The Use of Cyclodextrin Template-Based Metal Oxide Nanomaterials in the Development of Electrochemical Sensors for Phenolic Endocrine Disruptor Compounds

By

Milua Masikini

A thesis submitted in fulfillment of the requirements for the degree of
Magister Scientiae in the Department of Chemistry
University of the Western Cape
Cape Town / South Africa

Supervisor: Prof. Emmanuel I. Iwuoha
Co-supervisors: Dr Tesfaye T. Waryo and Prof. Priscilla G. Baker

November 2010.

KEY WORDS

Iron oxide

Oxy-hydroxy-iron

Hydroxy-iron

Metal oxide

Nanomaterials

β-cyclodextrin

Electrochemical Sensors

Phenolic Endocrine Disruptors

Bisphenol A

Tert-octylphenol

Cyclic voltammetry (CV)

Chronoamperometry (CA)

Electrochemical Impedance Spectroscopy (EIS)

ABSTRACT

Iron oxide nanoparticles were prepared using co-precipitation method in the presence and absence of beta-cyclodextrin (β-CD). Such materials were characterized using transmission electron microscopy (TEM), energy dispersive X-ray spectroscopy (EDX), attenuated total reflection Fourier transform infrared (ATR-FTIR), X-ray diffraction (XRD), cyclic voltammetry (CV), electrochemical impedance spectroscopy (EIS) and chronoamperometry (CA). The TEM shows that the surface morphology has no difference between nanoparticles prepared in the presence and absence of beta-cyclodextrin (β-CD), amorphous particles with high surface area and dimensions of about 100 nm by 500 nm. The amorphous states of nanoparticles are confirmed further by XRD. The ATR-FTIR analysis confirms inclusion complex between β-CD and nanoparticles. The nanoparticles synthesized were used to develop an electrochemical sensor for phenolic endocrine disruptors by modifying the surface area of glassy carbon electrode (GCE). Electrochemical characterization of the iron oxide β-CD nano-composites, studied in 0.1 M potassium chloride (KCl) using chronoamperometry, showed that the surface concentration of the adsorbed composite material was 8.5 x 10^{-8} mol/cm^2. Sensor analysis of bisphenol A (BPA) was carried out using cyclic voltammetry (CV) and square wave voltammetry (SWV) based on amperometric techniques which gave a linear range of 0.50 × 10^{-6} M to 50 × 10^{-6} M; limit of detection of 0.156 x 10^{-6} M and order of magnitude of linearity of 2.03. Hence, the sensor was further used to study 4-tert-octylphenol (TOP); the results showed that the sensitivity and the limit of detection were 11.31 nA L/mol and 0.249 x 10^{-6} M, respectively and order of magnitude of linearity of 2.00.

DECLARATION

"I declare that **The Use of Cyclodextrin Template-Based Metal Oxide Nanomaterials in the Development of Electrochemical Sensors for Phenolic Endocrine Disruptor Compounds** is my own work and that all sources quoted have been indicated and acknowledged by means of references."

Milua Masikini

Signed: …… Date: ……..

ACKNOWLEDGEMENTS

Firstly, I would like to give the Almighty God all the glory, honour and adoration for seeing me through this great journey. His presence, kept me saved at all the time in South Africa.

I would like to thank my supervisors, Professor Emmanuel Iwuoha and Professor Priscilla Baker, who gave me a precious opportunity to do my MSc as well as many valuable suggestions and great ideas.

Dr. Waryo Tesfaye is sincerely acknowledged for guiding me throughout the study and for his kindness and availability.

To the staff of the departments of Chemistry at UWC, thank you so much for the kind support that you accorded me during this period.

To SensorLab colleagues, Peter Ndangili, Lundi Ngqongwa, Chinwe Ikpo, Stephen Mailu, Natasha West, Dr Zelo Mangombo, Dr Faiza Ifthikar and all friends, your support and motivation are highly appreciated.

To my father, Mr. Milua Gabriel, my uncle Mosengo Edmond and his wife Mokabia Marie-José, brothers, sisters, cousins, nephews, nieces, for your prayers, supports and love. Thank you so much.

To my late mother, uncle, brother and sister, Mrs. Mbo Mokango, Mosengo Georges, Bienvenu Masikini and Clarisse Masikini, respectively, you left so earlier. May your souls rest in peace and I am sure we will meet in heaven.

Last but not least, I gratefully acknowledge the help and support of my brother Jean-Claude Masikini and his wife Matona Carmel.

To the National Research Foundation (NRF) of South Africa, thank you for awarding me an MSc bursary.

LIST OF PUBLICATIONS

1. **Milua Masikini**, Tesfaye T Waryo, Lundi Ngqongwa, Priscilla G Baker, and Emmanuel I Iwuoha, Hydroxy-iron/β-cyclodextrin-film amperometric sensor for the endocrine disruptors substance Bisphenol A in aqueous medium with reduced fouling effects. **(Analytical Letters 2010; in press).**

2. Lundi Ngqongwa, Tesfaye T Waryo, **Milua Masikini**, Priscilla G Baker, and Emmanuel I Iwuoha, Metal oxide/polyaniline-composite supercapacitor materials studied at carbon microelectrode surface. (**Submitted to Electroanalysis 2010**).

ABBREVIATIONS

A……	area of electrode
ATR-FTIR…….	attenuated total reflection Fourier transform infrared
APs……	alkyphenols
BPA……...	bisphenol A
C_0 …….	bulk concentration
CV……	cyclic voltammetry
CA…….	chronoamperometry
CDs……	cyclodextrins
D……	diffusion coefficient
E_i……	initial potential
E_λ ……..	switch potential
E^θ …….....	standard electrode potential
$E^{0'}$ …….....	formal electrode potential
E_p……...	peak potential
E_{pa}……..	anodic peak potential
E_{pc}……..	cathodic peak potential
ΔE_p……	peak to peak separation
EPA……...	environmental protection agency
EU…….	European Union
EDCs……	endocrine disruptors chemicals
I_{pc} …….	cathodic peak current
$I_{p(forward)}$ …….....	forward peak current
$I_{p(reverse)}$……...	reverse peak current

I_{pa}……..	anodic peak current
I_p……	peak current
Feox……...	iron oxide prepared in absence of beta cyclodextrin
Feox-bcd……	iron oxide prepared in presence of beta cyclodextrin
Feox-cobcd……	iron oxide coated with beta cyclodextrin
GCE……...	glassy carbon electrode
k^o……	standard rate constant
MAC……..	maximum admissible concentration
n ……	number of electrons transferred
NP……..	nonyphenol
NPs……	nanoparticles
Ph……..	phenol
R.....	gas constant
SEM……..	scanning electron microscopy
SWV……..	square wave voltammetry
TOP……...	4-tert-octylphenol
US……..	united states of America
v……	scan rate
WHO……	world health organisation
α. ……...	transfer coefficient
β-CD……..	beta-cyclodextrin
Γ ……	surface coverage

TABLE OF CONTENT

LIST OF SCHEMES

LIST OF TABLES

LIST OF FIGURES

CHAPTER 1

INTRODUCTION

1.1 Background

An endocrine disruptor compound mimics natural hormones, leading to their disruptive development and reproduction with consequences exemplified by a series of diseases such as male infertility, prostate cancer, breast cancer, obesity, etc. There is no doubt that the phenolic compounds in the materials of the containers and wrappers of food and drinks, cosmetic and household products make their way into the body fluids of consumers and the environment owing to their high solubility in oils/ fats and to some extent in water [1-3]. Nevertheless, controversy still surround the evidence supporting phenolic compounds as endocrine disruptors and their widely accepted effects on human health [4]. Improved chemical analysis and detection methods for phenolic compounds (e.g. bisphenol A, nonyphenol, chlorophenol) are necessary whether we are searching for more conclusive evidences on health hazards or we want to address these concerns and as a result need to monitor and control phenol concentrations and ensure that they are within the recommended safe limits in commercial food products, drinks and other consumables.

The most common techniques used for the determination of phenolic compounds in environmental samples include gas chromatography-mass spectrometry (GC-MS), high performance liquid chromatography-mass spectrometry (HPLC-MS) and liquid chromatography-mass spectrometry (LC-MS) with detection limits ranging from sub ppb values down to 2 x 10^{-17} ppb [1, 3, 5-7]. These techniques however present a significant disadvantage in term of cost since the requirements include trained personnel, consumption

of organic solvents and long analysis time (separation). Chemical sensor and biosensor devices in general and electrochemical sensors and biosensors in particular would be preferred to the above methods in light of the possibility of reagent-less detection and analysis, portability and non-expert operation.

The performance of an electrochemical sensor is determined by the nature of the material immobilized on the surface of the sensor and which interacts with analyte molecules and generates signals exclusive to the analyte and its concentration. However, it is well known that direct anodic decomposition of phenolic compounds at the metal electrode can result in the formation of insulating polyphenol film leading on electrode fouling [8]. In order to solve the above problem, synthetic diamond electrodes and various doped metal oxide electrodes, such as PbO_2, SnO_2, and TiO_2, have been employed as alternatives. We recently carried out a study to see if films of transition metal oxides with nanostructures in their native or template directed form could be used to generate better signal compared to traditional electrodes.

The method for the preparation of a nanomaterial may be partly dictated by its prospective applications. Thus, not all methods would be technically available for the preparation of nanomaterials used to develop analyte-recognition surfaces in sensor to be used in aqueous media. Some chemical techniques used for the preparation of nanomaterials and nanostructured materials and for controlling their particle sizes rely on molecular mechanisms which limit the space available for particle growth, for example, precipitation of ions in microemulsions, vesicles or polymer solutions [9]. In addition, such methods encounter difficulties in the separation of particles from the polymer, surfactant or ligands used as structure directors. Other often used techniques include hydrothermal reaction method, sol-gel methods, and gel impregnation. Due to the inherent difficulty in controlling

reactions under the conditions involved, procedures based on such techniques were found not to yield well defined materials in terms of crystal structure, particle size, size distribution, morphology and state of dispersion. In contrast, precipitation or coprecipitation of nanomaterials in liquid solutions offers an easy and cheap route and is especially attractive to chemical sensor researchers. Accordingly, this method was used for the synthesis of iron oxide nanoparticles [9-11].

In this work, we present the outcomes of our experiments with iron oxide synthesized in the presence and absence of β-cyclodextrin in the bulk or on the surface of the particles.

1.2 Motivation

During the past few decades, a rapid increase in the number of reproductive and developmental defects has been observed in humans and wildlife exposed to environmental compounds [12]. These concerns may occur from the potential of some xenobiotics, both natural and manmade, to interfere with normal endocrine function [13]. Groups of substances that are found in the environment and have the potential to induce negative effects on the endocrine systems of human and wildlife are defined as Endocrine Disrupting Chemicals (EDCs). It has been reported in the literature that the adverse health effects caused by EDCs in humans and wildlife are due to their estrogenic activities [14-19].

Phenolic compounds are significant and widespread pollutants in the environment and some of them display estrogenic or androgenic activities. Thus, human exposure to such phenolic compounds through an environment medium, indigestion of water, foodstuffs and products containing phenol may cause diverse diseases.

For instance, the presence of phenolic compounds even at low concentrations (1 μg/L), can affect the taste and the odour of water and fish. In the 1970s the US Environmental Protection Agency (EPA) presented a list of eleven priority pollutant phenols, characterized by a variety of substituents such as chloro, nitro and methyl groups, based on their toxic properties. EU directive (76/464/CEE) fixes the maximum admissible individual concentration for organic contaminants in drinking water at 0.1 μg/L and hence the determination of phenols in river and drinking water has become of great importance since the 1980s. The World Health Organisation (WHO) suggests guideline level concentrations lower than 200 μg/L for 2,4,6-trichlorophenol, 9 μg/L for pentachlorophenol, 10 μg/L for 2-Chlorophenol and 40 μg/L for 2,4-dichlorophenol. The Maximum Admissible Concentration (MAC) was fixed at 0.5 μg/L for the total phenol amount, which excludes those natural phenols that do not react with chlorine [20] and no-observed-adverse-effect level (NOAEL) for BPA at 5 mg/kg body weight/day, which is minimally five hundred-fold above conservative estimates of human exposure [21].

In view of the above risks for our environment, human and wildlife, there is no doubt that monitoring of the level of phenolic compounds with estrogenic or androgenic activities, is very necessary, with special emphasis on decontamination and detection method. The common techniques used for detection of phenolic endocrine disruptors are gas chromatography (GC), liquid chromatography (LC) and high performance liquid chromatography (HPLC). However, these methods require long pre-treatment, are time consuming, complex, and involve utilization of expensive and toxic reagents. Thus, preference is given to electrochemical methods because they are time saving, have fast response time, use cheap instrumentation, etc.

The electrochemical methods used for the detection and treatment could be through direct as well as indirect oxidation process. During indirect oxidation reactions, strong oxidants such as hypochlorite/chlorine, ozone and hydrogen peroxide are used for the oxidation of the phenolic compounds. However, the formation of chlorinated compounds one problem associated with the indirect electrochemical methods [20]. Contrarily, when the oxidation of phenolic pollutants are performed using direct electrochemical process, the pollutants are destroyed and/or detected by direct electron transfer reactions at the electrode and the efficiency of such method depends strongly on the electrode materials. For instance, Scheme 1 shows a representation of a GCE electrochemical phenol sensor system in which one of two pathways of phenol oxidation may occur at the electrode surface. In general, the oxidation of phenol begins with electron transfer that leads to phenoxy radicals. In pathway 1 the phenoxy radicals result in the formation of polymeric film, which can insulate and hence leads to fouling of the electrode surface. On the other hand, the phenoxy radicals may generate benzoquinone and hydroquinone which can be further degraded through ring opening to form various aliphatic acids, which in turn are further degraded to carbon dioxide and water [20].

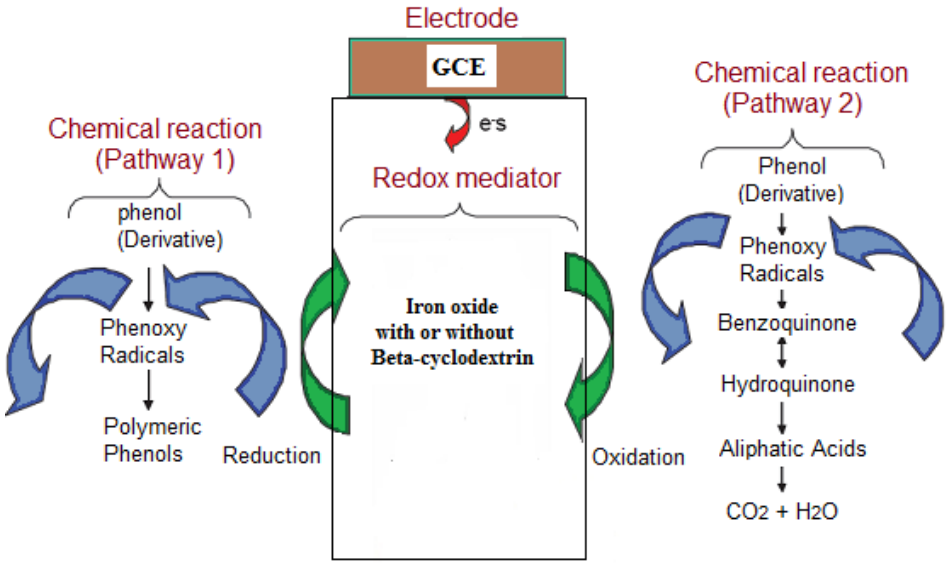

Scheme 1: Representation of a GCE/nanoparticle electrochemical phenolic sensor

1.3 Objectives

1.3.1 General objectives

The main aim of this research was to develop an electrochemical sensor for sensitive and rapid determination of the phenolic endocrine disruptors such as bisphenol A (BPA), 4-tert-octylphenol (TOP), nonylphenol, etc.

1.3.2 Specific objectives

The specific objectives include:

i. To synthesize chemically metal oxide nanoparticles in the presence and absence of β-cyclodextrin.

ii. To characterize the synthesized metal oxide nanoparticles by transmission electron microscopy (TEM), energy dispersive X-ray spectroscopy (EDX), Fourier transform infrared (FTIR) and X-ray diffraction (XRD);

iii. To develop an electrochemical sensor by drop coating the metal oxide prepared in the presence of β-cyclodextrin onto surface of glassy carbon electrode (GCE);

iv. To characterize the developed metal oxide sensors by cyclic voltammetry (CV), square wave (SW), chronoamperometry (CA) and electrochemical impedance spectroscopy (EIS) and to optimize the sensor parameters such as sensitivity, order of magnitude of linearity and limit of detection;

v. To apply the developed sensor for the detection of phenolic endocrine disruptors (e.g. bisphenol A and 4-tert-octylphenol).

1.4 Research framework

In line with the study objectives and the experiment programme, the research framework process is shown on the following Scheme.

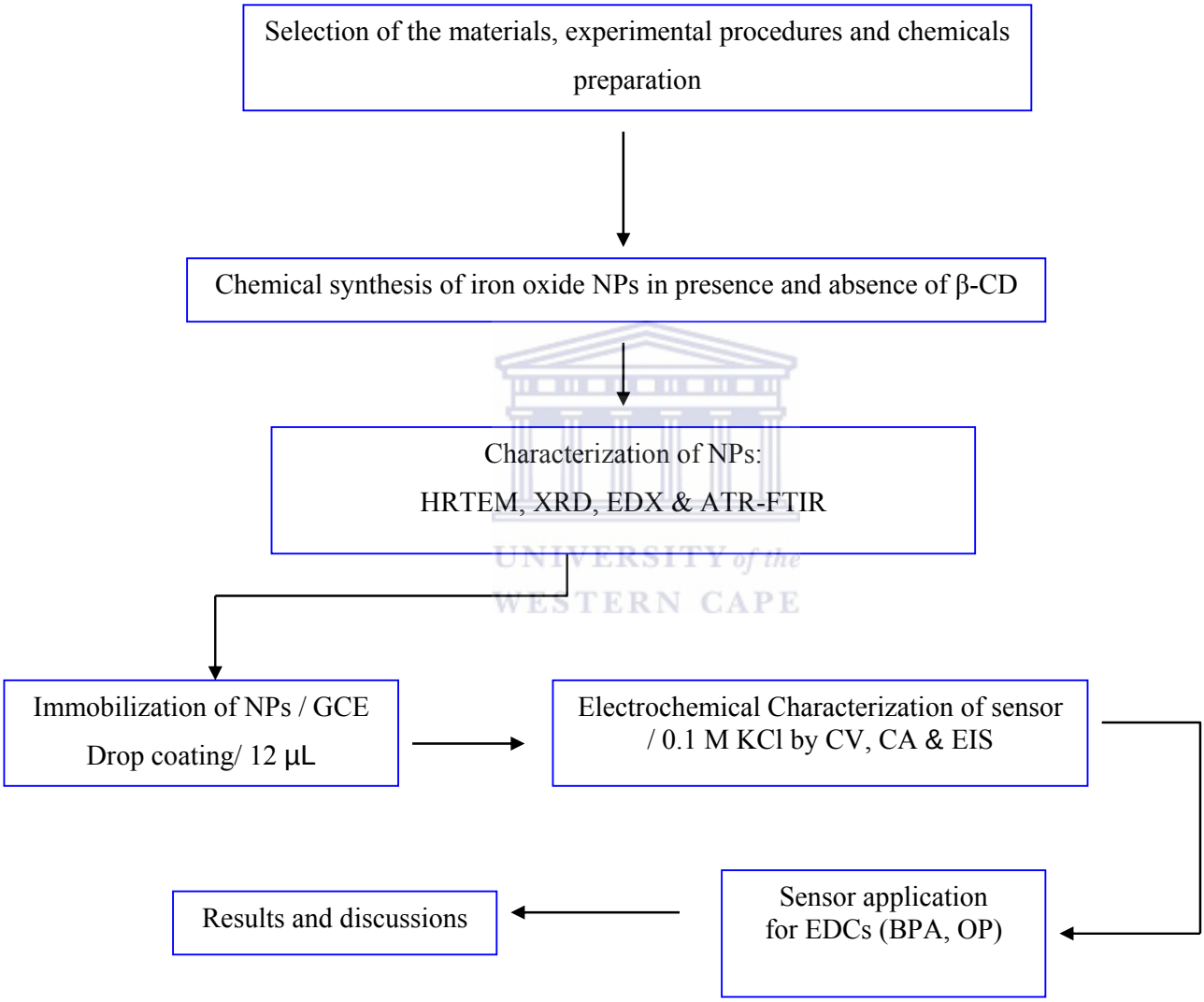

Scheme 2: Research framework.

1.5 Delimitations of the thesis

The main efforts of the thesis involve the following aspects:

i. Chemical preparation of iron oxides in presence and absence of β-cyclodextrin and their characterization using physical, analytical and electrochemical techniques.
ii. Investigation of iron oxide β-cyclodextrin composite and fabrication of an electrochemical sensor for phenolic endocrine disruptors.
iii. Performance of the developed sensor in the analysis of bisphenol A and 4-tert-octylphenol.

1.6 Thesis outline

The thesis will be presented as follows:

Chapter 1 gives an introduction into the various issues surrounding phenolic compounds that affect human life and wildlife, and as such require continuous monitoring through the use of various methods of detection. Different methods for the synthesis of metal oxide nanomaterials are also highlighted in this chapter together with the objectives of this study, research framework and delimitations of this study.

Chapter 2 presents reviews on endocrine disruptors; including a brief introduction, their sources, binding mechanism, health and environmental effects and properties. General phenols and phenolic endocrine disruptors, analytical techniques used for their detection; electrochemical phenol sensors as well as examples of some specific phenolic endocrine disruptors such as BPA and TOP, are also discussed in this chapter. Various synthesis routes for metal oxide nanoparticles and their applications in sensors in addition to cyclodextrins and their applications are included.

Chapter 3 describes the instrumentation, reagents, preparation of iron-oxide β-CD composite, various characterization techniques, fabrication and measurement of sensors, and preparation of the analytes (BPA, TOP).

Chapter 4 presents the results for the characterization of iron-oxide nanoparticles chemically prepared in the presence and absence of β-CD using different techniques such as TEM, EDX, ATR-FTIR and XRD. The results for the electrochemical characterization of the iron-oxide nanoparticles films investigated by CV, CA and EIS are also discussed.

Chapter 5 presents the results for the sensors responses to BPA using CV and SWV, the effect of scan rate on BPA –generated currents, as well as the sensors responses to TOP using CV and SWV. Analysis of ginger beer contaminated with BPA is also presented.

Chapter 6 summarizes the major conclusions drawn from the results of the research and the recommendations formulated for further studies.

CHAPTER 2

LITERATURE REVIEW

2.1 Introduction to endocrine disruptors chemicals (EDCs)

During the last few decades, international concern has been raised regarding the possible harmful effects of exposure to certain chemicals in the environment. This concern was initially centered on chemicals that may mimic the action of natural female hormones and were thus termed "environmental estrogens" [18, 22-23]. However, some chemicals can also affect the progeny of previously exposed parents [24]. Moreover, every year hundreds of these newly developed chemicals are released into the environment and the toxicity and health effects of these chemicals on human and animal wildlife are unknown [25]. These chemicals are now referred to as endocrine disrupting chemicals or EDCs. This class of compounds represent a wide range of chemicals that are found in our environment, food, and consumer products that interfere with hormone biosynthesis, metabolism, or action resulting in a deviation from normal homeostatic control or reproduction. Various definitions have been proposed for EDCs. The US Environmental Protection Agency (EPA) defines EDCs as exogenous agent that interferes with synthesis, secretion, transport, metabolism, binding action, or elimination of natural blood-borne hormones that are present in the body and are responsible for homeostasis, reproduction, and developmental process [26-27].

Some EDCs have similar structures to the natural hormone that they mimic or inhibit, while other EDCs have no resemblance at all. Therefore, EDCs belong to a class of substances which is defined by biological effect rather than chemical nature. For instance, various natural and synthetic chemical compounds including pharmaceuticals, pesticides, industrial chemicals and heavy metals have been identified as inducing estrogen-like responses [18, 28]

2.2 Endocrine system

The endocrine system is one of the body's main communication networks and is responsible for controlling and coordinating numerous body functions. It regulates all biological processes from conception of organism through adulthood and into old age regulating many functions of a body such as the development of the brain and nervous system, the growth and function of the reproductive system, metabolism and blood sugar levels.

Endocrine systems, also referred to as hormone systems, are found in mammals, non-mammalian vertebrates (e.g., fish, amphibians, reptiles and birds), and invertebrates (snails, lobster, insects and other species). In vertebrates the function of the endocrine system involves the regulation of a wide range of biological processes [18] and consists of:

- Glands located throughout the body.
- Hormones that are made by the glands and released into the bloodstream or the fluid surrounding cells.
- Receptors in various organs and tissues that recognize and respond to the hormones.

The normal function of the endocrine system therefore enables animals to control and regulate reproduction, development and behavior [18, 29]. The female ovaries, male testes, and pituitary, thyroid, and adrenal glands are major constituents of the endocrine system.

2.3 Endocrine disruptors chemicals: EDCs

2.3.1 Mechanism of EDCs

Endocrine disruptors are exogenous substances that alter function(s) of the endocrine system and consequently cause adverse health effects in an intact organism, or its progeny, or (sub)

populations [30]. Any substance that alters the function of endocrine system is termed an endocrine disruptor and is commonly referred to as "Endocrine Disrupting Chemicals" (EDCs). The endocrine system's function can be altered by different mechanisms such as:

a) mimicking or partly mimicking the sex steroid hormones estrogen (female sex hormone) and androgen (male sex hormone) by binding to their natural receptors either as agonists or antagonists.
b) altering the synthesis and breakdown of natural hormones.
c) modifying the production and functioning of hormone receptors.

Compounds that mimic estrogens are termed environmental estrogens and those that block hormone action are termed anti-estrogens or anti-androgens. The majority of researches on endocrine disruptors have been focused on environmental estrogens.

2.3.2 Sources of EDCs

Chemicals capable of acting as endocrine disruptors are ubiquitously found throughout the environment. They are grouped into two important groups [31-32]. The first group consists of natural compounds (e.g. phytoestrogens, bioflavanoids) that are naturally found in the environment [28, 33]. The second group consists of synthetic compounds (e.g. pesticides, herbicides, contraceptives, etc.) which are suspected to unintentionally [33] or intentionally [34] disrupt the endocrine systems of humans and wildlife. Giesy *et al*. [28]compiled a list of natural (Table 1) and synthetic compounds (Table 2) that are capable of disrupting the endocrine system.

Table 1: Examples of endocrine disrupting compounds: natural products[28]

Compound	Mode of action	Assay	Reference
Phytoestrogens			
Indole-3-carbinol	ER agonist	RER (MCF-7-luc), YES	[35-36]
β-Sitosterol	ER agonist, androgenic after metabolization	YES, in vivo fish	[35, 37]
Coumestrol	ER agonist	RER (MCF-7-luc), YES In vitro ER mediated PAP induction	[35-36] [38]
Enterolactone, enterodiol	Decreased aromatase enzyme activity	In vitro human cell culture system	[39]
Bioflavanoids			
Genistein	ER agonist Estrogenic	RER (ER-CALUX) In vitro and in vivo vitellogenin production	[38, 40] [41]
Biochanin A, daidzein, equol	ER agonists, estrogenic	In vitro and in vivo vitellogenin production In vitro ER mediated PAP induction	[41] [38]
Quercetin, naringenin, luteolin apigenin, chrysin, kaempferol, hydroxy- and methoxy-flavones	Estrogenic, antiestrogenic, ER agonist	CB-ER, RER, RER (MVLN)	[33, 42-43]
Mycoestrogens			
Zearalenone	ER agonist	CB-ER, RER, VTG in vitro	[33] [44]

YES, yeast based recombinant ER-reporter assay; E-screen, MCF-7 cell proliferation; CB-ER, in vitro competitive receptor binding assay; RER, in vitro recombinant receptor-reporter cell bioassay; VTG-in vitro, in vitro vitellogenin synthesis in cultured male trout hepatocytes.

Table 2: Examples of endocrine disrupting compounds: synthetic compounds [28]

Compound	Mode of action	Assay	Reference
Pharmaceuticals			
Flutamide	Antiandrogenic activity	YES	[45]
Tamoxifen	Antiestrogenic drug	in vitro cell line tests, in vivo	[46]
	binding to ER, antagonist or agonist	E-screen and other effects	[47-49]
Hydroxytamoxifen	Antiestrogenic and antiandrogenic activity	YES, E-screen and other effects	[45] [47]
Nafoxidine, clomiphene	ER agonist	YES	[35]
Ethynylestradiol	ER agonist	In vitro, in vivo	[37, 41]
Additives			
Parabens	ER agonists	CB-ER, YES, in vivo terotropic response	[50]
t-Butylhydroxyanisol	Estrogenic	E-screen	[51]
Pesticides			
Insecticides			
o,p0-DDT	ER agonist, antiandrogenic activity	YES, RER (ER-CALUX), VTG-in vitro	[35, 45] [40, 52]
o,p0-DDD, o,p0-DDE	ER agonists	YES	[35]
p,p0-DDE	Androgen receptor antagonist, weak ER and androgen receptor agonist	CB-androgen receptor, in vivo mice Study	[53]
	Antiadrogenic and weak antiestrogenic activity	YES	[45]
p,p0-DDD	ER agonist	YES, CB-ER, RER (MCF-7-luc)	[54]
p,p0-DDT	ER agonist, estrogenic	E-screen	[41]
Kepone	ER agonist, estrogenic—after metabolization	RER (ER-CALUX), E-screen, in vitrobin vivo	[40-41] [49]
Endosulfan, Dieldrin, lindane	ER agonist	RER (ER-CALUX)	[40]
Toxaphene	Estrogenic	E-screen	[55]
Methyl parathion	Estrogenic	YES, VTG—in vitro	[56]
		In vivo effects on estrus cycle in Mice	[57]
Chlordecone	Estrogenic	YES, VTG—in vitro	[56]
Chlordane	ER agonist	RER (ER-CALUX)	[40]
		In vivo—effects on endocrine function in mice	[58]

Table 2: Continued

Compound	Mode of action	Assay	Reference
Methoxychlor	ER agonist—after Metabolization	RER (ER-CALUX) in vitro + in vivo	[40, 49]
Carbamate insecticides (Aldicarb, Bendiocarb, Cabaryl, Methomyl, Oxamyl)	Endocrine modulators, non-ligand binding	in vitro modulation of estrogen and progesterone receptor in human breast and endometrial cancer cells	[54]
Pyrethroid insecticides (Sumithrin, Fenvalerate, D-trans Allethrin, Permethrin)	Estrogenic (different mechanisms)	In vitro pS2 gene expression E-screen	[59]
Fungicides			
Vinclozolin	Antiandrogen	In vitro androgen receptor binding assay, YES	[45, 60]
Dodemorph, Triadimefon, Biphenyl	Estrogenic	YES, VTG in vitro	[55]
Herbicides			
Atrazine	Estrogen, antiestrogen	RER (MCF-7-luc), in vivo	[36]
Simazine	Antiestrogen	In vivo	[61]
Alachlor, Nonachlor	ER agonists	YES, CB-ER, RER (MCF-7-luc)	[54]
Tributyltins	Androgenic	Imposex in snails, various in vivo effects in gastropods	[37, 62]
Industrial chemicals			
Phthalates			
Butylbenzylpthalate	ER agonist, antiandrogenic activity	In vitro + in vivo, E-screen, YES	[37, 45, 51, 63]
Dibutylpthalate	ER agonist	In vitro + in vivo	[37, 63]
Alkylphenols			
Nonylphenol	ER agonist, estrogenic	RER (MCF-7-luc, ER-CALUX), YES, number of in vitro and in vivo assays, E-screen, Vtg-in vitro	[35-36] [40-41, 49, 51, 64]
Octylphenol	ER agonist	RER (MCF-7-luc) Number of in vitro and in vivo assays	[64] [51]
Butylphenol, Pentylphenol	Estrogenic	E-screen	[41, 51]
Nonylphenol polyethoxylates and polyethoxycarboxylates	ER agonists	Number of in vitro and in vivo assay	[64]
Pentachlorophenol	Decrease in blood testosterone concentration	In vivo ewes feeding study	[65]
Bisphenol A	ER agonist	RER (MCF-7-luc, ER-CALUX), YES, VTG in vitro	[35-36]
		YES	[40, 51]
	Antiandrogenic activity		[45]

Table 2: Continued

Compound	Mode of action	Assay	Reference
Persistent organic pollutants			
PCDD	antiestrogenic—different mechanisms	In vivo + in vitro studies	[66]
PCBs	ER agonists or antagonists or other mechanism—depending on the substitution	RER (transient MCF-7-luc), E-screen, in vivo—vaginal cell cornification in mice	[51, 67]
Arochlor 1260 (PCBs mixture), Arochlor 1260	Estrogenic, effect on sexual differentiation, gonadal abnormalities	VTG in vitro, in vivo trout study	[51, 68]
Hydroxy-PCBs	ER agonists or antagonists	RER (MCF-7-luc), E-screen, CB-ER, in vivo—vaginal cell cornification in mice	[51, 67]. [65, 69]
PAHs	ER agonists—estrogenic, antiestrogenic—different mechanism	YES, E-screen RER (MCF-7-luc)	[70-71] [72-73]
6-hydroxy chrysene	Antiestrogenic	YES	[71]
Heavy metals			
Cations of cadmium, cobalt, copper, mercury, nickel, zinc	Depression or increases in testosterone production	In vitro substrate stimulated testosterone production by Leydig cells	[74]
Cadmium	Decrease in plasma testosterone and cortisol	In vivo juvenile rainbow trout Exposure	[75]
	Modification of pituitary hormone secretion	In vivo rat feeding exposure	[76]
Lead	Delayed sexual maturation, suppression of sex steroid biosynthesis	In vivo rat feeding study	[77]

Abbreviation as in Table 2.1.

2.3.3 Human health effects of endocrine disruptors

Currently, no adequate epidemiological data on human exist in order to make a solid conclusion regarding real links or correlations between endocrine disrupting compounds and human health [18]. Most of the evidence obtained for this possible link is derived from cases of pharmacological dosing, accidental exposure and occupational exposure [18]. The most well known link is between the development of cancer and other reproductive health problems in children and their mothers when the later took diethylstilbesterol (DES) while pregnant. Evidence of the possible relationship between exposure to the chemicals found in the environment and causing health effects in humans and wildlife published for the first time in 1992 were decreased sperm counts and male reproductive capabilities were recorded over 50 years [78-79]. Recently, a similar study was performed and correlated results were found [80].

Exposure to environmental estrogens and other endocrine disruptors can occur through three main pathways including ingestion, inhalation and dermal contact. In as much as there is no clear relationship between health effects and exposure to endocrine disruptors has been established [81] that there is so much yet be known about endocrine disruptors such as chemicals compositions, persistence in the environment and potential health effects, additional research is required including:

- large-scale human epidemiology studies relating specific health effects with exposure to endocrine disrupters.
- basic research into mechanisms of endocrine disruption.
- research into the effects of different types of exposure in the environment which may lead to unexpected effects e.g. mixtures of endocrine disruptors, long-term low dose exposure.
- exposure at different ages to see if humans are vulnerable to endocrine disruptors at any particular stage of life.
- exposure of individuals who may be especially susceptible.

More effort has been put into the study of chemicals that may disrupt the endocrine system because of its viability to health, especially reproductive health and the maintenance of the human species. One of the researchers in the endocrine disruptors area, John McLachlan, writes, “As patterns begin to emerge in environmental endocrine science, recognition of similarities to those associated with evolution and development should provide insights to mechanisms and outcomes. Without pattern recognition, there is not the ability to predict, and without prediction there is not the possibility to prevent” [82].

In wildlife, it was proven that endocrine disruptors can cause abnormalities and impaired reproductive performance, changes in immunity and behaviour and skeletal deformities in some species [81]. In humans, it has been reported over the recent decades, that adverse health effects are speculated due to exposure to endocrine-disrupting chemicals. These include heart disease, premature puberty, sex reversal (feminization of males), altered sex ratios, abnormal sexual behaviour, birth defects, decreased sperm density, decreased size of testes, breast cancer, ovarian cancer, testicular cancer, reproductive effects and thyroid dysfunction (Table 3) [18, 27, 78, 81].

Table 3: Examples of the health effects of chemical endocrine disruptors in humans [78]

Chemical	Use	Mechanism	Health Effect
Diethylstilbesterol (DES)	Medication	Mimics estrogen	In humans – female – vaginal cancer, reproductive tract abnormalities; male – abnormalities of the penis and testicles, semen abnormalities
Genistein	Naturally occurring in soybeans Resin in dental sealants,	Mimics estrogen, blocks testosterone	In adult humans – lowers cholesterol, may decrease breast cancer risk. In animals – infertility.
Bisphenol A	lining of food cans, and polycarbonate plastics	Mimics estrogen	In male mice – alters prostate size, decreases sperm production, affects behavior
Vinclozolin	Pesticide/fungicide	Inhibits testosterone	In male rodents – feminization, nipple development, abnormal penis development
Polychlorinated biphenyls (PCBs)	No longer made; still found as a pollutant	Inhibit thyroid hormones	In humans – delayed neurological development; IQ deficits
Dioxin	By-product of industrial processes including incineration	Decreases estrogen; decreases testosterone; alters thyroid hormone	In female rodents – delayed puberty, increased mammary cancers. In male rodents – decreased testosterone, penis and testicular abnormalities, feminized sexual behavior. In humans – decreased thyroid hormone levels; decreased testosterone; cancers

2.3.4. Important issues in endocrine disruption

Some of issues such as effects of age at exposure, mechanisms of action in the human body, identification of specific health problem, non-traditional dose-response dynamics, etc., have proven to be key to a full understanding of mechanisms of action and consequences of exposure to EDCs [27] and have been previously reviewed in detail by Gore *et al*. [83]. Some of these issues are listed below.

2.3.4.1. Age at exposure and latency from exposure

Research shows that consequences of an adult exposure to an EDC may be very different from exposure obtained by a developing fetus or infant [27]. In fact, exposure to EDC may cause the greatest risk during prenatal and early postnatal development when organ and neural systems are developing. Adverse consequences observed in animals, such as subfertility, premature reproductive senescence and cancer which are linked to early exposure to EDC, but may not be apparent early in life and may be manifested in adulthood or during aging [27, 84]. For example, NIEHS researchers at the University of Cincinnati and the University of Illinois found that exposure to low doses of environmental BPA and natural estrogens, estradiol during fetal development could affect the prostate genes behavior, and may lead to prostate cancer during aging [85]

2.3.4.2. Effects of exposure to multiple chemicals

In most cases, the effects of different classes of EDCs may be additive or even synergistic [27]. When individuals and/or populations are exposed to an EDC, other environmental pollutants are also involved because contamination of the environments is rarely due to a single compound.

2.3.4.3. Transgenerational effects

There is some evidence that EDCs may not only affect the individual directly exposed, but also children as well as future generations. Recent evidence suggests that the mechanism of transmission may in some cases involve the germline and may be nongenomic [27]. Another recent report supports above theory because prenatal exposure to vinclozolin or methoxychlor caused adverse effects on testis morphology and male fertility, and in addition these two chemicals caused epigenetic alterations in the DNA, specifically hyper- and hypomethylation. These effects were transmitted and alterations were observed in future generations [84].

Researchers from NIEHS have shown that the adverse effects of DES in mice can be passed to subsequent generations even though they were not directly exposed. The increased susceptibility of developing tumors was observed in both the granddaughters and grandsons of mice who were developmentally exposed to DES [86-87] and the mechanisms involved in the transmission of disease were shown to be epigenetic events [86, 88]. In fact, transgenerational effects may be transmitted, not because of mutation of the DNA sequence, but rather through modifications of factors that regulate gene expression such as DNA methylation and histone acetylation [27]. Transgenerational effects may also be associated with alterations in specific estrogen-responsive genes [84].

2.3.5 Phenolic compounds

2.3.5.1 Introduction to phenols

Phenols, sometimes called phenolics are defined as hydroxyl derivatives of benzene and its condensed nuclei [89-90]. Phenol and its derivatives are aromatic molecules containing hydroxyl, methyl, amide or sulphonic groups attached to the benzenoid ring structure [91-92].

The simplest class of the phenolic chemical is phenol. Its chemical formula is C_6H_5OH and its structure is that of a hydroxyl group (-OH) bonded to a phenyl ring (Fig. 1). In addition, phenol has synonyms include carbolic acid, benzophenol, and hydroxybenzene.

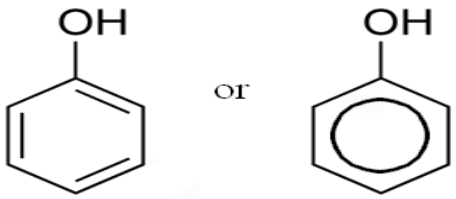

Figure 1: Phenol - the simplest of the phenols

Phenols are widespread, toxic, persistent and not easily removable from the environment [89, 93]. They are naturally produced as well as manmade (synthesized products). Naturally, phenols are constituent of coal tar and creosote, decomposing organic material, human and animal wastes, and as a compound found in many non-foods and foods [91]. In addition, they may also form during forest fires, by atmospheric degradation of benzene in the presence of light and can also be produced by the body and excreted as a metabolic product independent of external exposure or intake [91].

Phenols are commonly used in the production of plastics, plasticizers, drugs, dyestuffs, explosives, pesticides, detergents, stabilizers and antioxidants [89, 94-95], and their minor uses include the manufacture of paint and varnish removers, lacquers, paints, rubber, ink, illuminating gases, tanning dyes, perfumes, soaps and toys [96-97]. For example, production of phenol in term of volume exceeds three billion pounds annually in the United States and six billion pounds worldwide and is ranked in the top 50 in production volumes for chemicals; with the housing and construction industries accounting for about half of the phenol used in United States [98].

Phenols are introduced into the environment in different ways which include industrial effluents such as those from coal tar, gasoline, plastic, rubber proofing, disinfectants, pharmaceuticals, agricultural run-offs, chemical spills, steel industries, domestic waste-waters, wood preserving plants, brake and clutching industries, biocides application, etc.[89, 92-93, 99-102].

2.3.5.2 Phenols as endocrine disruptors

Some phenols have been reported to exhibit endocrine disrupting activities. Among phenolic compounds, bisphenol A and alkylphenols (nonylphenol and octylphenol) are the two important phenols that act as endocrine disruptors [91] and are the most widely detected in the environment [103]. Phenols can disrupt endocrine system in different ways:

- binding to hormone receptors thereby mimicking or antagonizing the action of the natural hormone, because of their molecular structure.
- altering synthesis or metabolism of natural hormone.
- interfering with signals between different components of the hypothalamus-pituitary-endocrine gland axes.

In addition, human exposure to phenols may occur through environment media, drinking water, foodstuffs or products containing phenol. Moreover, phenols are commonly absorbed by inhalation, ingestion, and through skin contact.

2.3.5.3 Properties of phenolic endocrine disruptors

Phenols known as endocrine disrupting chemicals (EDCs), present diversity in term of properties (physical and chemical), their mode of use, as well as their existence in the environment. The knowledge of some specific physical and chemical parameters of phenols

such as Log K_{ow}, solubility, Henry's law constant, vapour pressure, bioconcentration factor, and half-lives, K_{oc}, K_d, and diffusivity, is necessary, because these parameters as well as the nature of the media through which the phenols are migrating control environmental fate and transport of a contaminant. For example, studies have discovered that the rejection efficiency of EDCs by membranes is strongly dependant on EDCs' physicochemical properties, such as molecular weight, K_{ow}, water solubility, electrostatic property, etc. [104]. The physicochemical properties of some phenolic endocrine disruptors are summarized in Table 4, and structures of eleven EPA priority phenolic pollutants are presented in Figure 2.

Table 4: Physicochemical Properties of Selected phenols

Compounds	Main category	Chemical formula	Molecular weight (g/mol)	Water solubility (mg/L)	LogKow	pKa	Ref.
17β-estradiol (E2)	Natural estrogen	$C_{18}H_{24}O_2$	272.38	3.6	4.01	10.71	[104-106]
Estriol (E3)	Natural estrogen	$C_{18}H_{24}O_3$	288.4	441	2.45	10.4	[104-106]
17α-ethynylestradiol (EE2)	Pharmaceutical	$C_{20}H_{24}O_2$	296.41	11	3.67	10.4	[104-106]
Bisphenol A (BPA)	Industrial chemical	$C_{15}H_{16}O_2$	228.29	120	3.32	9.6	[104-106]
Nonylphenol (NP)	Industrial chemical	$C_{15}H_{24}O$	220.35	6	3.28	10.25	[104, 106]
Octylphenol (OP)	Industrial chemical	$C_{14}H_{22}O$	206.32	5	5.16	-	[104, 106]
4-tert-octylphenol	Industrial chemical	$C_{14}H_{22}O$	206.32	19	5.14	10.24	[104, 106]

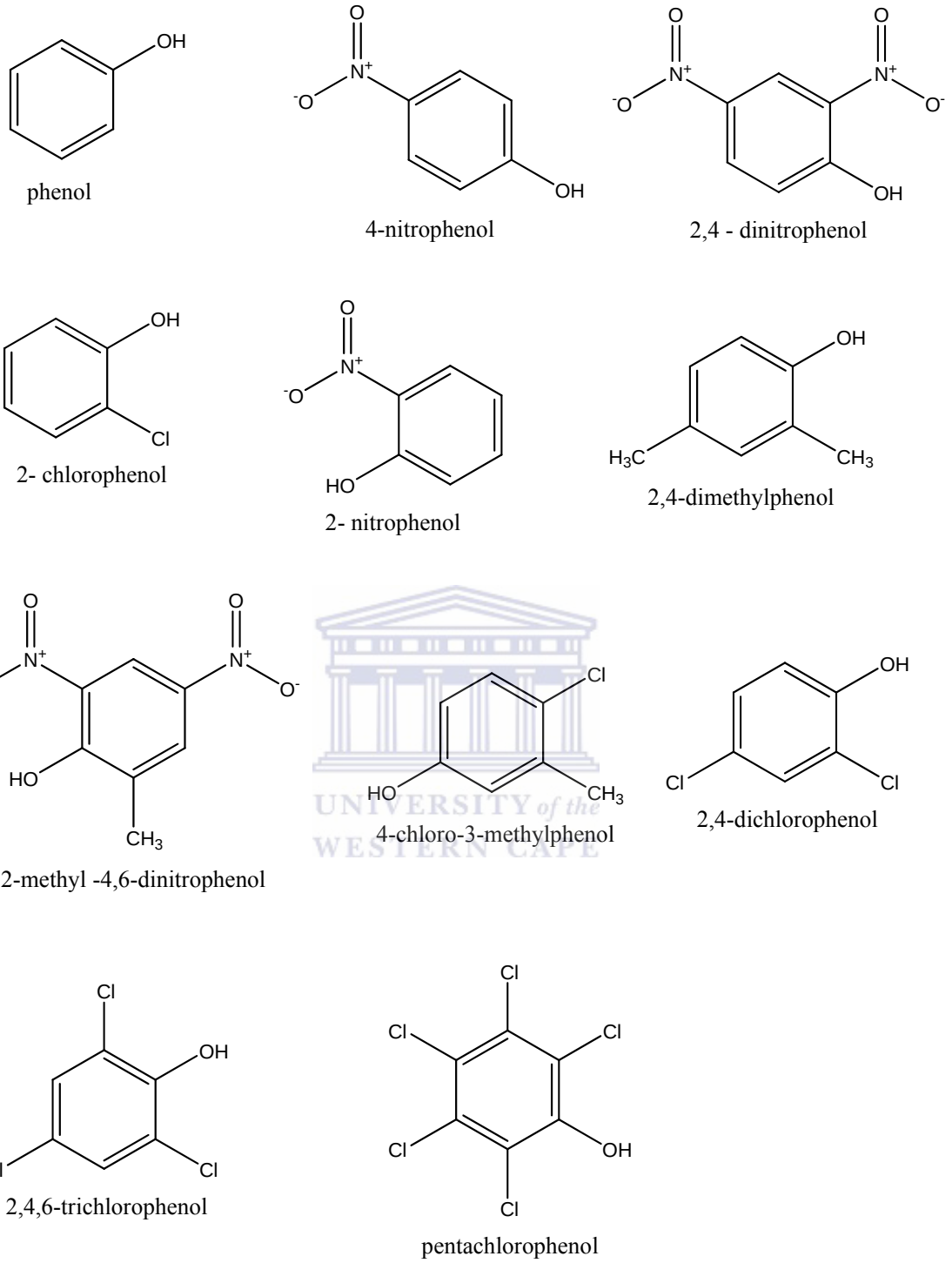

Figure 2: Chemical structures of eleven EPA priority phenols

2.3.5.4 Analytical methods for quantification of phenolic endocrine disruptors

The common techniques used for detection of phenolic endocrine disruptors are gas chromatography (GC), liquid chromatography (LC), high performance liquid chromatography (HPLC) [89, 107-108], coupled with different detectors such as mass spectrometry (MS) [107-108], fluorescence [108-109] and UV [108, 110]. Among all these separation techniques, gas chromatography (GC) is the commonly used for determination of estrogenic phenols [89, 107], because of advantages such as high resolution, rapid separation, low cost and easy linkage with sensitive and selective detectors [111]. The use of UV and fluorescence detection with HPLC, flame ionization detection (FID) and electrochemical detection (ECD) with GC as well mass spectrometric detection with both HPLC and GC have been reported [108, 112].

Phenols are very often present in the environment at low concentrations, thus a preconcentration technique is necessary .For that purpose solid-phase extraction (SPE) and solid-phase microextraction (SPME) are the most widely used [108, 112-114]. Mauricio *et al*. [115] used SPE followed by high-performance liquid chromatography (HPLC)-MS to determine levels of nonylphenol and octylphenol in water. SPE and capillary gas chromatography with electron capture detection was also used. In addition, Arditsoglou and Voutsa [116] developed a method to determine simultaneously phenolic compounds and steroid EDCs in aqueous and solid samples, based on a solid-phase extraction (SPE)-gas chromatography-mass spectrometry (GC-MS) method for water samples. Another alternative analytical technique, Capillary electrophoresis (CE), has also been used for the analysis of the phenols [117-118] and provide some advantages over other aforementioned analytical techniques such as high separation efficiency, small sample and electrolyte consumption and rapid analysis and has a great utility in routine analysis and monitoring processes in a number

of industrial fields [119]. However, the method can not identify neutral species and discern shape which is a disadvantage. For example, CE has been successfully applied to separate the eleven EPA priority phenols (Fig.2).

2.3.5.5 Electrochemical phenol sensors

Because of the disadvantages that traditional, analytical methods present, such as complex pre-treatment, complicated and expensive instrumentations, time-intensiveness and presence of professional operators, electrochemical methods are preferred because of cheap instrumentations, fast response, time saving etc. As long as there is no need for extensive separation alternating-current oscillopolarographic titration has been developed to be a simple, rapid, sensitive and inexpensive analytical tool for many applications in analytical, food and environmental science [119-120]. Although several electrochemical detection (ECD) methods have been used to detect phenols in conjunction with microfluidics, but amperometry remains one of the most popular [121]. In addition to instrumental methods, biological methods have improved to be very useful in the analysis of phenols in food and environmental samples. Among the methods, biosensors based on tyrosinase and perodidase has been developed for determination of phenols [122-124], among these methods. Alternatively, electrochemical detection of phenolic estrogenic compounds at carbon nanotube-modified glassy carbon electrode was reported [107]. The voltammetric behaviour of xenoestrogens, 4-nonylphenol (NP) and BPA at a platinum electrode has been compared with that of β-estradiol and other natural hormones [125]. Amperometric detection of river waters containing EDCs and phenols has also been employed by using a glassy carbon electrode (GCE), after preconcentration by SPME [126]. Moreover, carbon fiber electrodes were used for the electrochemical removal of BPA [127] and NP [128]. Amperometric determination of BPA using electrodes modified with adsorption enhancing agents like

cetyltrimethylammonium bromide, mesoporous silica, and layered Mg-Al-CO3 [129-131] ; electrochemical oxidation mediators such as cobalt phthalocyanine [132]; nickel tetraamino phthalocyanine [133] and dendrimer-quantum dot composite [134]; an amperometric enzyme biosensor made of immobilized tyrosinase [135-136]; microsomal cytochrome P450-3A4 (CYP3A4) nanobiosensor on GCE [137], have been also reported.

It is well known that direct oxidation of phenolic compounds at the metal electrode can result in the formation of an insulating polyphenol film leading to electrode fouling [8]. Measurement of charge transfer resistance related with BPA-adsorption with electrochemical impedance spectroscopy [138] is also an interesting approach in order to circumvent complications arising from electrode fouling by oxidative products of phenols. In the absence of sufficient selectivity, electrochemical BPA sensors could be exploited as detectors in tandem with a liquid chromatographic separation system [107, 139].

2.3.5.6 Example of some phenolic endocrine disruptors

2.3.5.6.1 Bisphenol A (BPA)

Bisphenol A (2,2-Bis-(4-hydroxyphenyl) propane), commonly abbreviated as BPA (Fig. 3), belongs to the phenol class of aromatic organic compounds with two phenol functional groups. It was synthesized for the first time over 100 years ago and was during the 1930s suspected as a possible synthetic estrogen from experiments on rats [91]. The effects of low-dose exposure to BPA on laboratory animals were first reported in 1997 [140]. Bisphenol A is mainly used as a monomer in the production of polycarbonate plastic and epoxy resins, and as a polymer additive to polyvinyl chloride plastic and some dental sealants. It is also used as an antioxidant in some plasticizers and a precursor to the flame retardants,

tetrabromobisphenol A. Bisphenol A can be found in some plastic water and baby bottles, plastic food containers, CDs and DVDs, household electronics, sports equipment, medical and dental materials, and the linings of some metal food and infant formula cans. Consequently, human exposure to BPA is ubiquitous, and is mainly through ingestion of tinned food [141-142], infant formula, maternal milk [141], or indirectly through maternal exposure, and the neonate [27]. Recently, the Center for Disease Control, using the human population as a reference, has published the results of a study which showed that 92.6% of over 2500 Americans had BPA in their urine [143]. In addition, the highest concentrations were found in children and adolescents than adults. Based on the statement that the main source of exposure is oral through food ingestion, the U.S. EPA has placed a safe human daily intake of BPA dose to be 50 µg/kg of body weight [27, 91].

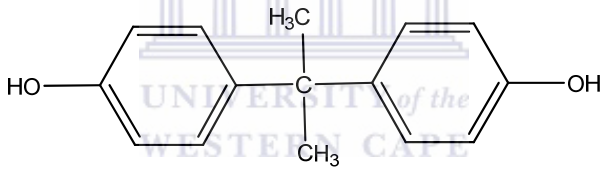

Bisphenol A

Figure 3: Chemical structure of BPA

Various studies published in the decade, have confirmed BPA as a endocrine disruptor and have found that laboratory animals exposed to low levels have increase risk of developing negative health effects such as diabetes, breast and prostate cancers, reproductive problems, decreased sperm count, early puberty, obesity, adverse effects on thyroid hormone, heart disease and neurological problems [27, 144-150].

2.3.5.6.2 Alkylphenols (APs)

Alkylphenols are a family of organic compounds obtained by the alkylation of phenols generally using from C_1 to C_{12} alkyls. The most important alkylphenols used are nonylphenol (NP) and octylphenol (OP) and their structures are shown in figure 4. In 1994, White *et al.*, published that nonylphenol ethoxylates (NPnEO) represented approximately 80% of the world market of alkylphenol ethoxylates and octylphenol ethoxylates (OPnEO) takes the remaining 20% [19].

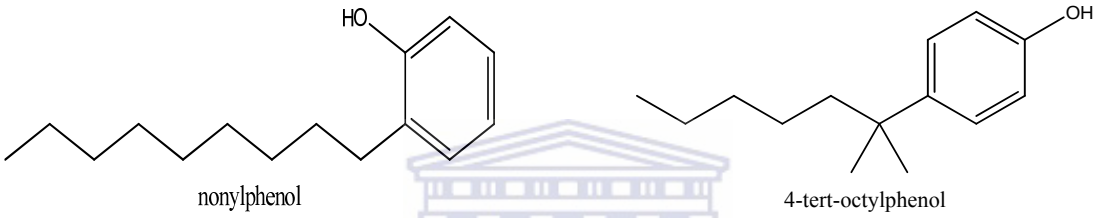

Figure 4: Chemical structure of nonylphenol and octylphenol

Alkylphenols such as nonylphenol and octylphenol have been used in industry for over 40 years and are mostly used for the production of alkylphenol ethoxylate (APE) surfactants (detergents), as additives for fuels and lubricants, polymer additives, antioxidants and as components in phenolic resins.

As a consequence of the wide-spread use for more than forty years, alkylphenols and alkylphenol ethoxylates have become ubiquitous environmental contaminants [151-152] and have even been found in foodstuffs [153]. Recently, since alkylphenols were found to exhibit estrogenic activity and may cause fertility problem in aquatic life particularly fish, issues about alkylphenols in the environment and human health have been raised. The major human exposure route to alkylphenols is air, contaminated drinking water (e.g. polluted rivers), absorption through skin (e.g. shampoos, cosmetics, spermicidal lubricants and domestic and

industrial detergents), inhalation and ingestion (e.g. pesticide sprays), contaminated food (e.g. fields spread with sewage sludge containing alkylphenols). Estrogenic activity (estrogen-mimicking) of alkylphenols was found for the first time in the 1930s when Dodds and Lawson reported the results of feeding 100 mg of 4-propylphenol to ovariectomized rats [154]. The next evidence for estrogenic effects of alkylphenols was published in 1978, by Mueller and Kim [155]. Unfortunately, no studies on the health and environmental implications of alkylphenols were done until Soto *et al*., published in 1991 effects of nonylphenol on cultured human breast cells [156]. Recently, more research has shown that the growth of these cells is increased by alkylphenols at concentrations 1000 to 10000 times higher than the estradiol levels required to produce the same growth. In addition, estrogenic effects of alkylphenols have been shown on rainbow trout hepatocytes, chicken embryo fibroblasts and a mouse estrogen receptor [19, 157]. Another Soto *et al*. study showed that, the low concentrations of 0.1 μM (20 μg/L) for octylphenol and 1 μM (220 μg/L) for nonylphenol can affect the growth of cultured human breast cancer cells [51]. Similar results were obtained by Routledge and Sumpter using the human estrogen receptor [158]. Recent research on estrogenic effects of nonylphenol, showed that lower concentration of 0.05 μg/L was sufficient to increase the number of eggs produced by minnows, as well as increasing vitellogenin levels [159]. The same study also suggested that nonylphenol could increase the levels of natural estrogen [159].

2.4 Metal oxide nanoparticles

2.4.1 Methods of synthesis of metal oxide nanoparticles

The synthesis of nanoparticles is a crucial step in both scientific research and the business area. Thus, there is a huge toolbox available to successfully synthesize both organic and

inorganic nanoparticles with diverse approaches. Among inorganic nanoparticles, metal oxide nanoparticles are the most attractive because of their intense use in science and technology. For the control of particle size and morphology, there are various physico-chemical methods or liquid-phase techniques, including co-precipitation, sol-gel chemistry, microemulsion, hydrothermal/solvothermal processing and template synthesis, and electrochemical deposition. These are some of the major methods for the synthesis of metal oxide nanoparticles, some of which will be developed in more detail below.

In this work, the co-precipitation method in aqueous medium (wet method) was used for the synthesis of metal oxide nanoparticles, specifically iron oxide.

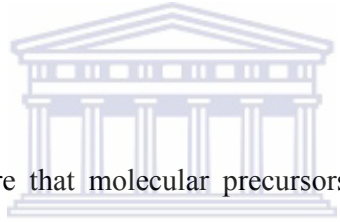

2.4.1.1 Sol-gel method

Sol-gel process is the procedure that molecular precursors, e.g. metal chlorides or metal alkoxides, react with certain solvent, e.g. H_2O or organic solvents, and form 3D metal oxide network via inorganic polymerization including hydrolysis/solvolysis and condensation reactions [160]. Aqueous sol-gel processes are generally used for the synthesis of metal oxide bulk materials as well as nanoparticles and two reaction mechanisms are involved, hydrolysis and condensation processes [160], as shown below. During the first step, which is hydrolysis, the metal alkoxide or metal chloride is hydrolyzed and an M-OH species is generated:

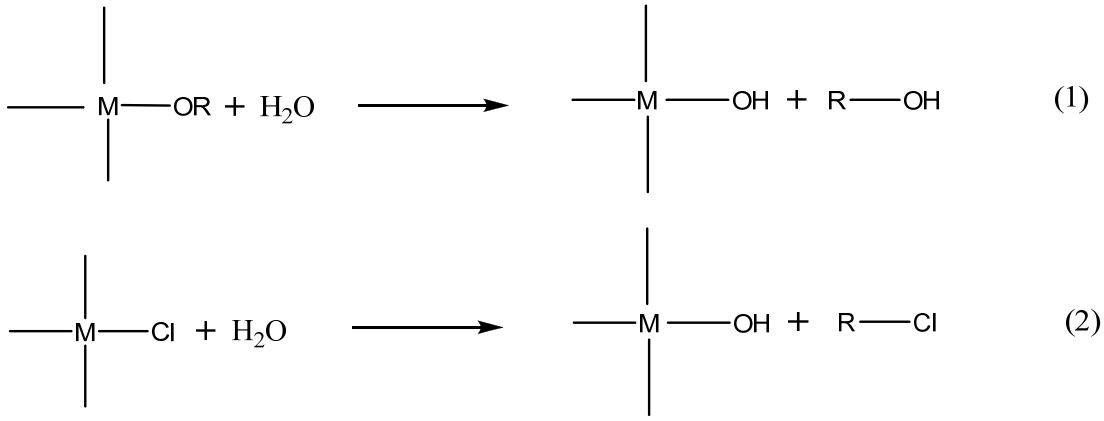

The second step, which is condensation, the hydroxy groups react with each other or another metal alkoxide/chloride and a 3D M-O-M is then formed leading to the propagation of the condensation reaction and resulting in the elimination of ROH, water or HCl.

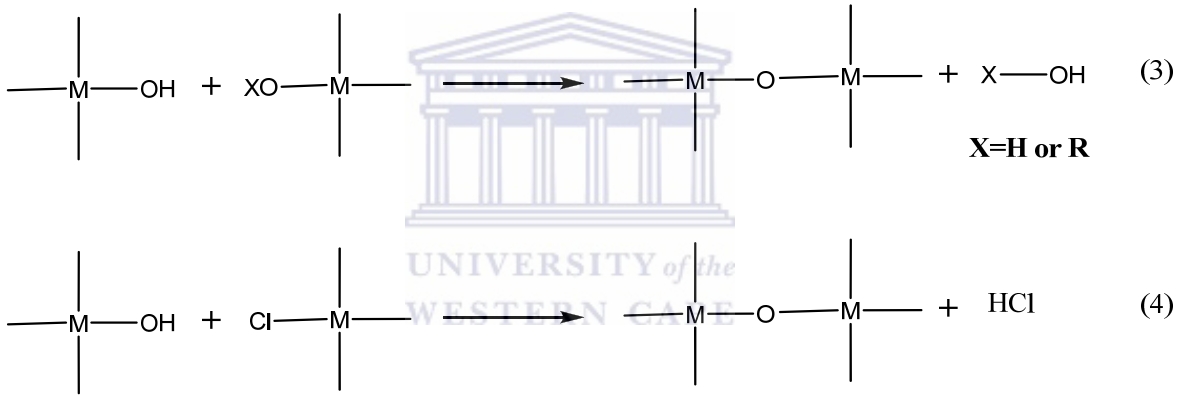

The aqueous sol-gel synthesis route has some advantages, such as high purity products and low processing temperatures. However, it also presents some disadvantages, of which the most important is that the method usually results in amorphous precipitates due to very fast hydrolysis and condensation processes and subsequent thermal treatment is necessary to obtain complete crystalline nanoparticles [160]. Another disadvantage of aqueous sol-gel synthesis is the difficulty in controlling the reaction parameters, such as the fast hydrolysis rate of the metal alkoxides, pH values, method of mixing, rate of oxidation and especially the nature and concentration of anions, which could all strongly impact on the morphology of the final products [161-162].

In order to overcome the difficulty of aqueous sol-gel routes a promising and popular sol-gel chemistry for the synthesis of metal oxide nanoparticles-the nonaqueous sol-gel route, has been introduced in which organic solvents, such as alcohols, ketones or amines are used as the liquid phase reactants. This method involves the reaction between metal oxide precursors, including organometallic complexes, metal halides, alkoxides and acetylacetonates, and alcohols or other inert organic solvents, such as amines and ketones. Compared with the aqueous method, the reaction mechanism of nonaqueous sol-gel chemistry is more complex. In spite of this disadvantage, nonaqueous method presents also some advantages, such as better control of particle, high crystallinity of the completed nanoparticles at relatively moderate temperatures (100-300°C) and homogeneous particle morphology, and control over particle sizes, shapes and compositions.

2.4.1.2 Hydrothermal synthesis

Hydrothermal synthesis is a method to produce metal oxide crystals from aqueous metal salt solutions through heating [163-164]. The equilibrium of the reaction of metal salt in water varies with temperature, and results in formation of metal hydroxide or metal oxides. An example of the synthesis of aluminium hydroxide from aluminium nitrate in water presented in the literature is shown below [163, 165-166]:

$$Al(NO_3)_3 + 3H_2O = Al(OH)_3 + 3HNO_3 \quad (5)$$

At higher temperatures, dehydrated products become predominant due to the further shift of the equilibrium.

$$Al(NO_3)_3 + 2H_2O = AlO(OH) + 3HNO_3 \quad (6)$$

$$Al(NO_3)_3 + 1.5H_2O = 0.5Al_2O_3 + 3HNO_3 \quad (7)$$

The hydrothermal synthesis method is generally used with a batch type autoclave, where aqueous solution is heated up slowly to 373–573 K and then aged for several hours or days. The above reaction takes place during the heating up period, leading to the formation of monomers, followed by nucleation and crystal growth. Because of the variation of the equilibrium with temperature, particles formed at lower temperatures dissolve again to re-crystallize at higher temperatures during the heating up period or the aging period. Consequently, hydrothermal method consumes a lot of time to obtain the crystals of equilibrium composition.

2.4.1.3 Microemulsion technique

Microemulsion is defined by Attwood as a system of water, oil, and amphiphilic compounds (surfactant and co-surfactant) which is a transparent, single optically isotropic, and thermodynamically stable liquid [167]. The concept of microemulsion was first introduced by Hoar and Schulman in 1943 by dispersing oil in an aqueous surfactant solution and adding an alcohol as a co-surfactant, leading to a transparent, stable formulation [168].

In recent years, microemulsion method has been developed to synthesize nanometer-size crystals. In addition the method is known to be a quite simple and rapid way to prepare nanocrystals and furthermore, it can synthesize ultrafine crystals with a grain size smaller than 2.4 nm [169]. Compared to conventional emulsions, the major differences are the size and shape of the particles, and stability [170]. For example, the size obtained is 10 – 200 nm in the case of microemulsions and 1 – 20 μm for conventional emulsions.

2.4.1.4 Coprecipitation method

This process involves dissolving a salt precursor, usually a chloride, oxychloride, or nitrate, e.g. $AlCl_3$ to make Al_2O_3, $Y(NO_3)_3$ to make Y_2O_3, and $ZrOCl_2$ to make ZrO_2 [171]. The metal hydroxide of the corresponding salt precursor is usually formed during the process and precipitate from water by adding a basic solution such as sodium hydroxide or ammonium hydroxide to the solution. The resulting chloride salts, i.e., NaCl or NH_4Cl, are then washed away and the hydroxide is calcined or dried after filtration or centrifugation and is washed again to obtain the final oxide. This method is an easy and cheap way to prepare metal oxide. In addition, it is useful in preparing composites of different oxides by coprecipitation of the corresponding hydroxides in the same solution. Nevertheless, the method presents a disadvantage - difficulty in controlling the particle size and size distribution. Frequently, the reaction is fast and then an uncontrolled precipitation takes place resulting in large particles [171].

2.4.1.4.1 Sonochemical coprecipitation

Sonochemical methods for the preparation of nanoparticles were pioneered by Suslick in 1991 [172]. The sonochemical method were useful in many areas of material science from the preparation of amorphous products [173-174] and insertion of nanomaterials into mesoporous materials [171, 175] to deposition of nanoparticles on ceramic and polymeric surfaces [176-177]. The method consists of breaking the chemical bond by applying high-power ultrasound waves generally between 20 kHz and 10 MHz. The acoustic cavitation is the main physical phenomenon responsible for the sonochemical process [171]. It has been reported that, the main events that occur during the preparation of nanoparticles by sonochemistry are creation, growth, and collapse of the solvent bubbles that are formed in the liquid [171]. Collapse of the solvent bubbles takes place only if the solute vapours diffuse

into the solvent bubble and the bubble reaches a certain size. Breaking of the chemical bonds in the solute occurs at very high temperatures (5000 –25,000 K) [172], and is obtained during the collapse. The organisation and crystallization of the nanoparticles are hindered by a high cooling (1011 K/s), which also occurs when collapse of the bubble takes place.

When the breaking of bonds in the precursor occurs in the gas phase, amorphous nanoparticles are obtained because of the fast kinetics of the reaction. On the other hand, if the breaking of bonds in the precursor occurs in a liquid phase then the products could be either amorphous or crystalline depending on the temperature in the ring region of the bubble, estimated by Suslick to be 1900 ◦C.

2.4.1.4.2 High-gravity reactive precipitation (HGRP)

High-gravity reactive precipitation is a new method to synthesize nanoparticles introduced by Chen *et al*. [171, 178] that was initially made for the preparation of metal carbonates and hydroxides. The method is based on Higee technology [171, 178], a novel technique, which consists of rotating a packed bed under a high-gravity environment, intensifying mass transfer and heat transfer in multiphase systems. The rate of mass transfer obtained by such technology between a gas and a liquid in a rotating packed bed is one to three orders of magnitude greater than that in a conventional packed bed.

Using HGRP method, Chen *et al*. adjusting some parameters of the reaction such as high-gravity levels, fluid flow rate, and reactant concentrations, were able to synthesize $CaCO_3$ particles with the particle size in the region of 17–36 nm. The same group used HGRP technique again for the synthesis of nanofibrils of $Al(OH)_3$ of 1–10 nm in diameter and 50–300 nm in length as well as $SrCO_3$ with a mean size of 40 nm in diameter.

Unfortunately, application of this technique has thus far been relatively limited and has not been extended to any other metal-oxide systems [171].

2.4.1.5 Templated techniques

In recent years, templated techniques have been used to obtain varieties of porous materials. In general, there are two types of templates in literature-soft template (surfactants) and hard template (porous solids such as carbon or silica) [171, 179]. When hard templates are used, the formation of porous material takes place in a confined space formed by the porosity of the template. Two types of hard templates have been employed in the template synthesis: active carbon [180] and mesoporous silica materials [171, 181-182]. However, the use of active carbons as templates during the synthesis has certain limitations since, at the high treatment temperature, infiltrated salts and the carbon may react with each other and destroy the target material. If during the synthesis the heat treatment is performed in air, the carbon may be quickly oxidized even at a relatively low temperature because of the catalytic effect of infiltrated salts. On the other hand, some metallic salts may produce metal instead of metal oxide as it is well known that at high temperature under inert temperatures, carbon is a good reducing agent. Commercial active carbons have been used as templates for the synthesis of various types of high-surface-area metal oxides (HSMO) [183], monodisperse and porous spheres of oxides as well phosphate [184]. To obtain ordered porous inorganic materials such as metal oxides and sulphides, mesostructured silica materials (MSMs) have been employed as templates [181-182]. In such synthesis using MSMs as a template, retention of surface silanol groups is required for effective impregnation of metal salts inside the pores. However, the surface silanol groups within the silica pores are usually affected during the removal of surfactant templates used for the synthesis of MSMs. To overcome such a problem, a recent and special technique called microwave digestion has been used [171].

Several people have used the mesostructured silica materials technique to synthesize high-surface-area metal oxides (HSMOs) e.g., Tian *et al*. [182] have synthesized various metal oxides (i.e., Fe_2O_3, Cr_2O_3, Co_2O_3). Although, their procedure presents some problems because of the expensive surfactants used as templating agents during the synthesis of MSM and a sophisticated method is used to remove those surfactants. Fuertes [185] has introduced an inexpensive and simple synthetic method for high-surface-area metal oxides (HSMOs) which has been successfully used to produce Mn_2O_3, Cr_2O_3, Al_2O_3, NiO, CeO_2, Co_2O_3, and Fe_2O_3. This method can also be used to synthesize metal sulphides and mixed metal oxides and consists of using porous silica templates (silica xerogel) synthesized without any surfactant. The xerogel is produced by a mixture formed exclusively by a silica source (sodium silicate), HCl, and water. The product obtained using Feurtes' method is not an ordered nanorod compare with the one obtained using the Santa Barbara Amorphous (SBA) template, but it is in the form of aggregates of nanoparticles and/or three-dimensional solid-containing confined pores [171].

Recently, Chane-Ching *et al*. [186] proposed a very simple and versatile method to synthesize various nanostructured metal oxides from surface-modified nanoparticle building blocks by using a liquid-crystal template. This approach consists of functionalizing the oxide nanoparticles with bifunctional organic anchors such as aminocaproic acid and taurine. When the addition of a copolymer surfactant is done, the functionalized nanoparticles slowly self-assemble on the copolymer chain through a second anchor site. By using this approach, the authors were able to synthesize several metal oxides like CeO_2, ZrO_2, and CeO_2–$Al(OH)_3$ composites.

2.4.1.6 Electrochemical deposition of metal oxide nanoparticles

Electrodeposition is the process of forming a film or a bulk material using an electrochemical process whereby the electrons are supplied by an external power supply. It is an important surface finishing procedure and in the broadest sense comprises the deposition of metals, alloys, oxides, polymers, and composites [187].

The advantage of in situ-immobilization methods for electrocatalysts in chemical sensing is incontestable [188]. Specially, electrosynthetic procedures enable us to reproducibly control various characteristics of modifier films. There are two major principles for electrochemically deposition of thin layers of metal oxide:

(i) by electrochemically changing either the pH in the vicinity of electrode surface or the oxidation state of the solution precursor [189]. This first approach is applicable for depositing substances such as siderite ($FeCO_3$), which are insoluble in alkaline medium, from an initially soluble precursor in acidic medium. Cathodic production of OH^- from species such as H_2O, which does not react with the precursor, seems to be the easiest way.

(ii) The second approach requires that the metal possesses at least two oxidation states that present large differences in solubility in the chosen medium [188]. Iron is a good example with Fe(II) being rather soluble and Fe(III) being almost insoluble in water. Green rusts ($Fe_4\ ^{II}Fe_2\ ^{III}O_4(OH)_{12}A.mH_2O$ with A^{2-} = anion), magnetite ($Fe^{II}Fe_2\ ^{II}O_4$) and goethite (α-FeOOH) could be synthesized according to this approach [189].

2.4.2 Iron oxide nanoparticles

Iron oxides exist in many forms in Nature, the three most common and very important technological forms include magnetite (Fe_3O_4), maghemite (γ-Fe_2O_3), and hematite (α-Fe_2O_3) [190-191]. Some of their physical and magnetic properties are summarized in Table 5.

Table 5: Physical and magnetic properties of iron oxides [191]

Property	**Oxide**		
	Hematite	***Magnetite***	***Maghemite***
Molecular formula	α-Fe_2O_3	Fe_3O_4	γ-Fe_2O_3
Density (g/cm^3)	5.26	5.18	4.87
Melting point (°C)	1350	1583-1597	-
Hardness	6.5	5.5	5
Type of magnetism	Weakly ferromagnetic or antiferromagnetic	Ferromagnetic	Ferrimagnetic
Curie temperature (K)	956	850	820-986
M_S at 300 K ($A\text{-}m^2/kg$)	0.3	92-100	60-80
Standard free energy of formation $\Delta G_f°$(kJ/mol)	-742.7	-1012.6	-711.1
Crystallographic system	Rhombohedral, hexagonal	Cubic	Cubic or tetrahedral
Structural type	Corundum	Inverse spinel	Defect spinel
Space group	R3c (hexagonal)	Fd3m	$P4_332$ (cubic); $P4_12_12$ (tetragonal)
Lattice parameter (nm)	a = 0.5034, c = 1.375 a_{Rh} = 0.5427, α = 55.3° (rhombohedral)	a = 0.8396	a = 0.83474 (cubic); a = 0.8347, c = 2.501 (tetragonal)

Among the three, hematite known also as ferric oxide, iron sesquioxide, red ochre, specularite, specular iron ore, kidney ore, or martite, is the oldest known of the iron oxides and is widespread in rocks and soils. It is extremely stable at ambient conditions, and is often the end product of the transformation of other iron oxides [191]. In its crystal structure, oxygen ions are in a hexagonal close-packed arrangement, with Fe(III) ions occupying octahedral sites. Magnetite, known also as black iron oxide, magnetic iron ore, loadstone, ferrous ferrite, or Hercules stone, has the strongest magnetism compare to any transition metal oxide [190-191]. In magnetite, oxygen ions arrangements are in a cubic close-packed.

In addition, magnetite has an inverse spinel structure with Fe(III) ions distributed randomly between octahedral and tetrahedral sites, with Fe(II) ions in octahedral sites [192]. Maghemite occurs in soils as a weathering product of magnetite, or as a product of heating of other iron oxides. It is metastable compared to hematite, and forms continuous solid solutions with magnetite [191]. The spinel structure of maghemite is similar to magnetite structure but contains vacancies in the cation sublattice. Two-thirds of the sites are filled with Fe(III) ions arranged regularly, with two filled sites being followed by one vacant site [190-191]. Moreover, in maghemite, the oxygen ions are arranged in a cubic structure.

The wet chemical routes to synthesis of magnetic nanoparticles are simpler, more tractable and more efficient with appreciable control over size, composition and sometimes even the shape of the nanoparticles [10, 193]. The synthesis of Iron oxides especially magnetite or maghemite can be done through the coprecipitation of Fe^{2+} and Fe^{3+} aqueous salt solutions by addition of a base [193]. However, the control of size, shape and composition of nanoparticles depends on certain parameters such as the type of salts used (e.g. chlorides, sulphates, nitrates, perchlorates, etc.), Fe^{2+} and Fe^{3+} ratio, pH and ionic strength of the media [10, 194]. Iron oxides (either Fe_3O_4 or γFe_2O_3) are usually prepared by adding a base to an aqueous mixture of Fe^{2+} and Fe^{3+} chloride at a 1:2 molar ratio. Scheme.3 shows the chemical reaction of Fe_3O_4 precipitation [10, 193].

$$Fe^{2+} + 2Fe^{3+} + 8OH^- \rightarrow Fe_3O_4 + 4H_2O \quad (8)$$

According to the thermodynamics of this reaction, complete precipitation of Fe_3O_4 should be expected at a pH between 8 and 14, with a stoichiometric ratio of 2:1 (Fe^{3+}/Fe^{2+}) in a non-oxidizing oxygen environment [10, 195].

Nevertheless, magnetite (Fe_3O_4) is not very stable and is sensitive to oxidation. Thus magnetite is transformed into maghemite (γFe_2O_3) in the presence of oxygen:

$$Fe_3O_4 + 2H^+ \rightarrow \gamma Fe_2O_3 + Fe^{2+} + H_2O \quad (9)$$

Or

$$Fe_3O_4 + 0.25O_2 + 4.5H_2O \rightarrow 3Fe(OH)_3 \quad (10)$$

$$Fe^{3+} + H_2O \xrightarrow{\text{Deprotonation}} Fe(OH)_x^{3-x}$$
$$Fe^{2+} + H_2O \xrightarrow{\text{Deprotonation}} Fe(OH)_y^{2-y}$$

$$Fe(OH)_x^{3-x} + Fe(OH)_y^{2-y} \xrightarrow[\text{Dehydration}]{\text{Oxidation}} Magnetite\,(Fe_3O_4)$$
$$\text{pH}\sim 9.0, 60^oC$$

Scheme 3: Reaction mechanism of magnetite particle formation from an aqueous mixture of ferrous and ferric chloride by addition of a base [10].

2.5 Characterization methods

2.5.1 Morphological and structural analysis techniques

2.5.1.1 Transmission Electron Microscopy (TEM)

The transmission electron microscope (TEM) has evolved over many years into a highly sophisticated instrument that has found widespread application across scientific disciplines. Because the TEM has an unparalleled ability to provide structural and chemical information over a range of length scales down to the level of atomic dimensions, it has developed into an indispensable tool for scientists who are interested in understanding the properties of nanostructured materials and in manipulating their behaviour [196].

The main application of transmission electron microscopy (TEM) is in the determination of the size, distribution and the morphology of synthesized nanoparticles. The principle of TEM works in much the same way as an optical microscope. A beam of electrons, generated by the high voltage electron emitter situated at the top of the lens column, interacts with the sample as it passes through the entire thickness of the sample and a series of magnifying magnetic lenses, where they are ultimately focused at the viewing screen at the bottom of the column. The TEM image is basically a projection of the entire item, including the surface and the internal structures. In this work TEM was used to determine the size, morphology and the crystallinity of the materials.

2.5.1.2 Scanning Electron Microscopy (SEM)

Scanning electron microscopy (SEM) is a versatile imaging technique capable of producing three-dimensional images of material surfaces. SEM is one of the most frequently used instruments in material research today because of the combination of high magnification, large depth of focus, greater resolution and ease of sample observation.

The basic operation in SEM entails the interaction of an accelerated highly monoenergetic electron beam, originating from the cathode filament, with the atoms at the sample surface. The electron beam is focused into a fine probe which is rastered over the sample. The scattered electrons are collected by a detector, modulated and amplified to produce an exact reconstruction of the sample surface and particle profile [197-198].

A requirement for effective performance is that the surface of the samples should be electrically conductive. During operation electrons are deposited onto the sample. These electrons must be conducted away to earth, thus conductive materials such as metals and

carbon can be placed directly into the SEM whereas non-metallic samples have to be coated with a gold metal layer to be observed. Many scanning electron microscopes have an energy dispersive spectrometer (EDX) detection system, which detects and displays most of the spectra of the elements contributing to the sample composition. In this work SEM was used to determine elemental composition of the materials.

2.5.1.3 X-Ray Diffraction (XRD)

X-ray diffraction (XRD) is a versatile, non-destructive technique that reveals detailed information about the chemical composition and crystallographic structure of natural and manufactured materials. It is an indispensable method for material characterization. XRD is a powerful tool in the study of crystallinity and atomic structure of materials and forms an integral part of the comprehensive characterization study of the consolidated composite carbon material. It is used extensively in the determination of the Bravais lattice types and unit cell dimensions. X-ray diffraction methods can be classified into two types: spectroscopic and photographic. The spectroscopic technique known as the X-ray powder diffractometry, or simply X-ray diffractometry, is the most widely used diffraction method. Because spectroscopic methods can replace most photographic methods, photographic techniques are not widely used as diffractometry in modern laboratories. However, photographic methods are used to determine unknown crystal structures [199].

In XRD, crystalline solids are bombarded with a collimated x-ray beam which causes crystal plane atoms, serving as diffraction gratings, to diffract x-rays in numerous angles. Each set of crystal planes or Miller indices (hkl) with inter-plane spacing (d_{hkl}) can give rise to diffraction at only one angle. The diffraction angle is defined from Bragg's law (eq.11), where the

intensities of the diffracted x-ray are measured and plotted against the corresponding Bragg angles (2θ) to produce a diffractogram.

$$n\lambda = 2d\sin\theta \tag{11}$$

where:

λ = wavelength of the X-rays

d = spacing of the planes in the crystal

2θ = angle of diffraction

The intensities of the diffraction peaks are proportional to the densities of the abundance of the corresponding crystal facets in the material lattice. Diffractograms are unique for different materials and can therefore qualitatively be used in material identification. For the purpose of this study XRD was used to investigate the crystallinity of the metal oxide nanoparticles synthesized.

2.5.1.4 Attenuated Total Reflection Fourier Transform Infrared (ATRFTIR)

Fourier transform infrared spectroscopy (FTIR) is the most widely used vibrational spectroscopic technique. FTIR is an infrared spectroscopy in which the Fourier transform method is used to obtain an infrared spectrum in a complete range of wave numbers simultaneously. It differs from the dispersive method, which entails creating a spectrum by collecting signals at each wave number separately. Currently, FTIR has almost totally replaced the dispersive method because FTIR has a much higher signal-to-noise ratio than that of dispersive method [199].

An ATR-FTIR operates by measuring the changes that occur in a totally internally reflected infrared beam when it comes into contact with a sample. An infrared beam is directed onto an optically dense crystal with a high refractive index at a certain angle. This internal reflectance creates an evanescent wave that extends beyond the surface of the crystal into the sample held in contact with the crystal. It is easier to think of this evanescent wave as a bubble of infrared that sits on the surface of the crystal and protrudes only a few microns (0.5 μ - 5 μ) beyond the crystal surface and into the sample. Consequently, there must be good contact between the sample and the crystal surface. In regions of the infrared spectrum where the sample absorbs energy, the evanescent wave will be attenuated or altered. The attenuated energy from each evanescent wave is passed back to the IR beam, which then exits at the opposite end of the crystal and is passed to the detector in the IR spectrometer. The system can generate an infrared spectrum.

For the technique to be successful, the following two requirements must be met:

- the sample must be in direct contact with the ATR crystal, because the evanescent wave or bubble only extends beyond the crystal 0.5 μ - 5 μ.
- the refractive index of the crystal must be significantly greater than that of the sample otherwise internal reflectance will not occur and the light will be transmitted rather than internally reflected in the crystal. Typically, ATR crystals have refractive index values between 2.38 and 4.01 at 2000/cm. It is safe to assume that the majority of solids and liquids have much lower refractive indices.

2.5.2 Electrochemical characterization methods

2.5.2.1 Cyclic voltammetry (CV)

Cyclic voltammetry (also called linear scan voltammetry) is an electrochemical technique that is classified under sweep techniques. In cyclic voltammetry, the root of the word voltammetry, "voltam-", refers to both potential ("volt-") and current ("am-"). During the voltammetric experiment some applied potential at a working electrode is varied at some scan rate in both forward and reverse directions while the current is simultaneously monitored. The basic instrumentation for the cyclic voltammetry analysis requires controlled potential equipment (potentiostat) and an electrochemical cell consisting of three electrodes. The analysis is normally carried out using an electrochemical analyser connected to a three electrode cell, containing the working electrode, reference electrode and auxiliary electrode. Figure 5 shows a three electrode cell system.

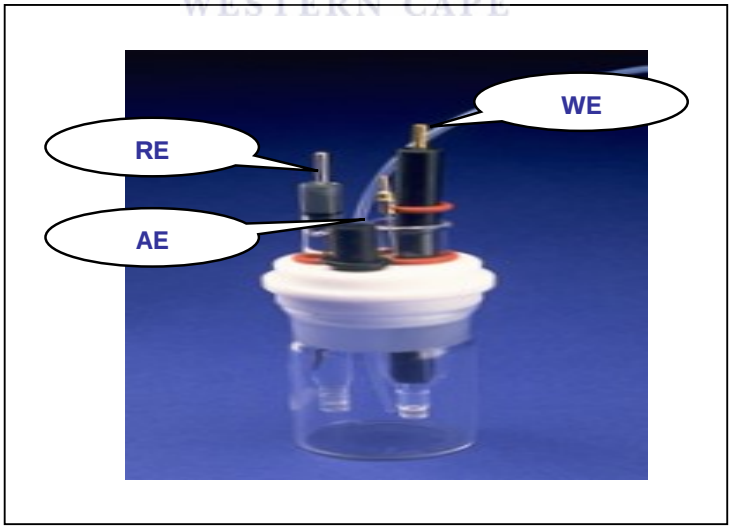

Figure 5: Schematic representation of an electrochemical cell consisting of three electrodes

The electrode where the reaction of interest takes place, is called working electrode. The common materials used for working electrode include platinum, gold and carbon (carbon can be in the form of graphite, glassy carbon, or diamond). These electrodes are generally encased in a rod of inert insulator with a disk exposed at one end and should not be susceptible to oxidation or reduction. In addition, it is very important that material used as a working electrode should not oxidise any ions in solution. The reference electrode provides a stable potential compared to the working electrode. Reference electrodes are used because their potentials are constant. There are different types of reference electrodes and the commonly used ones are the saturated calomel electrode (SCE), and the silver/silver chloride electrode Ag/AgCl. The counter electrode, also called the auxiliary or secondary electrode, can be made with any material which conducts easily and will not react with the bulk solution. The auxiliary electrode is usually made of platinum wire.

In cyclic voltammetry the potential is ramped from an initial potential (E_i) and at the end of its linear sweep, the direction of the potential scan is reversed, usually stopping at the initial potential. The potential may commence with additional cycles. The potential at which the change in direction occurs is also known as the switch potential (E_λ). The scan rate between E_i and E_λ is the same as that between E_λ and E_i and the values of the scan rate $v_{forward}$ and $v_{reverse}$ are always written with positive numbers.

Oxidation usually takes place during the forward part of the CV, if scanned from a negative to a positive potential. The reverse part of the CV will then represent reduction, with the potential running from a positive to a negative potential. However, if the potential is scanned from a positive to a negative value, then reduction would occur during the forward part of the CV scan and oxidation during the reverse CV scan. Important parameters are usually

obtained from cyclic voltammograms for analysis of reversible reaction properties and properties of an electroactive sample. These parameters include anodic and cathodic peak potentials, denoted as E_{pa} and E_{pc}, respectively as well as anodic and cathodic peak currents denoted as I_{pa} and I_{pc}, respectively. A typical cyclic voltammogram illustrating these parameters is shown in Figure 6.

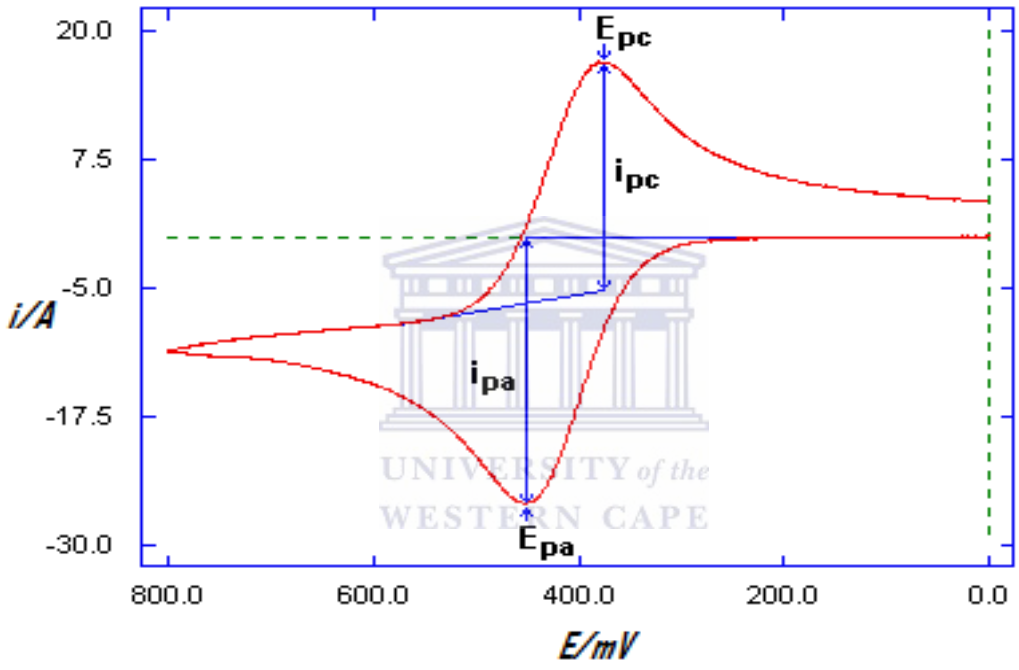

Figure 6: A typical cyclic voltammogram showing the basic peak parameters, E_{pa}, E_{pc}, I_{pa} and I_{pc}

In voltammetry the magnitude of the current is proportional to the concentration of the analyte. Thus the equality in size between I_p(forward) and I_p(reverse) implies a quantitative retrieval of electromodified material, which follows from Faraday's laws [20, 200]. In cyclic voltammetry, the position of both the cathodic and anodic peaks gives us thermodynamic

information of the redox couple used. The anodic and cathodic peak potentials also enable the calculation of the formal electrode potential, $E^{o'}$, as follows:

$$E^{0'} = \frac{E_{pa} + E_{pc}}{2} \qquad (12)$$

The formal electrode potential (normally called the formal potential or the formal redox potential) is in concept similar to the standard electrode potential, E^{θ} [20, 200].

a) Diagnostic criteria to identify a reversible process

To prove reversibility of the system when cyclic voltammetry is performed, the following conditions should be hold:

- the ratio of the currents passed at reduction (I_{pc}) and oxidation (I_{pa}) is near unity ($I_{pa} = I_{pc}$ or $I_{pa} / I_{pc} = 1$)
- the peak potentials (E_{pa} and E_{pc}) is independent of the scan rate, v
- the formal potential is positioned midway between E_{pa} and E_{pc}, so that $E^{o'} = (E_{pa} + E_{pc}) / 2$
- the peak current (I_p) is proportional to $v^{1/2}$
- the separation between the peak potentials E_{pa} and E_{pc} is 59 mV/n for an n-electron couple at 25 ºC or, $|E_{pa}-E_{pc}|$ would be 59 mV for a 1 electron process and 30 mV for a 2 electron process.

Some important information about the sample under investigation can be obtained from the peak parameters. This includes whether the electrochemical process displayed by the sample is reversible, irreversible or quasi-reversible. It also gives insight into how fast the electron transfer process is, relative to other processes such as diffusion [201]. For example, if the electron transfer is fast relative to the diffusion of electroactive species from the bulk solution

to the surface of the electrode, the reaction is said to be electrochemically reversible and the peak separation (ΔE_p) is given by equation 13 below.

$$\Delta E_p = \left| E_{pa} - E_{pc} \right| = 2.30 \frac{RT}{nF} \quad (13)$$

where ΔE_p is the peak separation (V), E_{pa} is the anodic peak potential (V), E_{pc} is the cathodic peak potential (V), n is the number of electrons transferred, F is the Faraday constant (96,485 C mol^{-1}), R is the gas constant (8.314 J mol^{-1} K^{-1}) and T is the absolute temperature (K). Thus, the peak separation can be used to determine the number of electrons transferred, and as a criterion for Nernstian behaviour [202]. This means that for reversible one-electron processes, the peak-to-peak separation assumes different values as a function of the temperature [200]. When the value of ΔE_p is measured, a departure of 10 – 20 mV from the theoretical value, especially at high scan rates, does not compromise the criterion for reversibility. This is due to the fact that the eventual presence of solution resistance, if not adequately compensated by the electrochemical instrumentation, tends to shift the forward/reverse peaks system, thereby increasing the relative value of ΔE_p [20, 200].

The chemical meaning of an electrochemical reversible process suggests that no important structural reorganisation accompanies the redox step. This will also be the case for an electrode process in which the rate of electron transfer is higher than the rate of mass transport.

b) The Randles-Sevčik equation

According to the Randles-Sevčik equation (eqn. 14) below, the magnitude of the peak current, I_p, in a cyclic voltammogram is a function of the temperature (T), bulk concentration (C_0), electrode area (A), the number of electrons transferred (n), the diffusion coefficient (D), and the speed at which the potential is scanned (v), [203]:

$$I_p = 0.4463nFA(nF/RT)^{1/2} D^{1/2}\nu^{1/2}C_0 \quad (14)$$

At 25 ºC the above equation reduce to [203-204]:

$$I_p = 2.686\times10^5 n^{3/2} A^{1/2} D^{1/2}\nu^{1/2}C_0 \quad (15)$$

where A is the electrode area (cm^2) and F, R, and T are as explained in equation 13.

Several voltammograms performed at different scan rates can lead to the preparation of several linear plots whose slopes could give further information about the redox properties of the sample in question. For instance, when the peak current is plotted against the square root of the scan rate, the slope of the linear plot can be used to estimate the diffusion coefficient according to the Randles-Sevčik equation.

The Randles-Sevčik equation is obeyed if a plot of peak current (I_p) against analyte concentration (C_0) yields a straight line. It also means that if the electrolyte composition is constant in terms of temperature, solvent, swamping electrolyte, then the Randles-Sevčik equation can be used to the determine the concentration of analyte by the construction of a suitable calibration curve [20, 204]. Furthermore, when the peak current is plotted against the square root of the scan rate, with I_p as the y-axis and $\nu^{1/2}$ as the x-axis, often called a Randles-Sevčik plot, a straight line should be obtained that passes through the origin, the slope of the linear plot can be used to determine the concentration of the analyte (C_0) if the diffusion coefficient D is known precisely, as shown in Figure 7. In addition, a Randles-Sevčik plot is also the best ways to determine an experimental value of the diffusion coefficient, D, if it is not available in literature, in the case of a reversible reaction [203].

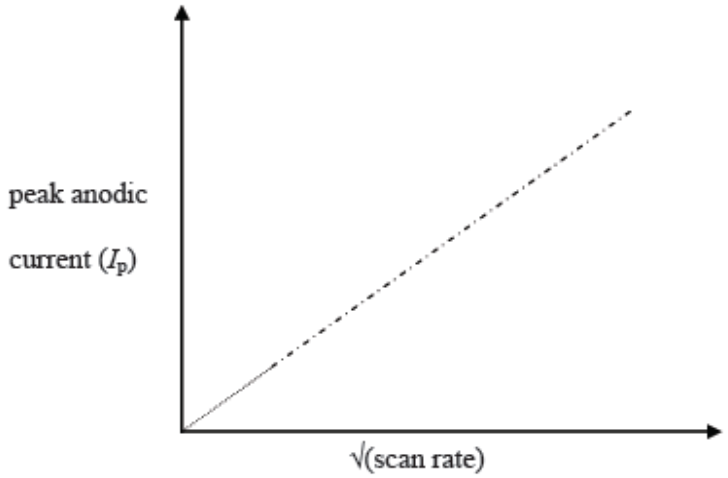

Figure 7: A Randles-Sevčik plot of I_p against $v^{½}$ [20].

From the Randles-Sevčik equation, it is also possible to calculate the other variables listed in equations 14 and 15. That is, if the peak current (I_p) at a certain scan rate (v) is measured, and the area of the electrode (A), the diffusion coefficient (D) and the concentration (C) of the species under study are known, one is able to calculate the number of electrons (n) involved in the redox change. Similarly, if the number of electrons (n) is known, one can calculate the diffusion coefficient (D) of the species, and any of the other variables.

When plotted, the log of peak current versus the log of scan rate gives a linear plot whose slope distinguishes between diffusion controlled peaks, adsorption controlled peaks or even a mixture of the two. When a slope of 0.5 is obtained, we have a diffusion controlled peak and a slope of 1 is for an adsorption peak. Moreover, when an intermediate value of the slope (0.5-1) is obtained, the suggested mechanism is mixed (diffusion-adsorption) [205].

c) Study of adsorption processes

Cyclic voltammetry can also be used for evaluating the interfacial behaviour of electroactive compounds. Both the reactant and the product can be involved in an adsorption –desorption

process. Such interfacial behaviour can occur in studies of numerous organic compounds, as well as of metal complexes (if the ligand is specifically adsorbed) [202]. In some cases, the sample to be characterized may be immobilised onto the surface of a working electrode (chemically modified electrodes). In such a case, the surface concentration (Γ) of the absorbed species could be estimated from a plot of current (I_p) versus scan rate (v) in accordance with the Brown Anson model using the equation [200, 202]:

$$I_p = \frac{n^2 F^2 \Gamma A \nu}{4RT} \tag{16}$$

where Γ is the surface concentration (mol/ cm^2).

During the reduction or adsorption of the adsorbed layer, the quantity of the charge (Q) consumed can also be used to calculate the surface coverage or surface concentration (Γ) [202]:

$$Q = nFA\Gamma \tag{17}$$

where Q is the charge in Coulomb (C) and Γ is a surface coverage in mol/ cm^2

d) Diagnostic criteria to identify an irreversible process

The most important characteristic of a cyclic voltammogram of a totally irreversible system is the total absence of a reverse peak. For totally irreversible systems the peak potential shifts with the scan rate. In addition, the individual peaks are reduced in size and widely separated as shown in Figure 8 (Curve A).

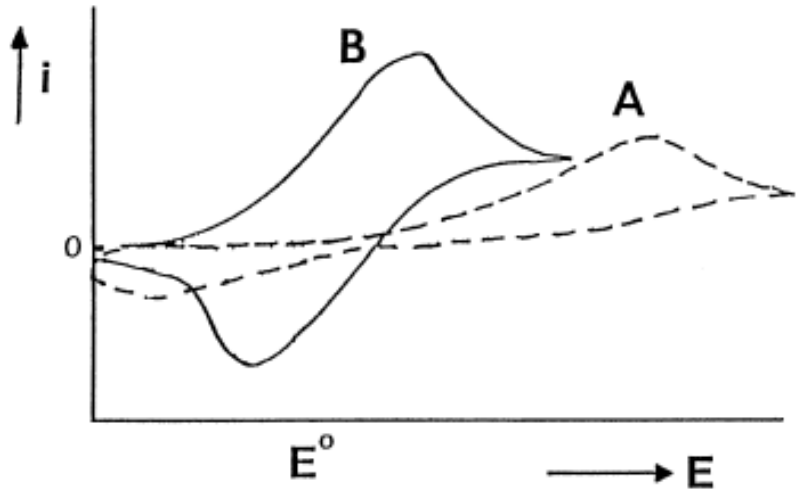

Figure 8: A typical cyclic voltammograms for an irreversible electrochemistry process (Curve A) and for a quasi-reversible process (Curve B) [202].

The following conditions are required to identify whether an electrochemical process is irreversible:

- there is no reverse peak
- the I_{pa} or I_{pc} is proportional to $\nu^{1/2}$
- the value of E_p shifts $-30/\alpha.n$ for each decade increase in v
- $\left|E_p - E_{p/2}\right| = \dfrac{48}{\alpha n} \quad mV$

The dependence of peak potential with scan rate for an irreversible process is expressed in the following equation [202]:

$$E_p = E^{o'} - \frac{RT}{\alpha nF}\left[0.78 - \ln\left(\frac{K^o}{D^{½}}\right) + \ln\left(\frac{\alpha nF\nu}{RT}\right)^{½}\right] \qquad (18)$$

where K^0 is heterogeneous rate constant and α is the transfer coefficient.

Thus, E_p occurs at higher potentials than $E^{0'}$, when the over-potential depends on K^0 and α. In a case where E_p independent of K^0, the shift of the peak potential could be compensated by an appropriate change of the scan rate. Therefore, when αn decreases, the voltammogram could become more drawn out. Equation 18 also allows for the calculation of the heterogeneous rate constant, K^0, if the values of $E^{o'}$ and D are known.

The peak current for an irreversible process is given by:

$$I_p = \left(2.99 \times 10^5\right) n\left(\alpha n\right)^{1/2} A C_0 D^{1/2} \nu^{1/2} \quad (19)$$

For the irreversible process, the peak current (I_p) is proportional to the bulk concentration (C_0) but can be lower in value depending on the value of the transfer coefficient (α).

Assuming that $\alpha = 0.5$, the ratio of reversible-to-irreversible peak current will be 1.27.

The chemical meaning of an irreversible electrochemical process implies that a large activation barrier to the electron transfer takes place causing breakage of the original molecular frame with the formation of new species [20, 200].

e) Diagnostic criteria to identify a quasi-reversible process

A quasi-reversible process refers to one occurring in the transition zone between reversible and irreversible behaviour. A typical cyclic voltammogram for a quasi-reversible process is shown in Figure 8 (Curve B). A quasi-reversible process is characterised by determining either the thermodynamic parameter $E^{o'}$(formal potential) or the kinetic parameters, α (transfer coefficient) and K^0 (rate constant) [20, 200].

For a quasi-reversible system the following conditions should hold:

- $|I_p|$ increases with $v^{1/2}$ but is not proportional to it

- $I_{pa} = I_{pc}$ or $I_{pa} / I_{pc} = 1$ provided $\alpha_c = \alpha_a = 0.5$
- ΔE_p is greater than $59/n$ mV and increases with increasing v
- E_{pc} shifts negatively with increasing v.

The current for quasi-reversible process (with $10^{-1} > K^0 > 10^{-5}$ cm/s) is controlled by both charge transfer and mass transport. In such a case, the shape of the CV is a function of $K^o/\sqrt{\pi aD}$ and $a = nFv/RT$. When the values of $K^o/\sqrt{\pi aD}$ increase, the quasi-reversible process approaches the reversible system and when its values decrease (i.e., at very fast scan rate) an irreversible process behaviour is observed. Compared to reversible system, cyclic voltammograms of a quasi-reversible system are more drawn-out and have a larger peak potential separation [202].

Furthermore, the chemical meaning of a quasi-reversible electrochemical process suggests that some important structural reorganisation accompanies the redox step, but it does not allow the molecular framework to undergo fragmentation [200].

2.5.2.2 Square wave voltammetry (SWV)

Square wave voltammetry is a type of pulse voltammetry that offers the advantage of speed and high sensitivity. An entire voltammogram is obtained in a few seconds or less. In addition, square wave voltammetry (SWV) has proved to be a suitable method to investigate redox reactions with overlapping waves. The excitation signal in SWV consists of a symmetrical square wave pulse of amplitude superimposed on staircase wave form of step height ΔE. The forward pulse coincides with the staircase step. A typical square wave voltammogram is shown in Figure 9 below.

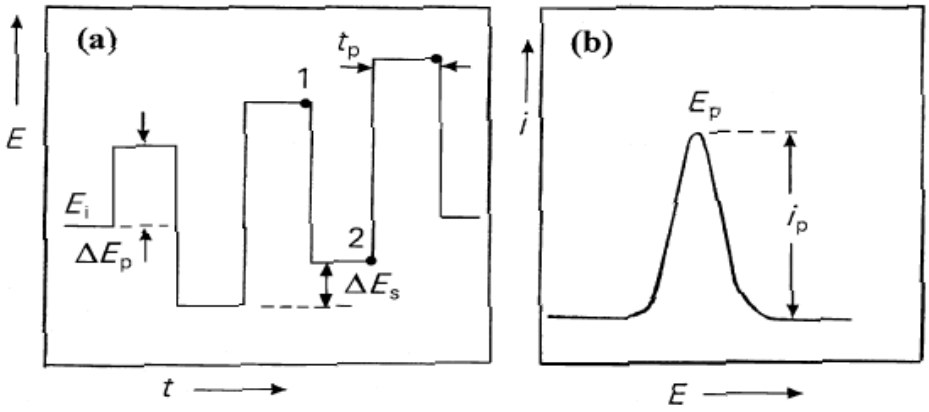

Figure 9: Excitation waveform of square wave voltammetry (Curve a) and response obtained by square wave voltammetry (Curve b).

The net current (I_{net}) is obtained by taking the difference between the forward and the reverse currents (I_{fwd}-I_{rev}) and is centred on the redox potential. In SWV, the peak height is directly proportional to the concentration of the electroactive species. Excellent sensitivity is achieved from the fact that the net current is larger than either the forward or the reverse components, since it is the difference between them and direct detection limit as low as 10^{-8} M are possible.

SWV presents some advantages over cyclic voltammetry. These advantages include excellent sensitivity and rejection of background currents. The scanning speed in SWV is also high and, coupled with computer control and signal averaging experiments, can be performed repetitively with increases in the signal to noise ratio. SWV is also applied in study of electrode kinetics with regard to preceding, following or catalytic homogeneous chemical reactions and determination of some species at trace levels.

2.5.2.3 Chronoamperometry (CA)

Chronoamperometry (CA) is an electrochemical technique in which the potential of the working electrode is stepped and the resulting current occurring at the electrode (caused by the potential step) is monitored as a function of time [206]. Because the experiment is diffusion controlled, after a certain time almost all molecules that are able to reach the electrode are reduced (oxidized). The analysis of CA data is based on the Cottrel equation which defines the current-time dependence for linear diffusion control.

$$I = nFAC_0\sqrt{\frac{D}{\pi t}} \tag{20}$$

where I is the current, n is the number of electrons, F is the Faradays constant, A is the area of the electrode, D is the diffusion coefficient, C_0 is the concentration and t is the time. This equation can be used to calculate the surface area of an electrode or the concentration of analyte in solution.

2.5.2.4 Electrochemical Impedance Spectroscopy (EIS)

Electrochemical impedance spectroscopy (EIS) is an excellent, non-destructive, accurate and rapid in-situ technique for examining processes occurring at electrode surfaces. A small amplitude AC (sinusoidal) excitation signal (potential or current), covering a wide range of frequencies, is applied to the system under investigation and the response (current or voltage or another signal of interest) is measured. This is in contrast to the usual spectroscopic techniques where interactions of electromagnetic waves and materials are measured as shown in scheme 4.

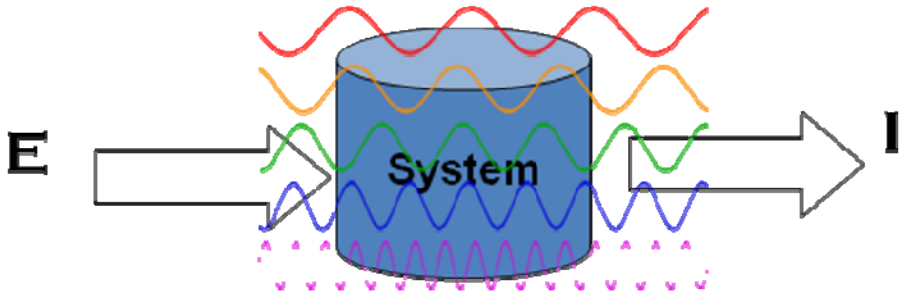

Scheme 4: Schematic of an impedance system.

In the previous techniques, such as cyclic voltammetry or another dynamic electroanalysis, an applied potential is either constant (potentiostatic) or changing (potentiodynamic) when ramped at a constant rate (v) of $V = dE/dt$. However, in impedance, a small perturbing potential is applied across a cell or sample that changes in a cyclic sinusoidal manner and generates a current resulting from the overpotential (η) caused by the difference of the potential from the equilibrium value. Over a time period, the averaged over potential is zero. Because the potential is only perturbing, it has the advantage of minimising the concentration change within the cell or sample after the experiment. The induced current alternates because the voltage changes in a cyclic manner, and hence the term alternating current (AC). The term impedance is therefore a measure of the ability of a circuit to resist the flow of an alternating current (AC). It is synonymous to resistance (R) used in direct current (DC), which is defined by Ohm's law (equation 21) as the ratio between voltage (E) and current (I) [203-204, 206-207]:

$$R = \frac{E}{I} \tag{21}$$

During a controlled-potential electrochemical impedance spectroscopy (EIS) experiment, the electrochemical cell is held at equilibrium at a fixed DC potential, and a small amplitude (5–10 mV) AC wave form is superimposed on the DC potential to generate a response from the

equilibrium position. The response to the applied perturbation, which is generally sinusoidal, can differ in phase and amplitude from the applied signal. This response is measured in terms of the AC impedance or the complex impedance, Z, of the system, which permits analysis of electrode process in relation to diffusion, kinetics, double layer, coupled homogeneous reactions, etc [207].

The ratio of the applied voltage (*E*) to measured current (*I*) is the impedance of the system (*Z* = *E*/*I*). Since an AC potential is applied to the cell, there will probably be a phase shift by an angle (φ) between the applied AC potential waveform and the AC current response. Therefore, the impedance can be represented using a vector diagram (Figure 10) displaying the in-phase and out-of-phase impedances, the total impedance, and the phase angle (φ).

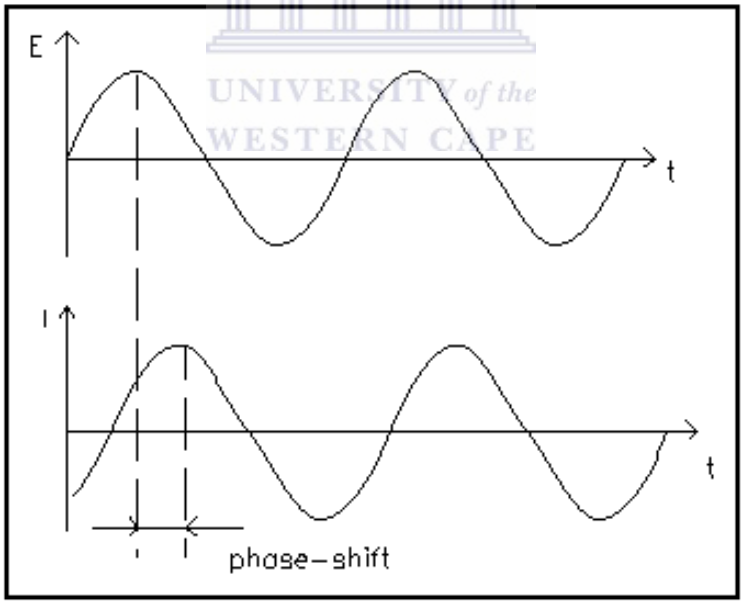

Figure 10: Sinusoidal current response to potential perturbation as a function of time.

Depending on the AC perturbation, the potential and current functions, at a particular frequency could be represented by the equations 22 and 23:

$$E(t) = E_c \sin(\omega t) \tag{22}$$

$$I(t) = I_c \sin(\omega t + \phi) \tag{23}$$

where E(t) is the potential at t, E_c is the amplitude of the signal, ω is the angular frequency (rad/s), also called the pulsation, defined as 2 π f with f being the frequency in Hertz (Hz) and φ is the phase angle between the two signals. I(t) and I_c represent the response current signal and amplitude, respectively.

Since the analysis of impedance spectra involved complex number, the in-phase and out-of-phase impedances are often referred to as real and imaginary impedances [207]. The complex impedance (Z) is made up of a resistive or real part Z', attributable to resistors (in phase with the applied voltage), and a reactive or imaginary part Z'', attributable to the contributions of capacitors (out of phase with the applied voltage by π/2) and /or inductors (out of phase with the applied voltage by -π/2). The impedance is related to the resistance (R), reactance (X) and capacitance (C) by the equation:

$$Z = R - jX \tag{24}$$

where $X = 1/\omega C$ and $\omega = 2\ \pi\ f$, ω is the applied angular frequency in rad/s and f is the frequency measured in Hertz (Hz).

The notation Z denotes the complete impedance, which has two components in terms of real (Z') and imaginary (Z''). They are related by the equation below:

$$Z = Z' - jZ'' \tag{25}$$

where $j = \sqrt{-1}$, and therefore, the term complex impedance can be used.

By considering a pure resistor that does not have any capacitance, its resistance when determined with a continuous current (DC) is R because its impedance is frequency independent. Hence we can write that:

$$Z = Z' = R \tag{26}$$

For an electric circuit or an electrochemical system, the transfer function from the potential (input function) to the current (output function) is called the admittance (Y) of the system [206], which is the inverse of impedance.

$$Y = 1/Z \tag{27}$$

2.5.2.4.1 Graphical representations of EIS

a) The Nyquist diagram

Nyquist plot is a plot of imaginary impedance, Z'', versus real impedance, Z'. The major inconvenience in this plot is that the frequency of each impedance point is not shown. However, frequency at some specific points of interest can be inserted for better interpretation. Nevertheless, even though its data is often poorly resolved, Nyquist plots are still more commonly displayed for historical reasons. A typical Nyquist plot is shown in Figure 11.

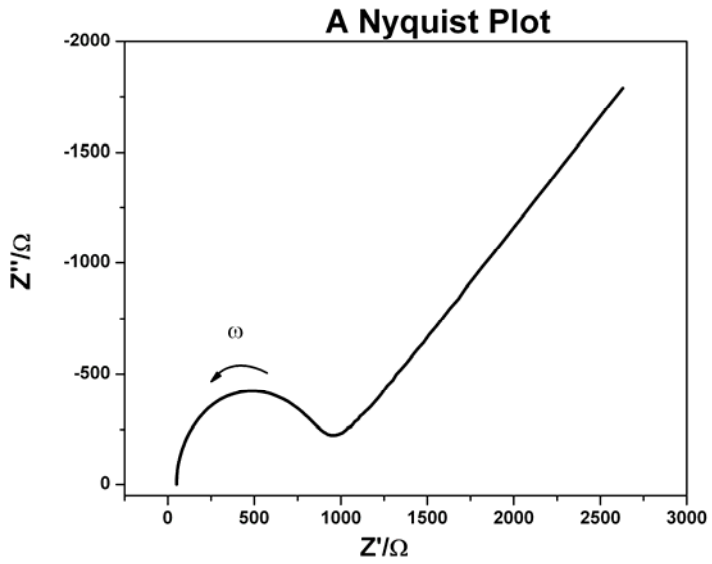

Figure 11: A typical Nyquist plot

The Nyquist diagram then gives a semi-circle going from the point at coordinates (*K*,0) when the angular frequency tends to zero, and finishing at the origin when the angular frequency tends to infinity [206].

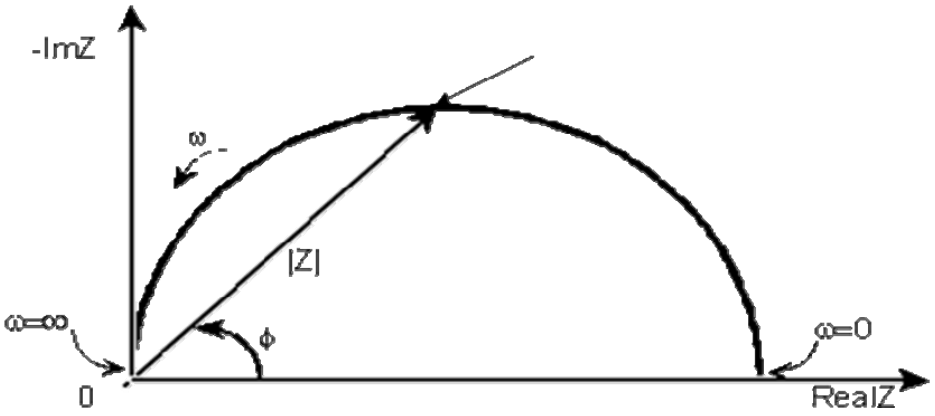

Figure 12: The Nyquist diagram showing how *Z* and ω are defined.

b) The Bode diagram

Another way to represent the impedance data is a bode plot, which is a plot of logarithm of the magnitude of impedance and phase angle versus the logarithm of frequency. The magnitude of impedance $|Z|$ measured in Ohms (Ω), is given by:

$$|Z| = \sqrt{Z'^2 + Z''^2} \tag{28}$$

Compared to a Nyquist plot, a Bode plot directly displays the frequency dependence. Moreover, because a logarithmic frequency scale is used, the data is also well resolved at all frequencies.

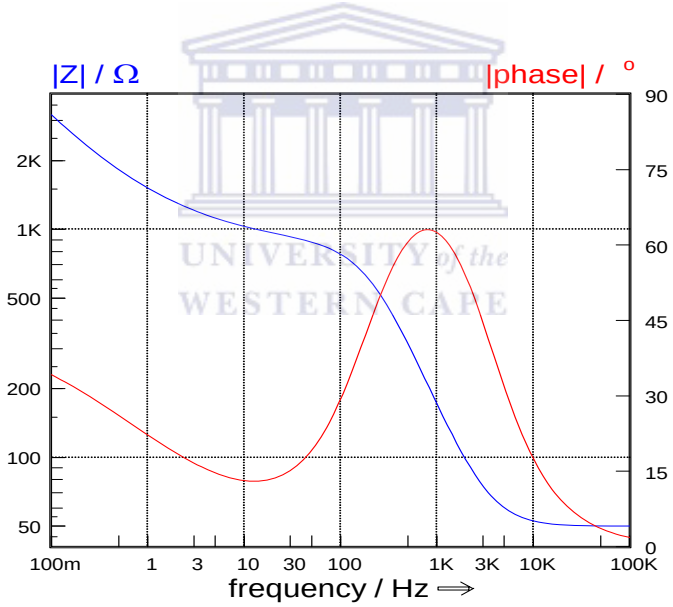

Figure 13: A typical Bode plot

2.5.2.4.2 Electrodes

At minimum two electrodes are needed to measure electrolyte-solution impedance, but usually three are used. The current is measured at the working electrode and is biofunctionalized with the probe. In order to establish a desired voltage between the working electrode and solution, electrical contact must be made with the solution using a reference

electrode and/or counter electrode. The reference electrode maintains a fixed, reproducible electrical potential between the metal contact and the solution allowing a known voltage to be applied. A simple piece of wire-a pseudo reference or quasi reference electrode can be sometimes sufficient [208]. The counter electrode supplies current to the solution to maintain the desired electrode-solution voltage, and is usually in electronic feedback with the reference electrode monitoring the solution voltage.

2.5.2.4.3 Instrumentation in electrochemical impedance spectroscopy

A potentiostat imposes a desired command voltage between the solution and working electrode while simultaneously measuring the current flowing between them. EIS analyzers are potentiostats designed especially for measuring AC impedance and have typical frequency ranges of 10 MHz-100 kHz. The presence of a computer is required to control both potentiostats and EIS analyzers. For the signal amplification and elimination of the background noise, digital post processing is commonly employed.

2.5.2.4.4 Data fitting

The measured impedance data can be used to extract equivalent values of resistances and capacitances if a circuit model is assumed a priori, though there is not a unique model or even necessarily a one-to-one correspondence between circuit elements and the underlying physical processes [208-209]. The common circuit used for impedance data is Randles equivalent circuit, which is composed of different elements such as resistors, capacitors and inductors joined in series and/or in parallel. Figure 14 shows typical Randles circuit. It is not always necessary to fit data to a model, and even the best models of the electrode-solution interface do not always perfectly fit experimental data without relevant fitting parameters. Sometimes the raw impedance is fit to a model and changes in model elements are reported

as the sensor output. Alternatively the impedance at a particular frequency is used. Depending on the values of the respective model circuit parameters, data at a particular frequency can contain information about various circuit elements or be influenced by a single element.

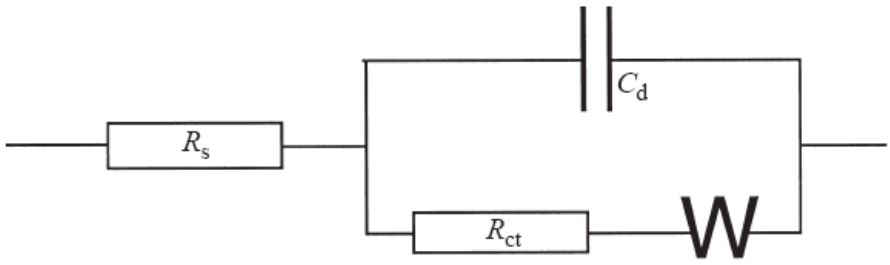

Figure 14: Randles equivalent circuit in series with the solution resistance.

Complex nonlinear least (CNLS) fitting [208, 210] is needed to incorporate both magnitude and phase and is available in several software packages such as LEVM, Z-view or Z-Plot and ZSimpWin. The Kramers-Kronig transform can act as an independent check against invalid experimental data [209].

2.5.2.4.5 Electrical circuit elements

Any electrochemical cell can be represented in terms of an equivalent electrical circuit that comprises a combination of resistances and capacitances. There could also be contribution of inductances at very high frequencies. Contributions to the resistance of a cell are the solution resistance (R_s), the charge transfer resistance (R_{ct}) and Warburg impedance (Z_w) while contribution to the capacitance could be as a capacitor (C) and constant phase element (CPE) [203, 207].

a) Solution resistance (R_s):

The solution resistance is the resistance between the working electrode and the reference electrode. This is indicated as a small offset on the real impedance axis. Its measurement is taken at the high frequency intercept close to the origin of the Nyquist plot. The resistance of an ionic solution depends on the ionic concentration and type of ions present in the electrolyte, temperature and the geometry of the area in which current is carried. In addition, the solution resistance, R_s, arises from the finite conductance of the ions in bulk solution, and thus is not generally affected by binding. In a bound space, with area A and length l, carrying a uniform current the resistance is defined as [207, 211]:

$$R_S = \rho \frac{l}{A} \tag{29}$$

where ρ is the solution resistivity. The reciprocal of ρ, called conductivity of the solution, k, is more frequently used to calculate the solution resistance. The relationship between conductivity of the solution and solution resistance is given by:

$$R_S = \frac{1}{k}\frac{l}{A} \tag{30}$$

$$k = \frac{l}{RA} \tag{31}$$

The units for k are siemens per meter (S/m). The siemens is the reciprocal of the ohm, (1 S = 1/ohm).

b) Charge transfer resistance (R_{ct}):

The charge transfer resistance is the resistance associated with the charge transfer mechanisms for electrode reactions. It is the resistance to electron transfer at the electrode interface. The charge transfer resistance (R_{ct}) is a manifestation of two effects (1) the energy

potential associated with the oxidation or reduction event at the electrode (i.e. the overpotential) and (2) the energy barrier of the redox species reaching the electrode due to electrostatic repulsion or steric hindrance [208]. It can be deduced from the kinetically controlled electrochemical reaction at low over-potentials. From the Buttler-Volmer equation which is the principal equation of electrochemical kinetics [206] (equation 32), the current (I) from the oxidation and reduction reactions is:

$$I = I_0\left[e^{\alpha nF\eta/RT} - e^{-(1-\alpha)nF\eta/RT}\right] \tag{32}$$

When $nF\eta/RT$ is well below unity, the linearization of the Butler-Volmer equation (32) is necessary to obtain:

$$I = I_0 nF\eta/RT \tag{33}$$

By analogy with Ohm's law [206], and when the over-potential, η, is very small and the electrochemical system is at equilibrium, the equation below is called charge transfer resistance.

$$R_{ct} = \frac{RT}{nFI_0} \tag{34}$$

where I_0 is the exchange current in Amperes (A) and R_{ct} is charge transfer resistance in ohms (Ω). Thus, the charge transfer impedance is equal to charge transfer resistance, given by the equation below:

$$Z_{R_{ct}} = R_{ct} = \frac{RT}{nFI_0} \tag{35}$$

From this equation the exchange current (I_o) can be calculated when R_{ct} is known. The charge transfer resistance (or charge transfer impedance) is estimated from the diameter of the semicircular region on the real impedance axis of the Nyquist plot. When the chemical system is kinetically sluggish, the R_{ct} will be very large and may display a limited frequency

region where mass transfer is a significant factor. However, if the system is kinetically facile, and the mass transfer always plays a role, the semicircular region is not well formed [204, 207].

c) Warburg impedance (Z_W):

This is the resistance associated with the diffusion of ions across the electrode/electrolyte interface. This impedance is associated with the difficulty of mass transport of electroactive species[207]. Layers of ions at the electrode interface behave like an RC element (i.e. a resistor and a capacitor in parallel) and this produces an infinite sum of RC elements called the Warburg impedance. The Warburg impedance (Z_w), only of physical importance in Faradaic EIS, represents the delay arising from diffusion of the electroactive species to the electrode [204, 208-209]. It is only appreciable at low frequencies and is affected by convection. It is characterised as a linear portion at an angle of 45°, and its Nyquist plot is a straight line with a slope of unity and its Bode plot is straight line having a slope of -0.5 on the Bode plot [203, 206]. The equation for the infinite Warburg impedance is given by [206, 211]:

$$Z_w = \frac{\sigma(1-j)}{\sqrt{\omega}} \tag{36}$$

With σ, the Warburg coefficient defined as:

$$\sigma = \frac{RT}{n^2F^2A\sqrt{2}}\left[\frac{1}{C_R\sqrt{D_R}} + \frac{1}{C_O\sqrt{D_O}}\right] \tag{37}$$

in which, ω is a radial frequency, D_O is the diffusion coefficient of the oxidant, D_R is the diffusion coefficient of the reductant, A is the surface area of the electrode, n is the number of electrons involved, C_O is the concentration of oxidant at the electrode surface, C_R is the concentration of reductant at the electrode surface, F is the Faradays constant, T is the temperature and R is the gas constant.

d) Capacitor (*C*):

The capacitance (*C*) is defined as the ability of an electrochemical system to store or retain charge [203]. An electrical double layer exists on the interface between an electrode and its surrounding electrolyte. This double layer is formed as ions from the solution "stick on" the electrode surface. The potential at the terminals of this double layer (capacitor) is proportional to its charge. The impedance of a capacitor is given by the following equation:

$$Z_{(c)} = Z'' = 1/j\omega C \tag{38}$$

e) Constant phase element (CPE):

The Constant Phase Element (CPE) is a non-intuitive circuit element that was discovered (or invented) while looking at the response of real-world systems. A constant phase element is also an equivalent electrical circuit component that models the behaviour of a double layer, which is an imperfect capacitor. In some systems the Nyquist plot was expected to be a semicircle with the center on the x-axis. However, the observed plot could certainly be the arc of a circle, but with the center some distance below the x-axis. These depressed semicircles have been explained by a number of phenomena, depending on the nature of the system being investigated. However, the common thread among these explanations is that some property of the system is not homogeneous or that there is some distribution (dispersion) of the value of some physical property of the system. The impedance of a CPE is represented by equation:

$$Z_{\mathrm{CPE}} = 1/Z = Y = Q_{\mathrm{o}}(j\omega)^{\mathrm{n}} \tag{39}$$

with $Q_0 = 1/|Z|$ at $\omega = 1$ rad/s

The constant phase element is independent of the frequency and its value is always - (90*n)°, with n from 0 to 1. When n = 1, CPE is an ideal capacitor and its impedance has the same equation as that for the impedance of a capacitor, where Q_0 =C:

$$Z_{CPE} = \frac{1}{j\omega Q_o} = \frac{1}{j\omega C} \quad (40)$$

when n = 0, CPE is a pure resistor.

2.5.2.4.6 Double layer capacitance

The electrical double layer is the array of charged particles and/or oriented dipoles that exists at all materials interface. In electrochemistry, double layer reflects the ionic zones formed in the solution to compensate for the excess of charge on the electrode [202].

When an electrode is polarized relative to the solution, it attracts ions of opposite charge. This tendency is countered by the randomizing thermal motion of the ions, but resulting in a local build-up of excess ions of opposite charge. Thus, any electric field arising at the electrode or within ionic solution decays exponentially because the excess ions screen the field. The characteristic length of this decay or Debye length is proportional to the square root of ion concentration [204, 208] (about 1 nm for biological ionic strengths). This effect creates a capacitance called double layer capacitance or diffuse layer capacitance. Ions adsorbed at bare electrodes increase the capacitance in accordance with the Gouy- Chapman-Stern model [204]. The double layer capacitance depends on the voltage because an increase in the electrode voltage attracts the diffuse ion layer, therefore increasing capacitance [204]. If an insulator (e.g. an insulating probe layer) covers the electrode, forming a capacitance, the double layer capacitance appears in series with it. Thus, measurement of the double layer capacitance can provide valuable insights into adsorption and desorption processes, as well as into the structure of the film-modified electrodes [202].

2.6 Chemical sensors

Chemical sensors are devices that convert chemical information (concentration, activity or partial pressure of the analyte) into a measurable signal [187]. Any chemical sensor contains two basic components: a receptor which is a chemical recognition unit and a transducer. Chemical sensors function on the interaction of a receptor with the analyte and transformation of chemical information into a form of energy that will be later converted by the transducer into a useful analytical signal. Chemical sensors can be classified into various groups according to the operating principle of the transducer. On the basis of the transducing element, they are categorized as electrochemical sensors, optical sensors, piezoelectric sensors and thermal sensors. Among all chemical sensors, electrochemical sensors present an important subclass in which an electrode is used as a transducer.

2.6.1 Electrochemical sensors

Electrochemical sensors are chemical sensors in which the chemical information is transduced into an electrical signal.

2.6.1.1 Principle of electrochemical sensors

Electrochemistry implies the transfer of charge from an electrode to another phase, which can be a solid or a liquid sample. During this process chemical changes take place at the electrodes and the charge is conducted through the bulk of the sample phase. Both the electrode reactions and/or the charge transport can be modulated chemically and serve as the basis of the sensing process [212]. On the basis of electrical signal which is recorded, electrochemistry can be divided into amperometric sensors, potentiometric sensors and conductimetric sensors. The structure of electrochemical sensors is shown in Scheme 5.

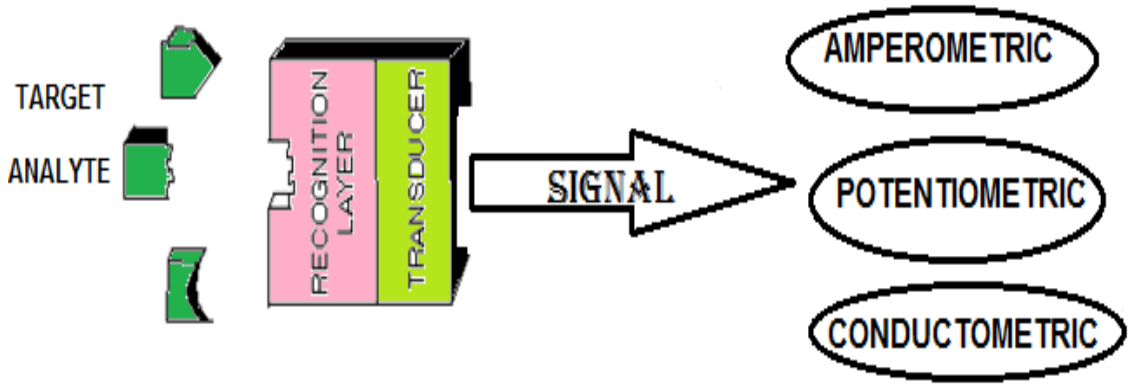

Scheme 5: Schematic representation of an electrochemical sensor.

2.6.1.2 Potentiometric sensors

In potentiometric sensors, the analytical information is obtained by converting the recognition process into a potential signal, which is proportional (in a logarithmic manner) to the concentration (activity) of species generated or consumed in the recognition event [213]. In such a device, use of reference electrode is required to provide a constant half-cell potential. The change in the potential is related to the concentration of the analyte in a logarithmic manner. Thus, the Nernst equation relates the potential difference at the interface to the activities of species i in sample phases (s) and the electrode phase (β) and is given by [212]:

$$E = E_0 + \frac{RT}{Z_i} \ln \frac{a_i^s}{a_i^\beta} \tag{41}$$

where E_0 is the standard electrode potential of the sensor electrode; a_i is the activity of the ion, R is the universal gas constant; T is the absolute temperature; F is the Faraday constant and Z_i is the valency of the ion. The ion-selective electrode (ISE) for the measurement of electrolytes and for obtaining the potential signal, is a common potentiometric sensor [212-213].

2.6.1.3 Amperometric sensors

Amperometry is a method of electrochemical analysis in which the signal of interest is a current that is linearly dependent upon the concentration of the analyte [213]. Amperometric sensors are based on the detection of electroactive species involved in the chemical or biological recognition process [212]. The signal transduction process is obtained by applying the potential to the working electrode at a constant value of a reference electrode and monitoring the current as a function of time. That applied potential serves as the driving force for the electron transfer reaction of the electroactive species. The resulting current is a reflection of the rate of the recognition event, and is proportional to the concentration of the target analyte, because it is a direct measure of the rate of the electron transfer reaction. In redox reactions at the working electrodes, electrons are moving from the analyte to the electrode or to the analyte from the electrode. The direction of flow of electrons can depend upon the properties of the analyte as long as it can be controlled by the electric potential applied to the working electrode [212]. An amperometric cell consists of two or three electrodes, which are working electrode, reference electrode and the counter (or auxiliary).

2.6.1.4 Conductometric sensors

Conductometric sensors are based on the measurement of electrolyte conductivity, which varies when the cell is exposed to different environments. The sensing effect is based on the change in of the number of mobile charge carriers in the electrolyte. If the electrodes are prevented from polarizing, the electrolyte shows ohmic behaviour. Conductivity measurements are generally performed with AC supply. Conductivity is a linear function of the ion concentration; therefore, it can be used for sensor applications. However, it is nonspecific for a given ion type. On the other hand, both the polarization and the limiting current operation mode must be avoided. Thus, small amplitude alternating bias is used for

the measurements with frequencies where the capacitive coupling is not determining the impedance measurement.

2.6.2 Application of nanoparticles in electrochemical sensors and biosensors

Various nanoparticles, such as metal nanoparticles, oxide nanoparticles, semiconductor nanoparticles, and even composite nanoparticles, have been widely used in electrochemical sensors and biosensors. Because of their unique properties, such nanoparticles play diverse role in electrochemical sensing. Thus, their main basic functions can be classified as: 1) immobilization of biomolecules; 2) catalysis of electrochemical reactions; 3) enhancement of electron transfer; 4) labelling biomolecules and 5) acting as reactant.

2.6.2.1 Immobilization of biomolecules

In the construction of a biosensor by immobilization of biomolecules, nanoparticles play a very important role due to their large specific surface area as well their high surface free energy by strongly adsorbing to biomolecules. It is well known that, the adsorption of biomolecules directly onto bare electrodes can often result in the denaturation of the biomolecules as well a loss in their bioactivity. However, the adsorption of such biomolecules onto the surfaces of nanoparticles help retain their bioactivity because of the biocompatibility of nanoparticles [214]. Biomolecules with various charges can be electrostatically adsorbed by nanoparticles since most of them carry charges. Besides the common electrostatic interaction, some nanoparticles can also immobilize biomolecules by other interactions [214]. For example, it is reported that gold nanoparticles can immobilize proteins through the covalent bonds formed between the gold atoms and the amine groups and cysteine residues of proteins [214]. The use of some nanoparticles in the immobilization of biomolecules can effectively increase the stability and maintain the activity of

biomolecules, which is a good option for biomolecular immobilization. However, the method presents also some weaknesses including the instability of some nanoparticles as well their tendency to aggregate. The resolution to problems lies in the choice of good technique combined with suitable immobilization methods.

Nanoparticles can also be used to immobilize other materials besides biomolecules to develop electrochemical sensors. Related works can be found in the publications of Willner's group [215-216].

Several works have been reported in the immobilization of enzymes with nanoparticles. In the early 1990s, Crumbliss *et al*. [217] immobilized several kinds of enzymes with gold nanoparticles and further fabricated different enzyme electrodes, and it was found that the prepared enzyme electrodes retained enzymatic activity. Many studies have been reported for the construction of biosensors based on the immobilization of different proteins with gold nanoparticles, such as horseradish peroxidise [218-219], microperoxidase-11 [220], tyrosinase [221] and haemoglobin [222]. Because of their good biocompatibility, SiO_2 nanoparticles have been also used for enzyme immobilization. Hu *et al*. immobilized several heme proteins with SiO_2 nanoparticles through the layer-by-layer assembly [223], and investigated the driving forces for the assembly procedure [224].

Electrochemical immunosensors based on the immobilization of an antigen or antibody with nanoparticles have also been extensively studied [214]. Yuan *et al*. [225] developed a reagentless amperometric immunosensor based on the immobilization of a 1-fetoprotein antibody onto gold nanoparticles, and the immunosensor exhibited good long-term stability. They also prepared a label-free immunosensor for Japanese B encephalitis vaccine [226] through the immobilization of related antibody with gold nanoparticles. In addition to the

most commonly used gold nanoparticles, other nanoparticles such as silver [227] and silica [228] have also been used for the immobilization of antibodies and antigens.

DNA, another type of biomolecule, can also be immobilized with nanoparticles and used for the construction of electrochemical DNA sensors. In order to immobilize DNA onto the surfaces of nanoparticles, the DNA strands are often modified with special functional groups that can interact strongly with certain nanoparticles. Fang and co-workers [229] immobilized the oligonucleotide with a mercaptohexyl group at the 5'-phosphate end onto 16 nm diameter gold nanoparticles, which were self-assembled on a cysteamine-modified gold electrode, and discovered that the saturated immobilization quantities of single-strand DNA on the modified electrode were about 10 times larger than that on a bare gold electrode.

2.6.2.2 Catalysis of electrochemical reactions

The use of nanoparticles with catalytic properties in electrochemical sensors and biosensors can decrease overpotentials of many analytically important electrochemical reactions, and in some cases improve the reversibility of some redox reactions, which are irreversible at unmodified electrodes [214]. For example, a sensitive NO microsensor was developed through the modification of a platinum microelectrode with gold nanoparticles in which the nanoparticles catalyze the electrochemical oxidation of NO with an overpotential decrease of about 250 mV [230]. The catalytic oxidation of NO was also obtained at a dense gold nanoparticle film modified electrodes [231]. Ohsaka and co-workers [232], based on the selective catalysis of gold nanoparticles on the oxidation of ascorbic acid, developed an electrochemical sensor for the selective detection of dopamine in the presence of ascorbic acid, and resulted in the decrease of the oxidation overpotential of ascorbic acid and the

effective separation of the oxidation potentials of ascorbic acid and dopamine, thus allowing the selective electrochemical detection.

Another type of nanoparticle that exhibit good catalytic properties is platinum nanoparticles, which have been used in electrochemical analysis. Niwa *et al*. [233] prepared a highly sensitive H_2O_2 sensor by modifying a carbon film electrode with platinum nanoparticles. The modified electrode exhibited sensitive response to H_2O_2, due to the catalytic oxidation of H_2O_2 by platinum nanoparticles. The H_2O_2 oxidation peak potential at that modified electrode was about 170 mV lower than that of the unmodified platinum electrode. Later on, by replacing platinum nanoparticles with Ni nanoparticles, the same group developed an electrochemical sensor for sugar determination [234]. The results proved that a graphite-like carbon film electrode containing 0.8% highly dispersed Ni nanoparticles had excellent electrocatalytic ability with regard to the electrooxidation of sugars, such as glucose, fructose, sucrose and lactose. In addition, the modified electrode exhibited a high oxidation peak current for the detection of sugars at comparatively low applied potentials, and the detection limits obtained were at least one order of magnitude lower, compared with the Ni-bulk electrode. Electrochemical sensors based on the catalytic properties of other metal nanoparticles have also been reported. For instance, copper nanoparticles was applied in amino acid detection [235].

Some non metal nanoparticles have been also used in electrochemical analysis systems because of their special catalytic properties. For example, a carbon paste electrode doped with copper oxide nanoparticles was developed for the detection of amikacin based on the catalytic properties of the copper oxide nanoparticles [236]. The oxidation current of amikacin at the prepared electrode was about 40 times higher than that at a bulk copper oxide

modified carbon paste electrode. Recently, Torresi *et al*. [237] reported the application of Prussian Blue nanoparticles with size of about 5 nm were immobilized onto ITO electrodes through the layer-by-layer technique, with the resulting electrodes exhibiting sensitive responses to H_2O_2 (103.5 mA/mM cm^2 for the electrode containing 15 bilayers) due to the catalytic reduction of H_2O_2 by the Prussian Blue nanoparticles.

2.6.2.3 Enhancement of electron transfer

When the electron transfer between electrodes and the active centres of enzymes are blocked because of bad direct electrical communication due to certain factors such as insulation, the conductivity properties of nanoparticles is useful for enhancing the electron transfer by acting as electron transfer mediators or electrical wires [214]. In fact, the arrangement between nanoparticles and biomolecules is another factor that contributes to the effective enhancement of electron transfer. Thus, synthesis of well defined and ordered nanoparticles is necessary to the construction of biosensors with greatly enhanced electron transfer properties. Metal nanoparticles, because of their good conductivity, are commonly used for suitable enhancement of electron transfer between electrodes and enzymes.

The work of Willner's group [238] is a well-known example concerning the enhancement of electron transfer between enzyme and electrode using nanoparticles. In this work, 1.4 nm gold nanoparticles were functionalized with N^6-(2-aminoethyl)-flavin adenine dinucleotide, reconstituted with apo-glucose oxidase and assembled on a thiolated monolayer associated with a gold electrode. The resulting enzyme electrode exhibited very fast electron transfer between the enzyme redox centre and the electrode with the gold nanoparticles as a mediator, and the electron transfer rate constant was found to be about seven times larger than that between glucose oxidase and its natural substrate, oxygen. Another example with gold

nanoparticles was done by Wang *et al*. [239], in which a gold electrode was modified with self assembled gold nanoparticles onto a three-dimensional silica gel network, and the direct electrochemistry of cytochrome c was obtained. In this case, these gold nanoparticles acted as a bridge to electron transfer between the protein and the electrode.

Silver nanoparticles, have also been used by Li *et al*. [240] to enhance the electron transfer between cytochrome c and electrode. Cytochrome c was immobilized on assembled silver nanoparticles onto pyrolytic graphite electrodes. It was reported that the silver nanoparticles act as the electrical bridge and enhances the electron transfer between cytochrome c and the electrode.

Metal oxide nanoparticles such as Fe_3O_4 [241] and MnO_2 [242], have been used to immobilize proteins and enhance their direct electrochemistry. Other metal oxide nanoparticles have been also used for the purpose. For instance, horseradish peroxidase was mixed with TiO_2 nanoparticles and immobilized onto pyrolytic graphite electrodes, which resulted in direct electron transfer [243]. Hemoglobin immobilized with ZrO_2 nanoparticles also exhibited direct electrochemistry at pyrolytic graphite electrodes and could be used for constructing mediator-free biosensors [244].

The use of semiconductor nanoparticles for the enhancement of electron transfer between redox proteins and electrode surfaces has also been reported [245]. For example, hemoglobin and CdS nanoparticles were mixed and immobilized onto pyrolytic graphite electrodes, and the immobilized hemoglobin exhibited direct electrochemistry.

2.6.2.4 Labeling biomolecules

The labeling of biomolecules, such as antigens, antibodies and DNA with nanoparticles plays an increasingly important role in developing sensitive electrochemical biosensors. Such labeling of biomolecules with nanoparticles help the biological entities retain their bioactivity as well as interact with their counterparts, and help in the determination of analyte concentration based on the electrochemical detection of the nanoparticles. Metal and semiconductor nanoparticles are most used to label biomolecules, and stripping voltammetry represents a major technique for measuring the dissolved ions because stripping voltammetry is a very powerful electrochemical analytical technique for trace metal measurements [246].

Among all the metal nanoparticles, gold nanoparticles are the most frequently used in both immunosensors and DNA sensors labeling. For example, Limoges's group [247] has reported a sensitive electrochemical immunosensor for goat immunoglobulin G based on a gold nanoparticle label. The primary donkey anti-goat immunoglobulin G was immobilized on a microwell surface and interacted with the goat immunoglobulin G to be determined, and then gold nanoparticle- labeled donkey anti-goat immunoglobulin G was added to conjugate with the analyte. The solubilized gold ions were electrochemically reduced and accumulated on carbon screen-printed electrode using anodic stripping voltammetry for the detection. Based on a similar electrochemical method, Limoges *et al*. [248] developed a sensitive DNA- sensor based on the labeling of oligonucleotide with 20 nm gold nanoparticles. The sensor could detect the 406-base human cytomegalovirus DNA sequence at a concentration of 5 pM.

Silver nanoparticles and certain core-shell metal nanoparticles have also been reported in the labeling of biomolecules. An electrochemical DNA biosensor based on a silver nanoparticle label was able to detect the target oligonucleotides at levels as low as 0.5 pM [249]. Fang *et al*. [250] labeled 5'-alkanethiol capped oligonucleotide probes with gold-coated copper core-

shell nanoparticles, and developed an electrochemical DNA sensor based on the indirect determination of solubilized Cu^{2+} ions by anodic stripping voltammetry. Similarly, Wang *et al*. [251] described a method for monitoring DNA hybridization based on electrochemical stripping detection of an iron tracer by labeling the DNA probe with gold coated iron core-shell nanoparticles. The iron-containing nanoparticles were first dissolved followed by hybridization of the DNA, and the released iron ions were determined by cathodic stripping voltammetry in the presence of the 1-nitroso-2- naphthol ligands and a bromate catalyst.

Recently, semiconductor nanoparticles have been extensively used as labels in electrochemical biosensors, especially DNA sensors [252]. For example, thiolated oligonucleotides labeled with CdS semiconductor nanoparticles were employed as tags for the detection of DNA hybridization events [253]. Dissolution of the CdS nanoparticles with 1 M nitric acid, and the chronopotentiometric stripping measurements of the dissolved Cd^{2+} ions with a mercury-film electrode provided the electrical signal for the DNA analysis. Using a similar principle, Wang *et al*. [254] developed a method for the simultaneous analysis of different DNA targets by Stripping voltammetry. Three different nucleic acids were immobilized on three different kinds of magnetic particles and hybridized with different DNA targets. DNA probes labeled with different semiconductor nanoparticles, such as ZnS, CdS and PbS nanoparticles, were added and hybridized with their complementary DNA targets.

Oxide nanoparticles can also be used as labels for biomolecules. Fang and co-workers [255] have reported the application of tris (2, 2'-bipyridyl) cobalt (III) [$Co(bpy)_3^{3+}$]-doped SiO_2 nanoparticles as oligonucleotide labels for electrochemical detection of DNA hybridization on a glassy carbon electrode by differential pulse voltammetry.

2.6.2.5 Nanoparticles acting as reactant

Due to their high surface energy, nanoparticles are chemically more active than the related bulk materials. The application of this special reactivity of nanoparticles in electrochemical sensors and biosensors has not been extensively studied, and more attention should be paid to this field [214]. Among all nanoparticle materials, MnO_2 with unique reactive properties was the most used. Besides MnO_2, other nanoparticles with similar properties such as PbO_2 and CeO_2 could also be used to construct electrochemical sensors and biosensors. For example, it is well known that bulk MnO_2 can catalyze the decomposition of H_2O_2, while MnO_2 nanoparticles can react with H_2O_2 directly [256]. Therefore, the active properties and special reactivity of the metal nanoparticles present an advantage for the construction of novel electrochemical sensors and biosensors.

Based on the special reactivity of MnO_2 nanoparticles, Chen's group [256] has developed a biosensor in which glucose oxidase and MnO_2 nanoparticles were co-immobilized on the gate of an ion-sensitive field effect transistor (ISFET), with the resulting glucose biosensor showing a significant pH increase at the sensitive membrane with increasing glucose concentration. This is essentially different from the pH changes of conventional ISFET-based glucose biosensors. Using a similar response mechanism to Chen's group, a sensitive biosensor for lactate was later developed based on the layer-by- layer assembly of MnO_2 nanoparticles and lactate oxidase on an ISFET [257]. Its response to lactate was about 50 times higher than that of the biosensor without MnO_2 nanoparticles.

Reaction between MnO_2 nanoparticles and ascorbic acid was also used to construct a sensitive ISFET-based ascorbic acid sensor [258]. MnO_2 nanoparticles were simply deposited on the gate of an ISFET, where the latter's reaction with ascorbic acid produced hydroxyl

ions, related to the concentration of ascorbic acid that could be monitored by the ISFET. The obtained sensor was more stable and sensitive than the enzyme-based ISFET sensor, and it could be easily prepared and renewed. In addition, the reaction of MnO_2 nanoparticles with ascorbic acid has also been used to eliminate interference in a glucose biosensor [259]. A chitosan film containing MnO_2 nanoparticles was introduced on the surface of an amperometric glucose biosensor, and the MnO_2 nanoparticles could effectively oxidize ascorbic acid to an electrochemically inactive product before it reached the electrode surface.

2.7 Cyclodextrins (CDs)

2.7.1 History of cyclodextrins

Cyclodextrins (CDs) were first described by Villiers in 1891[260]. About 15 years later, an Austrian microbiologist, Franz Schardinger [261-262], laid the foundation of the cyclodextrin chemistry in 1903-1911 and identified both alpha- and beta-cyclodextrin. In the 1930s, Freudenberg identified gamma-cyclodextrin and suggested that larger cyclodextrins could exist. Freudenberg and co-workers [263] showed that cyclodextrins were cyclic oligosaccharides formed by glucose units. However, they were not widely used until after the 1950s, when French and co-workers modified the chemical process for the production of CDs [264] and somewhat later Cramer and co-workers [263] described their ability to form inclusion complexes. However, the availability of cyclodextrins and high production costs greatly limited their research and application until the 1970s [265-266]. The advancement of biotechnology has resulted in dramatic improvements in cyclodextrin production, which has lowered their production costs, leading to the availability of highly purified cyclodextrins and cyclodextrin derivatives at relatively inexpensive cost [267].

2.7.2 Chemical structure, property and complexation phenomenon of cyclodextrins

A cyclodextrin (CD) is a cyclic oligomer of α-D-glucose formed by the action of certain enzymes on starch [268]. CDs are generally crystalline, water-soluble, cyclic, homogeneous, non-reducing, and belong to the family of cyclic oligosaccharides formed by various D-glucopyranose units. The three major CDs are α-cyclodextrin (Schardinger's α-dextrin, cyclomaltohexaose, cyclohexaglucan, cyclohexaamylose, α-CD) comprised of six glucopyranose units, β-cyclodextrin (Schardinger's β-dextrin, cyclomaltoheptaose, cycloheptaglucan, cycloheptaamylose, β-CD) comprised of seven units and γ-cyclodextrin (Schardinger's γ-dextrin, cyclomaltooctaose, cyclooctaglucan, cyclooctaamylose, γ-CD) comprised of eight such units (Figure 15). Maestre *et al*.,2007 [269] studied complexation phenomenon of CDs containing more than eight glucopyranose units.

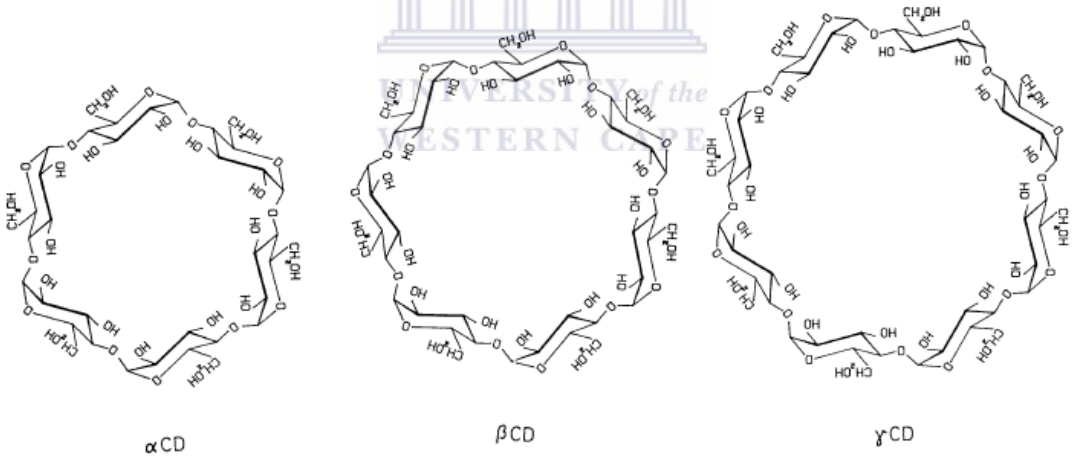

Figure 15: Chemical structure of α-, β- and γ-CDs.

The most important property of CDs is their ability to form inclusion complexes with many appropriately sized organic and inorganic ions and molecules in aqueous, non-aqueous and mixed media [270]. The host-guest complex formed results by entrapping hydrophobic guest molecules into their cavity without the formation of any chemical bonds thereby neither

changing the structure of the host or guest. This complexation ability is due to the chemical structure of CDs and the glucopyranose units' conformation. The glucopyranose units in cyclodextrin molecules are in the chair conformation. Therefore, the hydroxyl functional groups are orientated to the cone exterior with the primary hydroxyl groups of the sugar residues at the narrow and wider edges, giving it a hydrophilic outer surface. The central cavity is formed by the skeletal carbons and ethereal oxygens of glucose residues, which gives the CD molecule a comparatively hydrophobic inner cavity. The polarity of this cavity has been estimated to be similar to that of an aqueous ethanolic or methanolic solution [271]. The main driving forces for complexation are weak Van der Waals forces, hydrogen bonds, and hydrophobic interactions that keep the complex together. Therefore, the complexation process can be considered as a replacement of water molecules with guest molecules.

Generally, in an aqueous solution, the cyclodextrin cavity which is slightly apolar, is occupied by water molecules that are energetically unfavourable (polar-apolar interaction). Therefore, the water molecules inside the cavity have fewer tendencies to form hydrogen bonds in the same way as in solution and result in a higher enthalpy and energy. When hydrophobic guest molecules are incorporated into the cavity of the cyclodextrin, the energy of the system is lowered by substituting these enthalpy-rich water molecules with those hydrophobic guest molecules which are less polar than water (Figure 16) to form the complex. Therefore, one, two, or three CD molecules can contain one or more entrapped guest molecules. Most frequently, the host-guest ratio is 1:1. This is the essence of molecular encapsulation (Figure 16). However, 2:1, 1:2, 2:2, and higher order complex equilibria almost always exist simultaneously in the system [262, 271].

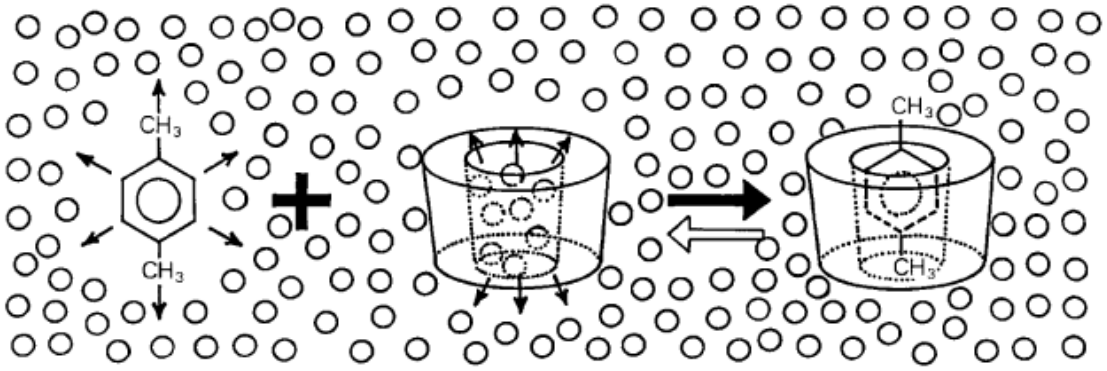

Figure 16: Example of complexation between cyclodextrin (host) and *p*-xylene (guest)[262].

In addition, the host-guest inclusion complex is determined both by the CDs' inner cavity size and by the appropriate size of those organic and inorganic guests. Only the guest molecules with suitable shape and size (with diameter of 0.5 to 0.8 nm) can be incorporated into the CDs' inner cavity to form inclusion complexes. The cavity size of CDs is dependent on the number of glucose in the molecule [271] as shown in Figure 17 and Table 6. Comparing the size cavities of α-CD, β-CD and γ-CD, α-CD has the smallest cavity size of the three CDs which is insufficient for many compounds. γ-CD has the largest cavity size, but its price in the market is higher than the other CDs. Therefore, β-CD is most widely used in research and manufacturing due to its cost and suitable cavity size for most molecules (drugs) [271].

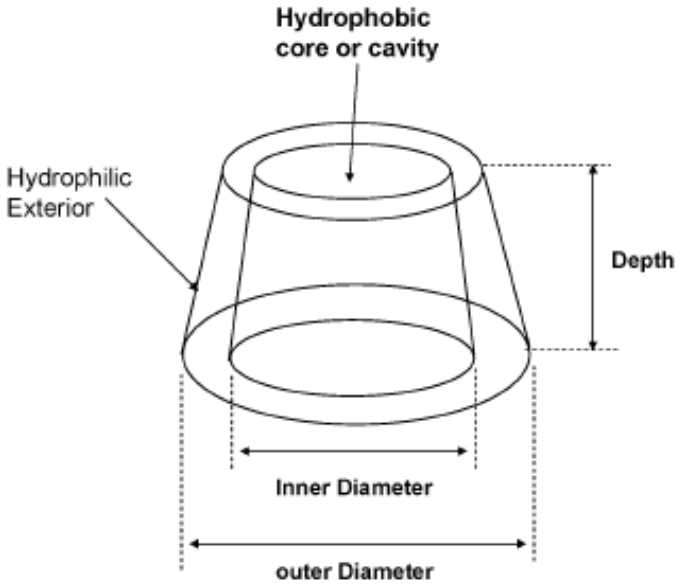

Figure 17: Dimensions and hydrophilic/hydrophobic regions of the CD molecules [271].

Table 6: Characteristics of α, β and γ-CDs [271]

	α	β	γ
Number of Glucose units	6	7	8
Molecular Weight [g/mol]	972	1135	1297
H_2O solubility [g/100mL]	14.5	1.85	23.2
pK_a	12.33	12.2	12.08
Inner diameter [nm]	0.45-0.57	0.62-0.78	0.79-0.95
Outer diameter [nm]	1.37	1.53	1.69
Depth / Height	0.79	0.79	0.79
Cavity volume [nm^3]	0.174	0.262	0.472

Due to the limitation of size and apolar character of the CD cavity, complexation is obviously not suitable for all compounds. For example, inorganic salts such as KCl and NaCl are generally recognized as not being suitable for CD complexation. In addition, solubilization of compounds using cyclodextrin complexation is not suitable for very small molecules, or those that are too large such as peptides, proteins, enzymes, sugars and polysaccharides

[271]. In general, to form an applicable complex with β-CD, compounds (e.g. drugs) have to fit the requirements below with few exceptions:

- more than 5 atoms (C, P, S, and N) should form the skeleton of the drug molecule;
- solubility in water of less than 10 mg/ml;
- melting point temperature below 250 ºC;
- contains the molecule consists of less than 5 condensed rings;
- molecular weight between 100 and 400;

2.7.3 Application of cyclodextrins

The formation of inclusion complexes is widely used and provides numerous advantages in pharmaceutical, food, cosmetic and chemical industries. Among all these applications, the most thoroughly studied field of application of CDs is in the pharmaceutical industry specifically in the use of CDs in drug formulations [262].

In pharmaceutical industry, CDs have been used to increase drug bioavailability in formulations and to improve light, thermal and oxidative stability of drug molecules through the formation of cyclodextrin complexes [271]. For instance, β-CD was reported to increase the bioavailability of poorly soluble drugs by increasing the drug solubility [271]. In addition, cyclodextrins can also be used to reduce or prevent dermal, gastrointestinal or ocular irritation, reduce or mask unpleasant tastes or odour, prevent adverse drug-ingredient interactions (drug-drug or drug-additive) and to convert oils and liquid drugs into microcrystalline or amorphous powders [271-272].

In cosmetic industry, CDs are mainly used to increase the water solubility of lipophilic materials; to convert the liquid or oily materials to powder form; to increase the physical and chemical stability of guest molecules by protecting against decomposition, oxidation,

hydrolysis, or loss by evaporation; to provide the controlled release of active ingredients; to reduce or prevent skin irritation; to prevent interactions between various formulation ingredients; to improve the absorption of various compounds into skin; stabilize emulsions; and to reduce or eliminate the bad odour of certain components [262, 273].

In the food industry, CDs are employed in the preparation of cholesterol free products; the stabilization of volatile or unstable compounds and the reduction of unwanted tastes and odour. For instance, in the production of low-cholesterol butter, β-CD is used to remove the cholesterol from the butter [262].

In the chemical industry, a rapid increase in the number of applications of CDs is observed. For example, in the conservation of wood products, aqueous cyclodextrin solutions are added to water-insoluble fungicides to impregnate the wood structures (door and window frames). CDs are also used to reduce high viscosity in order to facilitate spraying of polyurethane thickening agent containing emulsion- type coatings. In electrochemistry, CDs either added to solution or immobilized onto the electrode surface can be helpful for stereoselective organic electrosynthesis and electrocatalytic reactions.

CHAPTER 3

EXPERIMENTAL

3.1 Instrumentation

Electrochemistry experiments were carried out with a Basi Epsilon –Ec-ver.2.00.71_XP electrochemistry work station (for cyclic voltammetry, square wave and chronoamperometry) and electrochemical impedance spectroscopy (EIS) measurements were recorded with Zahner IM6ex Germany using electrodes from BioAnalytical systems, BAS, US in three-electrode electrochemical cell as shown in Figure 5. Hydrodynamic amperograms and voltammograms for all electrochemical experiments were recorded with a computer interfaced to the Basi Epsilon electrochemical workstation (Scheme 6). Iron oxide modified glassy carbon and unmodified glassy carbon electrodes (GCE) of area 0.071 cm^2 and 3 mm of diameter, were used as the working electrodes. A platinum wire from Sigma Aldrich and Ag/AgCl electrodes from BAS were used as auxiliary and reference electrodes, respectively. Alumina powders and microcloth pads were obtained from Buehler, IL, US and were used for the polishing of the GCE.

Attenuated total reflectance Fourier transform infrared (ATR-FT-IR) was recorded with a Perkin Elmer model Spectrum 100 series. The X-ray diffraction (XRD) was performed by using a Bruker AXS D8 Advance diffractometer. The studies on the morphology and size distribution of the iron oxide nanomaterial were performed by using a high resolution transmission electron microscope (HRTEM) from Tecnai G^2F20 X-Twin MAT (US) and JEOL JSM-7500F scanning electron microscope from US.

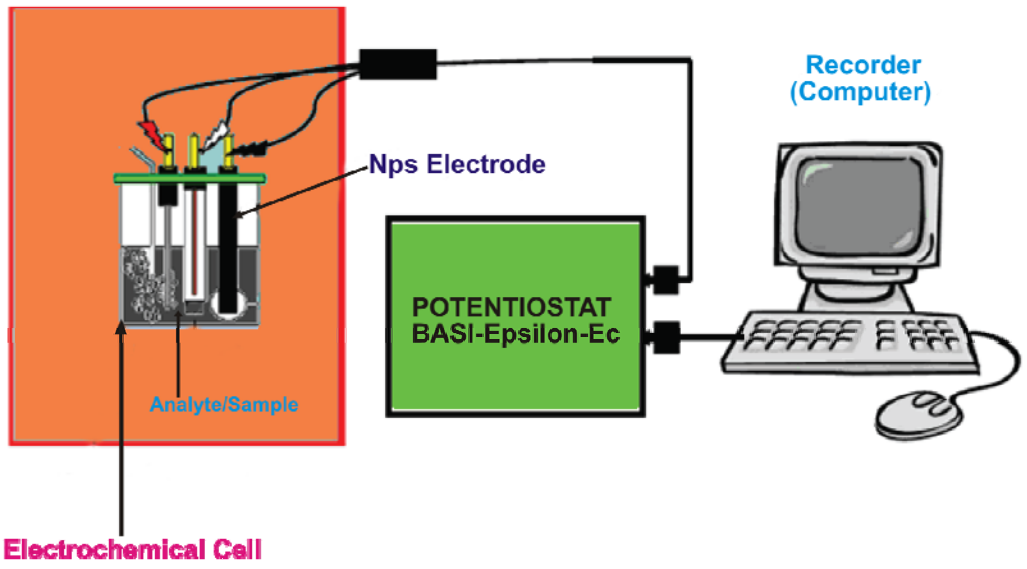

Scheme 6: Major components of the electroanalytical system used for the electrochemical measurements.

3.2 Reagents

Ferrous chloride tetrahydrate ($FeCl_2.4H_2O$), ferric chloride hexahydrate ($FeCl_3.6H_2O$), sodium hydroxide (NaOH), bisphenol A (BPA), 4-tert-octylphenol (TOP) and absolute ethanol were purchased from Sigma- Aldrich. Methanol (95.5 %) was obtained from Kimix. Potassium chloride (KCl) was obtained from Fluka. β-cyclodextrin (β-CD) was obtained from Sigma-Aldrich. Potassium ferricyanide $K_3Fe(CN)_6$ and Potassium ferrocyanide $K_4Fe(CN)_6$ were obtain from UniLAB. All the chemicals were used as received.

Deionized water (18.2 MΩ cm) purified by a Milli-Q^{TM} system (Millipore) was used as the reagent water for aqueous solution preparation and analytical grade argon (Afrox, South Africa) was used to degas the system.

3.3 Preparation of iron oxide- beta-cyclodextrin composite nanomaterial

The synthesis of the iron oxide/ beta -cyclodextrin nanomaterial was carried out based on a literature procedure with slight modification [274]. Briefly, a β-cyclodextrin solution (60 mL, 0.015M) was heated at 90 °C with continuous stirring for 30 min; then, 1600 µL of 5 M NaOH was added to the solution and followed by drop wise addition of 60 ml ferrite solution containing a stoichiometric ratio of 1:2 ferrous chloride tetrahydrate (0.005 M) and ferric chloride hexahydrate (0.005 M). The resulting suspension (solution) was digested at 90 °C for 30 min under a stirred, refluxing system. The reaction mixture was then allowed to cool to room temperature and centrifuged at 1400 rpm to separate particles. Resulting residues were washed three times with deionized water. The washed product was then immediately dispersed in water under-sonication or after being left to dry in desiccators.

The iron oxide nanomaterial without β-cyclodextrin was prepared for control purposes according to the same procedure. Furthermore, we attempted to prepare iron-oxide nanomaterial coated with β-cyclodextrin by centrifuging (1400 rpm, 5 min) a 1 mL suspension of the control iron oxide product, then adding 1 mL of β-cyclodextrin solution (0.015 M) to the resulting residue after decantation, and allowing the resulting mixture to stand for 5 min after sonication (10 min). The suspension of the presumably cyclodextrin

coated iron oxide nanomaterial was separated by centrifugation, rinsed with water in order to remove any loosely adsorbed molecules of cyclodextrin, and finally re-suspended in water.

3.4 Characterization of iron oxide nanoparticles

3.4.1 Electrochemical characterization

3.4.1.1 Cyclic voltammetry (CV)

Cyclic voltammetry characterization was carried out using the instrument described in Section 3.1 (Scheme 6). The characterization solution contained 10 mL of 0.1 M KCl. The iron oxide-β-cyclodextrin composite nanoparticle (Feox-bcd) modified GCE was cathodically scanned from -1300 mV to 0 mV at 50 mV/s and at different scan rates. The electrochemical behaviours of the surface of the modified electrodes were also investigated using $K_3[Fe(CN)_6]$ as a redox probe by cyclic voltammetry.

3.4.1.2 Chronoamperometry (CA)

The chronoamperometry characterization of Feox-bcd was performed using the same instrumentation as in the cyclic voltammetry characterization. A potential of 1200 mV was imposed until the cathodic current degraded to a constant value for 65 s in order to convert any lower oxidation state oxy-iron species into the iron(III)-based species. This was followed by application of a second potential step of -1300 mV for 65 s in order to convert all the oxy-

iron(III) species into iron(II)-based species. The charge obtained was used to estimate the effective surface coverage of the electroactive oxy-iron species using the following Formula 42 [137, 275] and the mass of the oxy-iron species (Formula 43).

$$\Gamma = \frac{Q}{nFA} \tag{42}$$

$$m = \frac{QM_{\mathrm{w}}}{nF} \tag{43}$$

where Q is the Faradaic charge (corrected for baseline), n is number of electrons transferred, F is Faraday's constant, M_{W} is the molecular weight and A is the geometric area of the electrode.

3.4.1.3 Electrochemical Impedance Spectroscopy (EIS)

Electrochemical impedance spectroscopy (EIS) measurements, recorded with Zahner IM6ex, Germany, were used to estimate the ionic conductivity of electrochemically synthesized iron oxide synthesized in the presence and absence of β-cyclodextrin and coated with β-cyclodextrin in $[Fe(CN)_6]^{3-/4-}$ prepared in KCl (0.1 M), at a perturbation amplitude of 10 mV within the frequency range of 100 kHz to 100 mHz.

3.4.2 Transmission Electron Microscopy (TEM)

The studies on the morphology and size distribution of the iron oxide nanomaterial were performed by using a high resolution transmission electron microscope (HRTEM) of Tecnai G^2F20 X-Twin MAT (US) operating at 200 kV field emission.

Specimens for high resolution transmission electron microscopy (HRTEM) were prepared by dispersion in ethanol using an ultrasonic bath. A few drops of the dispersed material was then placed on a carbon-coated copper grid and allowed to dry by evaporation under an infra-red lamp before loading the grid onto the microscope.

3.4.3 Scanning Electron Microscopy (SEM-EDX)

Scanning electron microscopy was used to characterize the surface morphology of iron oxide nanoparticles prepared in the presence and absence of β-cyclodextrin as well as the coated one, and to determine elemental composition and/or atomic percentage of the samples. The images were recorded using a Hitachi X-650 analyzer using the secondary electron (SE) mode with interchangeable accelerating voltages of 25 kV, and a maximum resolution of 20 μm. The chemical composition of the sample was obtained by energy dispersive x-ray spectroscopy (EDX) which was coupled to the SEM machine. The samples for SEM/EDX were prepared by drop-coating 10 μL of iron oxide nanomaterial onto a carbon adhesive mounted on aluminium stubs followed by drying under a lamp.

3.4.4 Attenuated Total Reflection Fourier Transform Infrared (ATRFTIR)

ATR-FTIR spectra were recorded in the range 4000-300 cm^{-1} using a Perkin Elmer model Spectrum 100 series. The samples were prepared from the particle suspension in deionised water by drop-coating 8 μL of the iron oxide nanomaterial and β-cyclodextrin suspension on cellophane and drying under a lamp.

3.4.5 X-Ray Diffraction (XRD)

X-ray diffraction (XRD) for the phase identification of a crystal of the iron oxide nanomaterial was performed by using a Bruker AXS D8 Advance diffractometer (voltage 40 KV; current 40 mA). The XRD spectra were recorded in the range 10-100 degrees. The samples were prepared from the particle suspension in deionized water by drop-coating 20 μL of the suspension on the glass and drying under a lamp.

3.5 Fabrication of the sensors

The glassy carbon electrode surface was polished consecutively with aqueous slurries of 1.0, 0.3, and 0.05 μm alumina powders on a microcloth pad (Bühler), gently rinsed with deionized water then ultrasonicated for 5 min in ethanol in order to remove residual polishing material. After rinsing once more with water, the electrode surface was left to dry under a nitrogen (air) stream and modified as follows. An aliquot (12 μL) of the iron-oxide dispersed in water was drop-coated onto the clean and dry glassy carbon electrode surface and dried in open air under a lamp for 30 min. The film of material cast on the electrode surface was then gently rinsed with deionized water. The ferric oxide-β-cyclodextrin composite film-modified electrode obtained in this way was denoted as Feox-bcd/GCE. The sensor prepared using the β-cyclodextrin-coated iron-oxide nanomaterial was referred to as Feox-cobcd/GCE and the one prepared in the absence of β-cyclodextrin, the control sensor, was referred to as Feox/GCE.

3.6 Sensor measurements

The sensors' amperometric responses to target analytes (bisphenol A and 4-tert-octylphenol) in a deaerated aqueous KCl solution (10 mL, 0.1 M) were studied by cyclic voltammetry and square wave voltammetry. Their responses at different concentrations were recorded by spiking successively increasing volumes of the appropriate analyte stock solution. Deaeration was carried out by passing UHP argon gas through the electrolyte for 5 min before measurement and maintaining a blanket of the gas over the solution throughout the duration of the experiment. Cyclic voltammetry and square wave measurements were studied between 0 and 1000 mV where no redox peak occurred for both the modified and unmodified GCE in the blank supporting electrolyte at a scan rate of 100 mV/s for bisphenol A and 50 mV/s for 4-tert-octyphenol. All the electrochemical experiments with the sensors were carried out at 25 °C. Electrochemical impedance spectroscopy (EIS) measurements were used to estimate the ionic conductivity of electrochemically iron oxide synthesized in the presence and absence of β-cyclodextrin as well as coated one in $[Fe(CN)_6]^{-3/-4}$ prepared in KCl (0.1 M), at a perturbation amplitude of 10 mV within the frequency range of 100 kHz to 100 mHz.

3.7 Preparation and analysis of bisphenol A

A 1 M stock solution of bisphenol A (BPA) was prepared in ethanol (absolute) and kept in a refrigerator at 4 °C. A fresh 10 x 10^{-3} M second stock solution was prepared before every experiment from the first stock solution in a mixture of ethanol/water (40:60 v/v) and a 100 x 10^{-6} M third stock solution from the second one was prepared in pure water. The electrochemical properties of BPA at the iron oxide modified glassy carbon electrode were examined in 0.1 M KCl using cyclic voltammetry (CV) and square wave voltammetry (SWV).

3.8 Preparation and analysis of 4-tert- octylphenol

A 1 M stock solution of 4-tert-octylphenol (TOP) was prepared in methanol and kept in a refrigerator at 4 °C. A fresh 10 x 10^{-3} M second stock solution was prepared before every experiment from the first stock solution in a mixture of methanol/water (40:60 v/v) and a 100 x 10^{-6} M third stock solution from the second one was prepared in deionized water. The electrochemical behaviour of TOP at an iron oxide modified glassy carbon electrode was examined in 0.1 M KCl using cyclic voltammetry (CV) and square wave (SW) voltammetry.

3.9 Interference studies

It well known that several inorganic and organic compounds can interfere with the detection of the analyte of interest. In this work, particular attention was given to cations and anions such as Ca^{2+}, Mg^{2+}, Cu^{2+}, Na^{+}, NO_3^{-}, Cl^{-}, and SO_4^{2-}. Solutions containing 0.1 M each of these ions were prepared. Each solution was mixed with 10 μM of BPA at a ratio of 1:10. SWV was carried out on all of the resulting mixtures. The catalytic currents emanating from the mixtures of these solutions were compared to that obtained from 10 μM of BPA. Expressed as a ratio of $I_{(BPA)}/I_{(BPA+\text{ suspected interferences})}$, the value obtained was used to assess the level of possible interference by all investigated substances.

3.10 Real sample application

A real sample application of the sensor GCE//Feox-bcd was demonstrated using a sample of a commercial soft drink known as STONEY GINGER BEER (S05F10D, Coca-Cola Co., Bar code: is 5 449000 106421). According to the information provided on the can, the sample

from this drink contained the ingredients: carbonated water, sugar, citric acid, stabilisers, preservatives, sodium benzoate and sorbate, and flavourant. The samples were analyzed by the standard addition method using four replicate sensors. The responses from the sensors were normalized with respect to their responses to a standard solution of BPA.

CHAPTER 4

RESULTS AND DISCUSSION

4.1 Characterization of the iron oxide nanoparticles

4.1.1 Electrochemical characterization

4.1.1.1 Cyclic voltammetry

Electrochemical behaviour of the surface of the modified electrodes (GCE) was investigated in aqueous potassium chloride solution (0.1 M) by cyclic voltammetry.

According to the voltammograms Figure 18, each of the oxy-iron films exhibited two pairs of anodic and cathodic peaks. The CVs do show the successful immobilization of the films (Feox, Feox-bcd and Feox-cobcd) and their electroactivity. The origin of the two pairs of peaks could be either of the following: a) the existence of two different electroactive phases (polymorphs) an oxy-iron (III) with different formal potentials; b) the presence of a following electrochemical reaction producing another oxide/hydroxide/ or soluble product (cathodic dissolution).

Because of the motive of solvation of the Fe^{2+}, the electrode reaction which yields free Fe^{2+} ions would exhibit a pre-peak relative to the main electrode reaction that yields another insoluble phase. It has already been known that phase composition is one of the factors controlling the electrochemical properties of iron oxides [276]. Possible iron(III) oxide/hydroxide products include: $Fe(OH)_3$, FeOOH (goethite and lepidocrocite),

$Fe_2O_3.½H_2O$ (ferrihydrite), and Fe_2O_3 (hematite and maghemite). While reports indicate that it is mostly difficult to reduce crystalline ferric oxides in the absence of protons and complexing agents, the reduction of amorphous FeOOH, γ-FeOOH (lepidocrite), and δ-FeOOH in a neutral media was reported to occur yielding Fe_3O_4 as a secondary phase [276]. Once formed Fe_3O_4 (or Fe_2O_3.FeO) can also be reduced reversibly in neutral media into FeO [277-278].

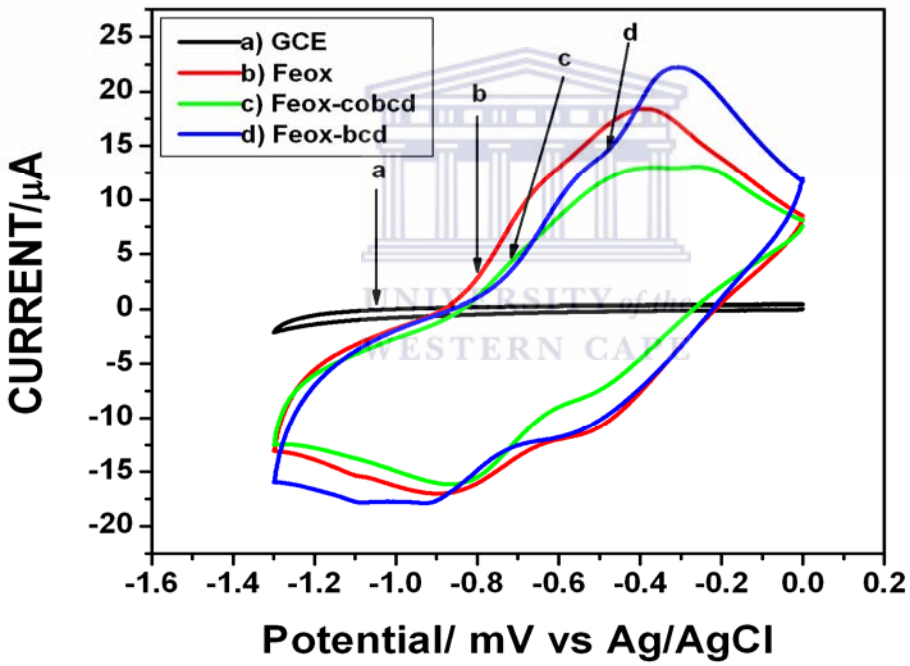

Figure 18: Cyclic voltammograms of bare GCE (a), Feox (b), Feox-cobcd (c) and Feox-bcd (d) in 0.1 M KCl at scan rate of 50 mV/s.

The above literature background may be used to propose a tentative equation for the electrode reaction responsible for the two pairs of peaks observed in cyclic voltammograms of our oxy-iron products shown in Figure 18:

$3FeOOH\ (s) + e^- \rightarrow Fe_2O_3.FeO\ (s) + H_2O\ (l) + OH^-(aq.)$ $\quad E°'_1 = -0.46$ (0.1 M KCl)

$Fe_2O_3.FeO\ (s) + H_2O\ (l) + 2e^- \rightarrow 3FeO\ (s) + 2OH^-\ (aq.)$ $\quad E°'_2 = -0.76$ (0.1 M KCl)

In case the origin of the double redox peaks was the occurrence of a pre-peak of cathodic dissolution, then the electrode reactions may be written as follows:

$FeOOH\ (s) + H_2O + e^- \rightarrow Fe^{2+}\ (aq) + 3OH^-\ (aq)$ $\quad E°'_1 = -0.46$ (0.1 M KCl)

$3FeOOH\ (s) + e^- \rightarrow Fe_2O_3.FeO\ (s) + H_2O\ (l) + OH^-(aq.)$ $\quad E°'_2 = -0.76$ (0.1 M KCl)

Figure 19 shows the peaks for Feox-bcd at different scan rate (from 10 to 200 mV/s). However, the peaks c are observed only at scan rates greater than 30 mVs^{-1}. At scan rates lower than 30 mV/s, peak c is not observed due to the effect of fast oxidation electron transfer reaction.

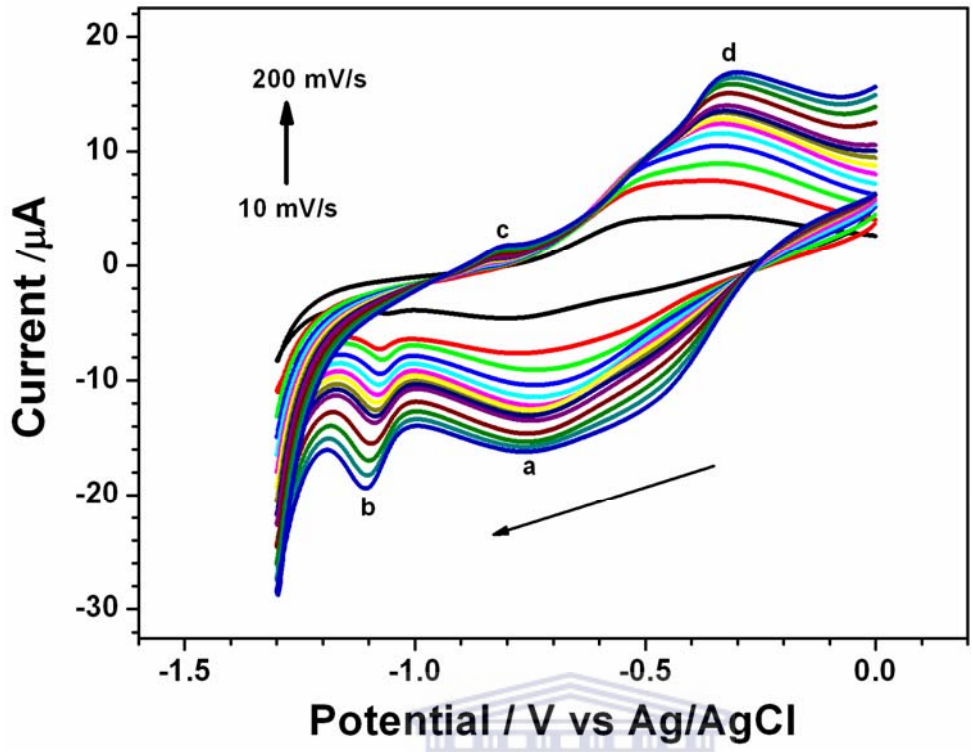

Figure 19: Multiscan voltammograms of Feox-bcd characterization in 0.1 M KCl at different scan rates (10 to 200 mV/s).

In order to shed light on the rate limiting process behind the observed electrochemical activity of the film of Feox-bcd (Fig.19) , log-log plots of peak current versus scan rate were studied [205]. The plots of the log of peak current versus log of scan rate for Feox-bcd (Figure 20 and appendix A) show the peaks current increased linearly with log of scan rate in the range of 10 – 200 mV/s according to the equations: log I_{pa} = 0.12494 + 0.5561 x log ν, (R = 0.993); log I_{pb}= 0.1924 + 0.4790 x log ν, (R= 0.993); log I_{pc}= -3.0659 + 1.4545 x log ν, (R= 0.993) and log I_{pd}= 0.06681 + 0.5910 x log ν, (R= 0.990); for peaks a, b, c and d respectively. It was observed that, all plots had non-zero intercept because of the non-Faradaic current and the plots emanating from peak b were the most linear. Thus, the rate of the redox process involving the Feox-bcd (Figure 19) film was limited by a diffusion step for peak b, adsorption for peak c and both diffusion and adsorption for the peaks a and d. This is assigned to the characteristic of thick electroactive films.

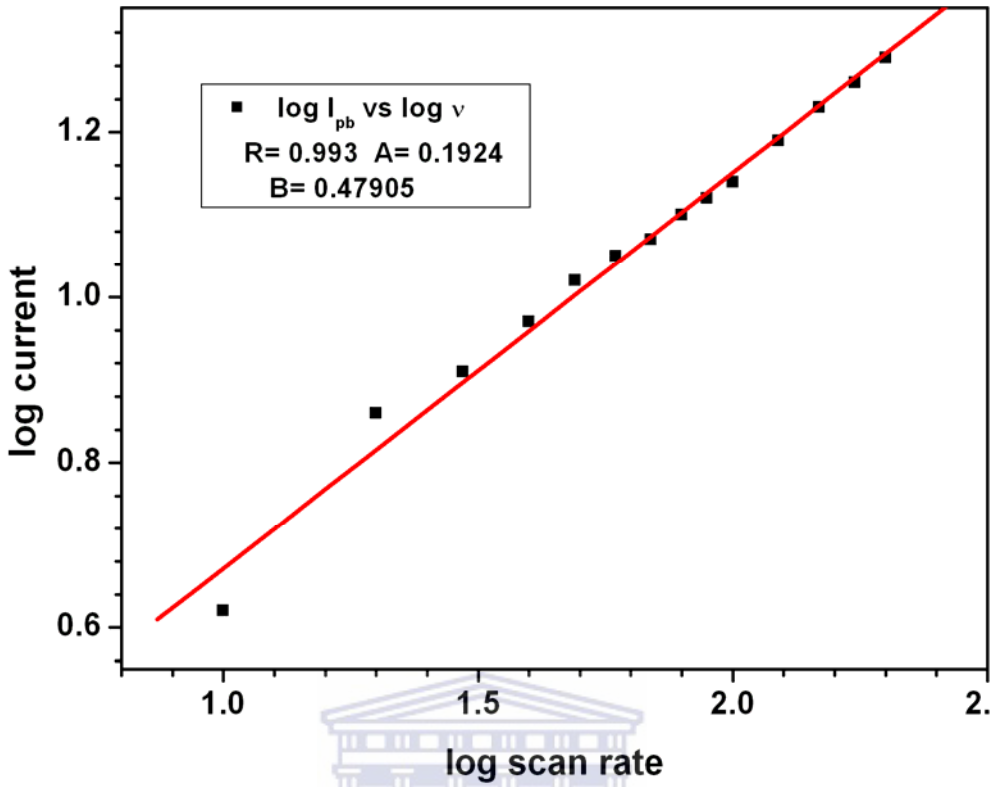

Figure 20: A plot of log peak current versus log scan rate for peak b.

Electrochemical behaviour of the surface of the modified electrode was also investigated using $K_3[Fe(CN)_6]$ as a redox probe by cyclic voltammetry. Figure 21 shows the cyclic voltammograms of bare GCE (a), Feox/GCE (b), Feox-cobcd/GCE (c) and Feox-bcd/GCE (d) obtained in the presence of 5 mM $K_3[Fe(CN)_6]$ in the supporting electrolyte (0.1 M KCl). The bare GCE showed a well defined redox peak with peak-to-peak separation (ΔE_p) of 87 mV. The modified GCE, compared to the unmodified GCE, showed an increase in ΔE_p (174; 225; 406 mV, for Feox, Feox-cobcd and Feox-bcd, respectively) and a decrease in peak currents (I_p). Thus, the iron-oxide films appear to have slightly impeded the kinetics of the $K_3[Fe(CN)_6]$ redox system. However, in the absence of electrochemical mediation or catalysis, the observed changes in I_p and ΔE_p could also be caused by an uncompensated ohmic drop as a result of the film. In addition, since nanoparticles have charge (negative charge for iron oxide), and the negative charge of $Fe(CN)_6^{3-}$ could also explain the situation

because of the electrostatic repulsion between the two negatives charges. So the immobilization of iron-oxide films onto the surface of the GCE could decrease the rate of electron transfer between electrode surface and $K_3[Fe(CN)_6]$ species.

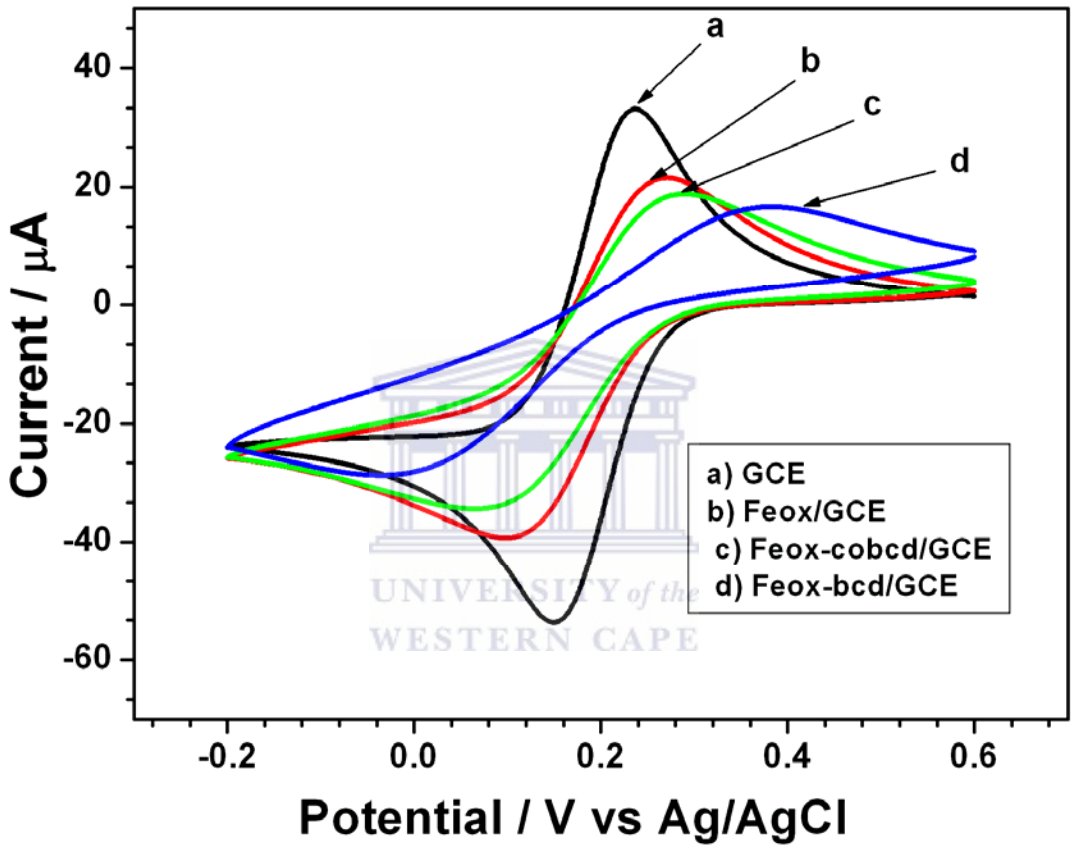

Figure 21: Cyclic voltammograms of GCE (curve a), Feox/GCE (curve b), Feox-cobcd/GCE (curve c) and Feox-bcd/GCE (curve d) in the presence of $K_3[Fe(CN)_6]$ 5 mM in aqueous KCl (0.1 M), at scan rate of 50 mV/s.

4.1.1.2 Chronoamperometry (CA)

In order to quantify molar ratios of the Fe(II) and Fe(III) species, and the surface coverage of iron-oxide films onto the surface of glassy carbon electrode, a chronoamperometric experiment was carried out (Fig. 22). Feox-bcd was employed for estimation of mass and surface coverage using the Formulas 42 and 43 (section 3.4.1.2). Based on the data we got using the formula 43, the effective surface concentration of electroactive iron-oxide species was thus estimated to be 2.9 $x10^{-7}$ mole cm^{-2} (16 μg cm^{-2}). The same data was exploited to find the ratio of iron(II) to iron(III) species which indicated the iron in film was almost (95%) in the iron(III) form. The same composition may be assumed for the iron-oxide products without β-cyclodextrin as well.

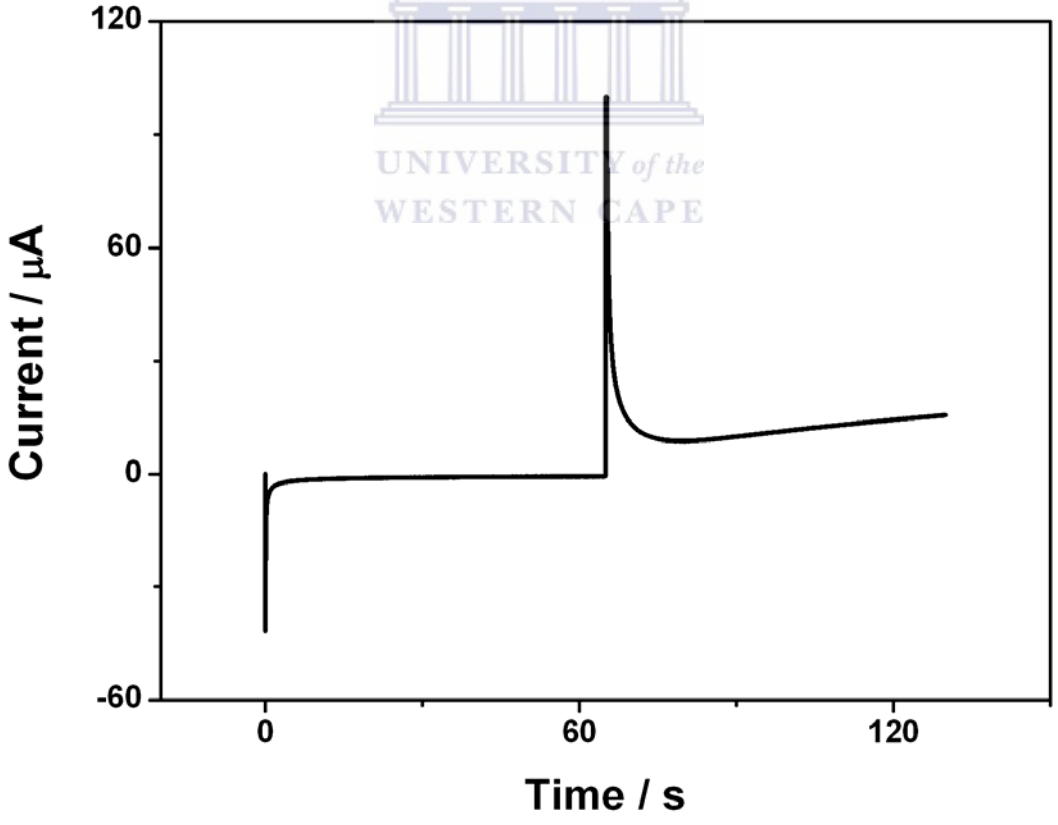

Figure 22: Chronoamperomogram of Feox-bcd

4.1.1.3 Electrochemical Impedance Spectroscopy (EIS)

The electrochemical impedance spectroscopy (EIS) experiments were carried-out for further characterization of the modified electrode. Figure 23 shows the Nyquist diagrams for the bare GCE (a), Feox/GCE (b), Feox-cobcd/GCE (c) and Feox-bcd/GCE (d) in the presence of $Fe(CN)_6^{3-/4-}$ (5 mM) in the supporting electrolyte (0.1 M KCl) and Randle's equivalent circuit (insert) used for fitting the corresponding data by replacing the double layer capacitance with a constant phase element (CPE). Solutions resistances (Rs) recorded were similar for both the unmodified GCE and the modified GCE. In the range of frequencies of interrogation chosen, the diffusion impedance was not fully exhibited, and the results shown (Fig.23) are meant only for qualitatively comparing charge transfer resistances (R_{ct}). It can be seen that the lowest value of electron transfer resistance (R_{ct} = 1.288 kΩ) was obtained for the bare GCE. When Feox, Feox-cobcd and Feox-bcd were dropped on the surface of the GCE, the charge transfer resistance, R_{ct}, increased markedly (2.283 kΩ, 3.355 kΩ and 4.51 kΩ) for Feox, Feox-cobcd and Feox-bcd respectively, which could be attributed to the iron-oxide films themselves, therefore increasing the activation energy of the interfacial electron transfer that involving the $Fe(CN)_6^{3-/4-}$ redox system. This indicates a more sluggish electron transfer rate at the iron oxide films interfaces compared to that of bare glassy carbon electrode and corroborate the electrostatic repulsion phenomena observed in the CVs (see section 4.1.1.1). Since a charge barrier for anions at the surface of the electrode can be formed if inclusion occurs [279] and specific adsorption of ions can affect the redox reaction at the electrode [280], therefore, the increase of R_{ct} observed for iron oxide prepared in the absence (Feox) and the presence of β-CD (Feox-bcd) as well as the coated one (Feox-cobcd) can be explained by the presence of β-CD in Feox-bcd and Feox-cobcd due to inclusion complex between iron oxide and β-CD which has formed a charge barrier for anions ($Fe(CN)_6^{3-/4-}$ and Fe_2O_3.FeO) at the surface of the electrode thereby increasing the charge transfer resistance.

On the other hand, the difference of R_{ct} observed between Feox-bcd and Feox-cobcd can be discussed as a result of an enhancement of the electrostatic repulsion caused by the specific inclusion complex of iron-oxide and β-CD for Feox-bcd, and the incomplete repulsion between the two negative charge (iron-oxide and redox probe) due to nonspecific inclusion complex of iron-oxide and β-CD for Feox-cobcd. It can also be seen that, all the curves have a semi-circle and a linear portion, which correspond to kinetic in the higher frequency region and mass transfer via diffusion processes in the lower frequency region, respectively (Figure 23).

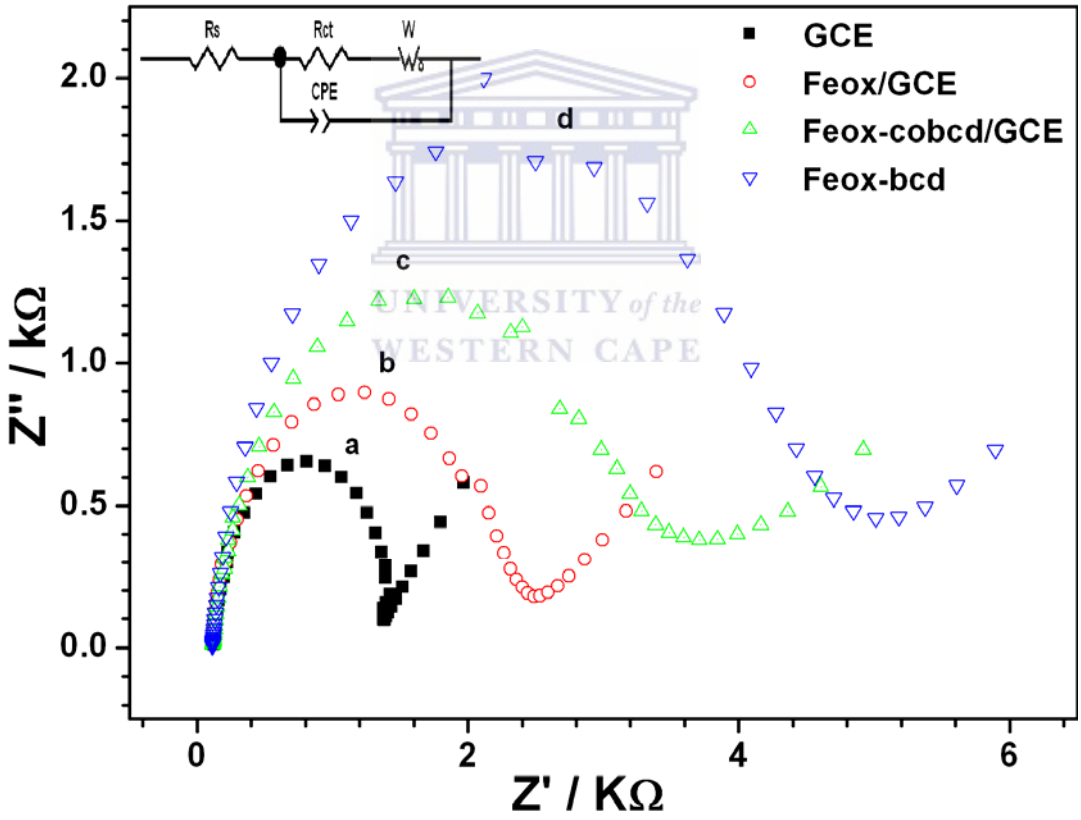

Figure 23: Nyquist plots of GCE (curve a), Feox/GCE (curve b), Feox-cobcd/GCE (curve c) and Feox-bcd/GCE (curve d) in the presence of $[Fe(CN)_6]^{-3/-4}$ 5 x 10^{-3} M in aqueous 0.1 M KCl. Insert circuit used for fitting.

4.1.2 Transmission Electron Microscopy (TEM)

Figure 24a and b, shows transmission electron micrograph of two iron oxide nanomaterials prepared in absence and presence of β-cyclodextrin and their corresponding electron diffraction patters, respectively. Both the micrographs and the diffraction patterns showed that the presence of beta-cyclodextrin did not cause any obvious change in morphology of the iron oxide nanomaterials. In both cases, the products appeared to be composed of highly amorphous particles [281] with high surface area and dimensions about 100 nm by 500 nm.

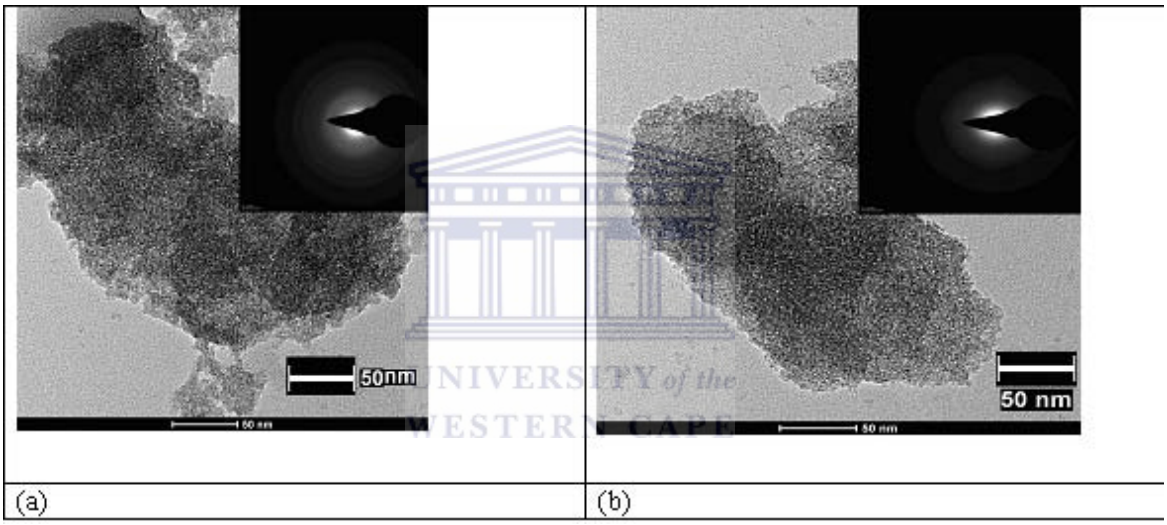

Figure 24: TEM images and ED pattern of the iron oxide material which was prepared in absence (a) and in presence (b) of β-CD and their corresponding electron diffraction patters (insert).

4.1.3 X-Ray Diffraction (XRD)

The extent of crystallinity of the iron oxide nanoparticles was determined using X-ray diffraction. Figure 25 shows, the X-ray diffraction patterns of the iron oxides nanoparticles prepared in presence and absence of β-cyclodextrin, and coated with β-cyclodextrin. As it can be seen no peaks were observed that were a result of the nanomaterials. The absence of peak reflects that the materials are amorphous. This XRD results correlates with those of electron

diffraction patters from TEM and confirm the amorphous nature of the iron oxides nanomaterials. Peaks observed in the figure could be due to the glass sample holder used [282].

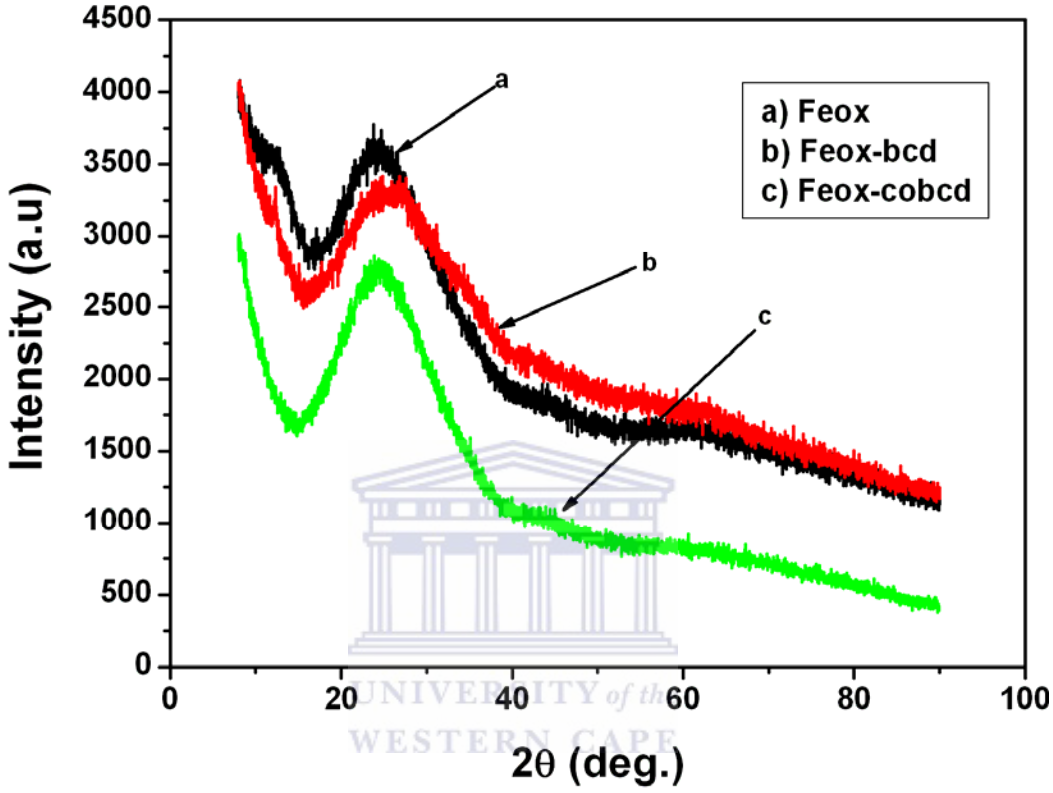

Figure 25: XRD of the iron oxide material prepared in the absence (a) and in the presence (b) of β-CD and of the iron oxide material coated with β-CD (c).

4.1.4 Attenuated Total Reflection Fourier Transform Infrared (ATRFTIR)

Figure 26 shows the infrared transmission spectra of the iron oxide materials which were prepared in the absence (Feox) and presence (Feox-bcd) of β-cyclodextrin in the reaction mixture. The figure shows the corresponding spectra of the pure β-cyclodextrin (β-CD) itself and that of the iron oxide material which was coated with β-CD after its preparation (Feox-cobcd). The assignments of the respective absorption bands in the corresponding spectra are listed in Table 7 after correlating the spectra with handbook values and previous reports. The peaks around 3371 cm^{-1} and 1644 cm^{-1} are assigned to the O-H stretching and bending modes

of water, respectively owing to the adsorbed water in the sample and the hydroxyl group on β-cyclodextrin [274, 283-285]. The absorption peaks observed at 664 cm^{-1} and 587 cm^{-1} are due to stretching vibrations of the metal-oxygen bond characteristic of the metal oxide [274, 283] and the peak at (594 -594 cm^{-1}) can be attributed to Fe_3O_4 [285]. The other absorption peaks at 2928 cm^{-1} and at (800-1500 cm^{-1}) could be related to C-H bonds, C-C bonds and C-O bonds caracteristique of β-cyclodextrins [284-286].

The spectra of the iron oxide nanoparticles which were synthesized in the presence of β-cyclodextrin exhibited no significant difference from the spectra of iron oxide nanoparticles which were coated post-synthesis with β-cyclodextrin. Furthermore, the appearance of some peaks (for example 1158 and 1028 cm^{-1}) similar to those of pure beta-cyclodextrin confirmed the attachment of β-cyclodextrin on the surface of nanoparticles in both cases. Otherwise, we can conclude that, there is inclusion complex between β-cyclodextrin and iron oxide nanoparticles.

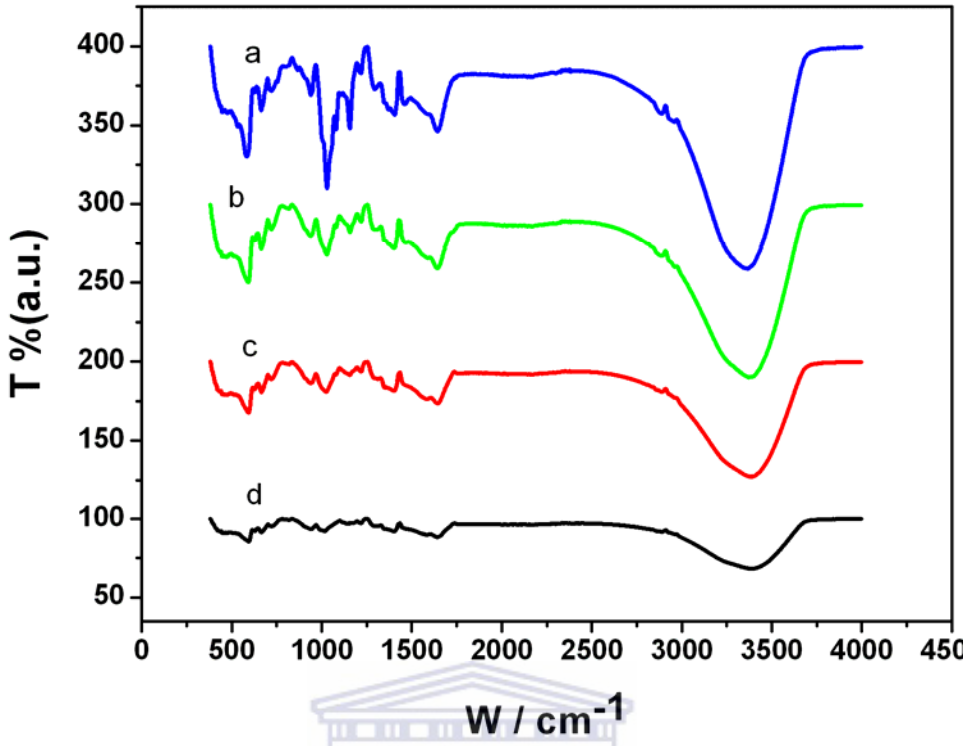

Figure 26: ATR-FTIR of pure β-CD (a), Feox-bcd (b), Feox-cobcd (c) and Feox (d).

Table 7: Assignments of the absorption bands (cm^{-1}) in the FTIR spectra in Figure 25.

Pure β-CD/ cm^{-1}	Feox-cobcd/ cm^{-1}	Feox-bcd/ cm^{-1}	Feox/ cm^{-1}	Assignments
3307	3369	3371	3392	ν^* H-O….H
2928 ; 2881	2960 ; 2875	2887	-	ν^*_{as} C-H of $-CH_2$
1644 – 1407	1643 – 1399	1644 – 1403	1643	δ^* H-C-OH
1294	1288	-	-	δ^* H-C-OH
1155	1158	1156	-	ν^*_s C-O-C
863 – 1207	936 – 1220	938 – 1216	-	C-C
-	663	664	663	M - O
-	587	594	594	Fe - O

Legend: ν^*: stretching vibration; ν^*_{as} : asymmetrical stretching vibration; ν^*_s : symmetrical stretching vibration; δ^* : deformation; M : metal

4.1.5 Elemental composition

The iron oxide nanoparticles Feox, Feox-bcd and Feox-cobcd were then subjected to EDX analysis to determine the percentage atomic composition of the atoms present in each of them. The comparison of the EDX spectra of Feox (Figure 27) with that of Feox-bcd (Appendix B1) and Feox-cobcd (Appendix B2) can conclude that iron oxides were successfully prepared. Feox revealed percentage atomic compositions of 46.82 Fe, 37.74 O and 07.73 C. The presence of carbon element in Feox could be explained by the carbon adhesive used as a sample holder, while the Feox-bcd and Feox-cobcd spectra showed the increase in carbon percentage as a result of attachment of β-CD. The atomic composition of other iron oxides was 45.70 Fe, 35.92 O and 11.15 C; and 37.36 Fe, 39.56 O and 17.33 C, for Feox-bcd and Feox-cobcd respectively. The trace amounts of Si, Na, Ca and S observed in the spectra can be due to the impurities present in the base and salt used for the synthesis of the nanoparticles and/or sample holder used during EDX measurement. EDX results correlates with those of FTIR by confirming the successful attachment of β-CD in iron oxide or inclusion complex during the chemical preparation and coating.

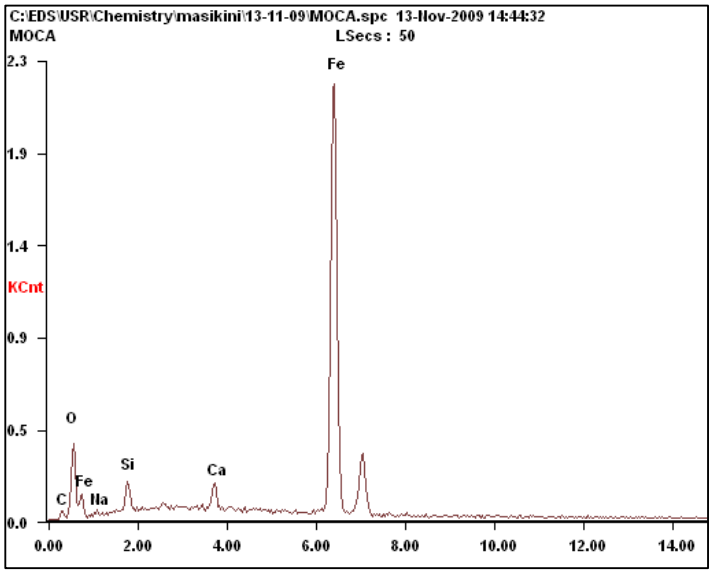

Figure 27: EDX spectrum for Feox.

CHAPTER 5

RESULTS AND DISCUSSION

5.1 Iron oxide nanoparticles sensors response to bisphenol A

5.1.1 Electrochemical property of BPA at iron oxide modified glassy carbon electrode

As the main objective of the study was to develop sensors for selected endocrine disruptor molecules, the electrochemical behavior of bisphenol A (BPA) as a model endocrine disruptor was investigated Figure 28 shows an overlay of cyclic voltammograms of bisphenol A (BPA) at the bare GCE, Feox-cobcd/GCE, Feox-bcd/GCE and Feox/GCE in aqueous KCl (0.1 M).

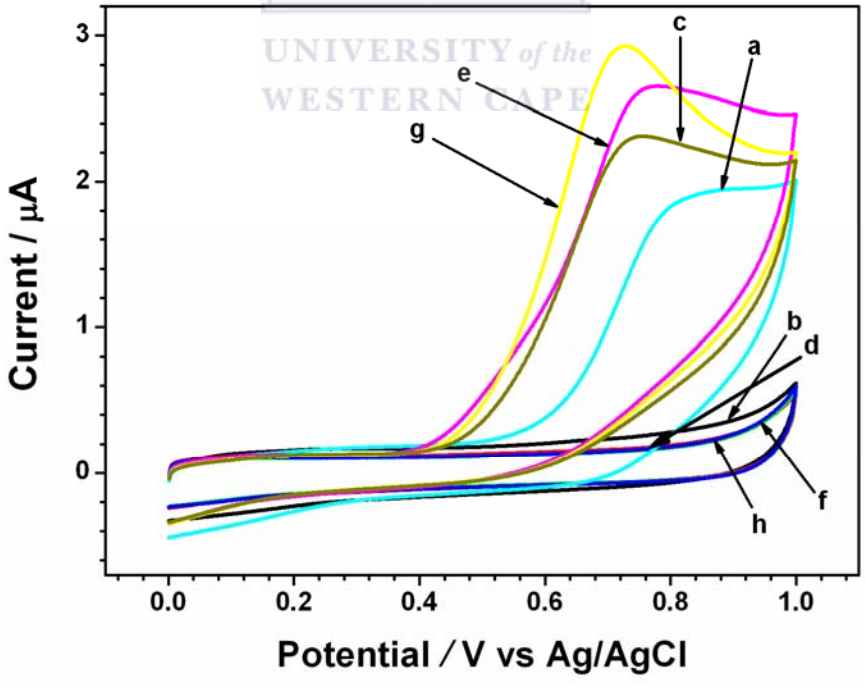

Figure 28: Cyclic voltammograms of bisphenol A (50 x 10^{-6} M) at the bare GCE (curve a), Feox-cobcd/GCE (curve c), Feox-bcd/GCE (curve e) and Feox (curve g) in aq. KCl (0.1 M). Curves b, d, f and h represent CVs at 0 M BPA.

The response of the modified electrodes as BPA sensors were studied between 0 and 1000 mV where no redox peak occurred for both the modified and unmodified GCE in the blank supporting electrolyte. On addition of BPA to the supporting electrolyte, an irreversible oxidation peak was observed at all sensors. Compared to the bare GCE, the BPA oxidation peaks at the three modified electrodes were observed at potentials which were more anodic by about 100 mV. Thus, the iron-oxide material exhibited an electrocatalytic effect. This is actually an advantage gained over the bare GCE for sensing applications. They were also more well-defined because of enhanced sharpness. The peak currents were as well enhanced when compared to the GCE, the highest being for the Feox/GCE. The iron-oxide film without incorporated β-CD showed the highest current-peak height (2.929 μA) and the lowest peak potential (727 mV). On the incorporation of the β-CD either through co-deposition or post-synthetic coating, the respective peak positions shifted to higher values but still smaller by about 60 mV than that which was recorded for the bare GCE. The peak heights were as well improved relative to the bare GCE. For the modified electrodes in this work, oxidation peaks of BPA were observed between 730 - 770 mV (vs Ag/AgCl). It is also observed that, the iron-oxide film shifted the anodic peak potential to less positive values compared to that of the bare GCE. Possible causes include: chemical reduction of the iron(III) species which could be re-oxidized (electrochemically mediation), electrocatalysis, stabilization of BPA oxidation products, and enhancement of BPA adsorption by acting as an adsorbent leading to increased pre-concentration.

The fact that no reduction peak of BPA was observed at both of the modified and the unmodified GCE is in agreement with the literatures [131-133]. But this observation does not indicate that the electrochemical reaction of BPA is irreversible. Furthermore, when multiple cyclic scans were recorded, the oxidation peak was observed only during the first scan for all

electrodes (Figure not shown). This indicates the occurrence of a fouling phenomenon, arising from the oxidative polymeric products of BPA, which resulted in blockade of other BPA molecules from reaching the sensing layer. Thus, the oxidation peak current in the first anodic sweep is recorded for BPA analysis in this work. Most of the proceeding results and discussions will focus more on the BPA sensor developed with Feox-bcd because of its outstanding analytical performance as compared to the bare GCE, Feox, and Feox-cobcd.

5.1.2 Effect of scan rate

From the relationship between the peak current and scan rate, useful information concerning electrode mechanism can be obtained. Hence, the adsorption behavior of BPA over the surface of the modified electrode was investigated by means of cyclic voltammetry. Figure 29, shows cyclic voltammograms of BPA at Feox-bcd/GCE with various scan rates. It can be seen that the oxidation peak current increased with increasing scan rate.

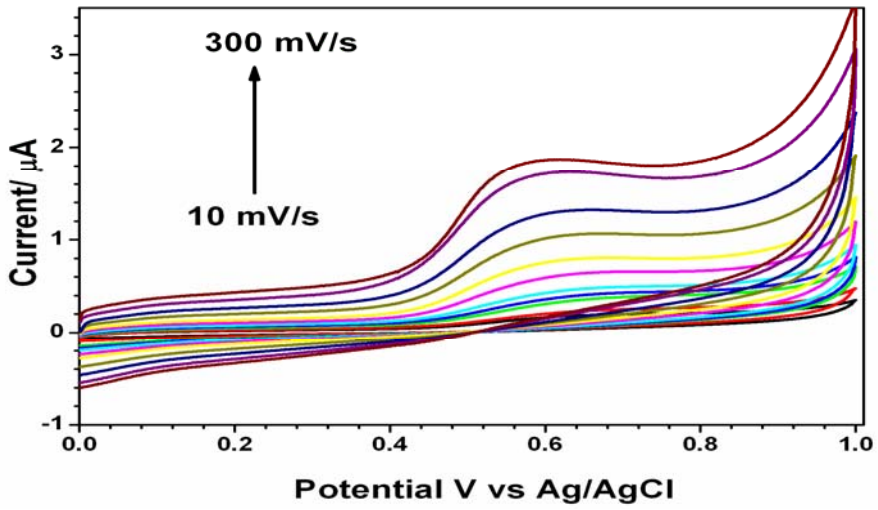

Figure 29: Cyclic voltammograms of 5 x 10^{-6} M BPA in 0.1 M KCl at different scan rate (10 – 300 mV/s).

As shown in Figure 30, the plot of peak current versus scan rate, the peak current increased linearly (R = 0.997) with the scan rate in the range of 10 – 300 mV/s according to: I_{pa} = 0.121 + 0.00599ν; where I_{pa} is in μA and v is in mV/s. Thus, the oxidation of BPA on Feox-bcd/GCE is an adsorption-controlled process, which can be used to pre-concentrate BPA onto the surface of Feox-bcd/GCE for improving BPA detection limit. Furthermore, the plot of E_{pa} versus ln v did not show linear correlation (data not shown); however it was noted that there was a general tendency of E_{pa} to be constant, but at scan rates ≥ 100 mV/s it exhibited an apparent slight shift to increasingly smaller anodic values contrary to the behaviour expected from an irreversible electrode process. The data were collected by starting with the highest scan rate (300 mV/s) and moving to the smallest scan rate (10 mV/s), in order to minimize fouling. Thus, the gradual non-linear anodic shift to higher potentials with decreasing scan rate may arise from temporal factors like the deposition of additional fouling substances originating from the polymerization of oxidized BPA. The observed general tendency of the anodic peak potential to be constant may indicate that the oxidation of BPA was indeed reversible. It is well-known form literature that the direct oxidation of phenolic compounds via one-electron or two-electron transfer would generate a phenoxy radical, or phenoxonium ion and quinone, respectively [127, 131]. Oxidation of phenolic compounds to quinone can be suppressed by applying a low overpotential. According to previous reports, with regard to the oxidation of phenolic compounds [131-132, 134], the anodic oxidation of BPA in this work, has been attributed to the aromatic-ring in the BPA and the formation of phenoxonium ion via a two-electron and two proton process. This is then followed by C–O and/or C–C coupling of two phenoxonium ions or one phenoxonium ion and a phenolic radical to form a neutral dimer. The mechanism of the overall reaction can be described as oxidation, followed by de-protonation, another oxidation and de-protonation process, and finally coupling. The

resulting BPA dimer is non-conducting film, which continuously adds to the insulation of the electrode.

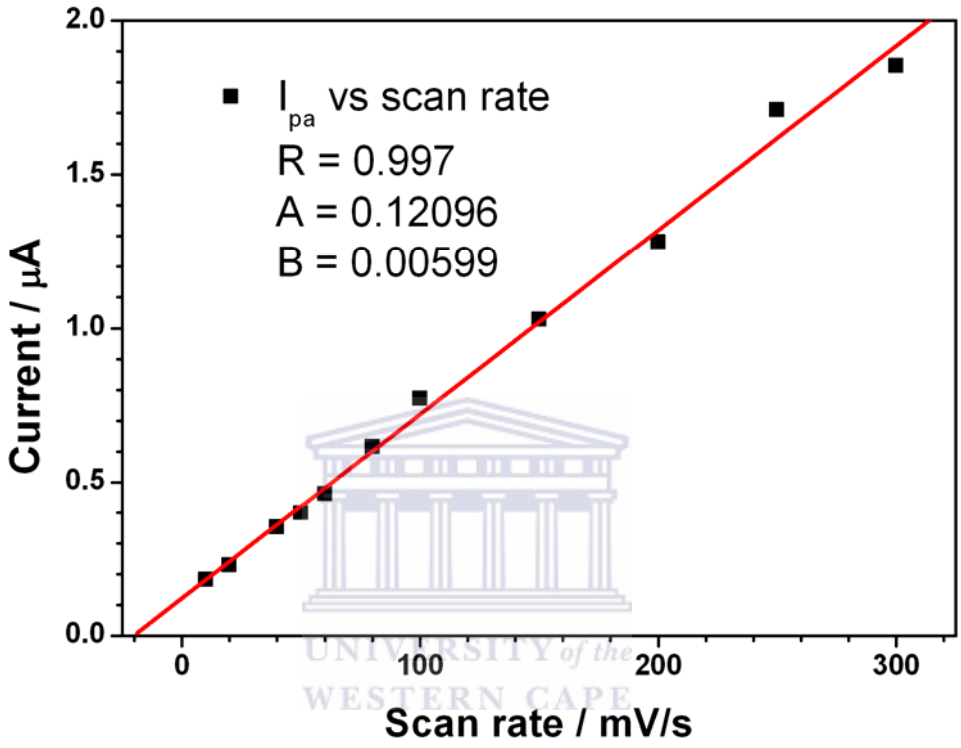

Figure 30: Effect of scan rate on the oxidation peak current of 5 x 10^{-6} M BPA in 0.1 M KCl

5.1.3 Amperometric bisphenol A sensor

The figures below show the cyclic voltammetric (Fig. 31) and square wave (Fig. 32) responses of Feox-bcd/GCE at different concentrations of BPA in 0.1 M KCl at scan rate of 100 mV/s. In each case only one cycle scans were recorded for the reasons explained in section 5.1.1. Peak potentials successively shifted to more anodic values with increasing concentration in both cases. The observations were consistent with adsorption effects.

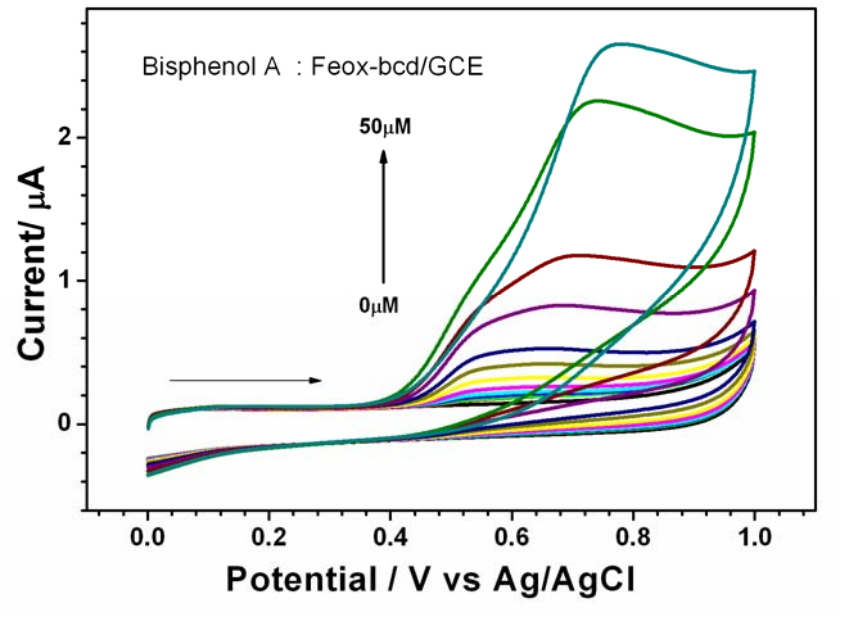

Figure 31: CV response of Feox-bcd/GCE at different concentration of BPA in 0.1 M KCl. Scan rate 100 mV/s.

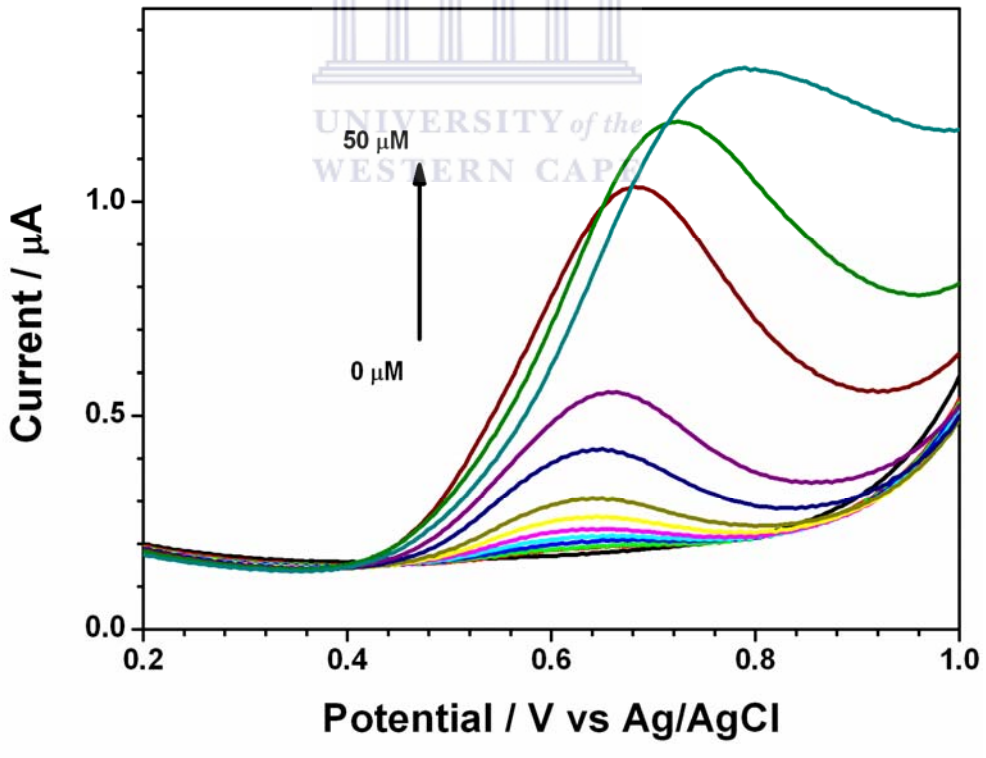

Figure 32: SWV response of Feox-bcd/GCE at different concentration of BPA in 0.1 M KCl. Scan rate 100 mV/s.

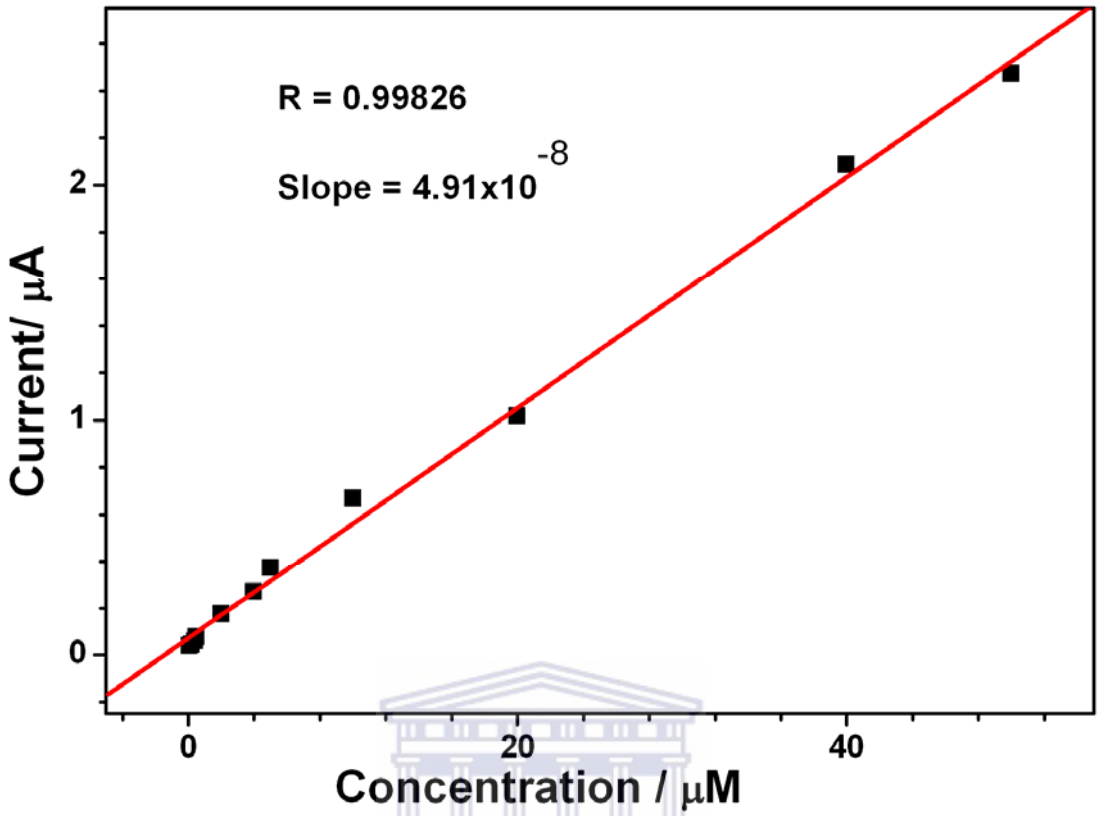

Figure 33: Calibration curve of peak current vs BPA concentration for iron oxide nanoparticle with beta cyclodextrin modified glassy carbon electrode.

Figure 33 shows the peak current increased linearly (R = 0.998) with increasing concentration of BPA in the range of 4 x 10^{-7} M to 50 x 10^{-6} M. The corresponding sensitivity and detection limits were 49.1 nA L/mol and 0.156 x 10^{-6} M, respectively.

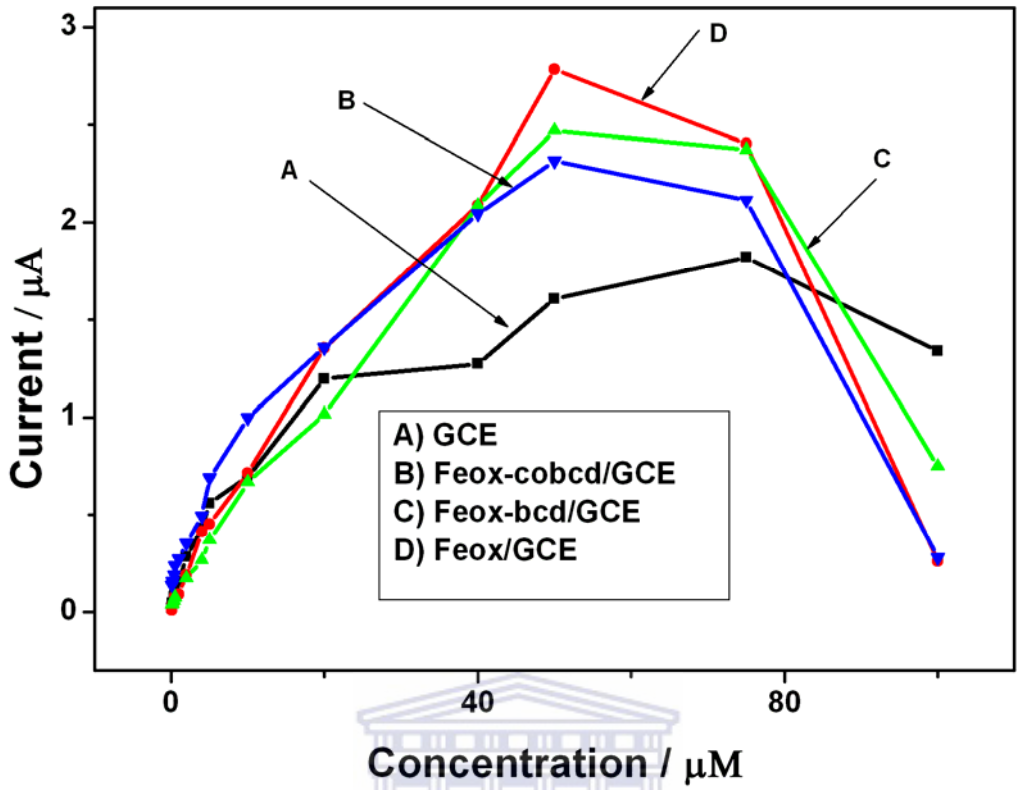

Figure 34:Cyclic voltammetric responses of the bare GCE (curve A), Feox-cobcd/GCE (curve B), Feox-bcd/GCE (curve C) and Feox/GCE (curve D) to different concentration of BPA in 0.1M KCl. Current values at respective peak potentials of CVs were recorded at 100 mV/s

In order to compare the linearity, sensitivity, and levels of fouling of the different sensors under discussion, the cyclic voltammograms of BPA were recorded at different concentrations (10^{-7} M to 10^{-4} M) for bare and the three modified electrodes (GCE, Feox-bcd, Feox-cobcd and Feox) in KCl (0.1 M). Figure 34 shows the current increased with increasing concentration of BPA in the range of 10^{-7} M to 50 x 10^{-6} M for Feox/GCE, Feox-bcd/GCE and Feox-cobcd/GCE, and then it started to decline. The same result is observed on the GCE but the decrease start at 20 x 10^{-6} M. Obviously, the decrease of current showed that fouling occurred at concentrations higher than 50 x 10^{-6} M BPA for Feox, Feox-bcd and Feox-cobcd. Among the currently reported sensors, both the Feox-bcd and Feox films exhibited two orders (2.09 and 2.03) of magnitude showing one order of magnitude improvement over the bare

GCE (0.99). However, the level of linearity of the calibration curve for the Feox-bcd made it most superior for practical applications. Its operating potential (770 mV) was better than the bare GCE by about 60 mV.

5.1.4 Reproducibility, stability and interference

Stability and reproducibility are key elements of electrode performance. The reproducibility of Feox/GCE, Feox-cobcd/GCE and Feox-bcd/GCE, were investigated in the presence of 10 x 10^{-6} M BPA in KCl (0.1 M). The relative standard deviation (RSD) for six parallel measurement of 10 x 10^{-6} M BPA were 5.03 %; 9.23 % and 1.7 %, respectively when measured with square wave voltammetry (SWV). Thus, results indicated that the reproducibility of the electrodes were within experimental error. The relative standard deviation (RSD) obtained from stability studies of Feox/GCE, Feox-bcd/GCE and Feox-cobcd/GCE, were out of experimental error. Thus results indicated that the sensors are single shoot sensors and as such can be used only once. Some inorganic ions were tested to check their levels of interference in BPA by square wave (SWV). The results indicated that 10- fold concentration of Ca^{+2}, Mg^{+2}, Cu^{+2}, Na^{+}, NO_3^{-}, Cl^{-}, SO_4^{-2} have no influence on the signals of BPA with deviations of 2.3%, 0.96%, and 0.8% for Feox, Feox-cobcd and Feox-bcd, respectively.

5.2 Iron oxide nanoparticles sensors response to TOP

5.2.1 Electrochemical property of TOP at iron-oxide modified glassy carbon electrode

In order to test our sensors response to others phenols, 4-tert-octyphenol was used. Figure 35 shows an overlay of cyclic voltammograms of 4-tert-octylphenol (TOP) at the bare GCE, Feox-bcd/GCE and Feox/GCE in aq. KCl (0.1 M).

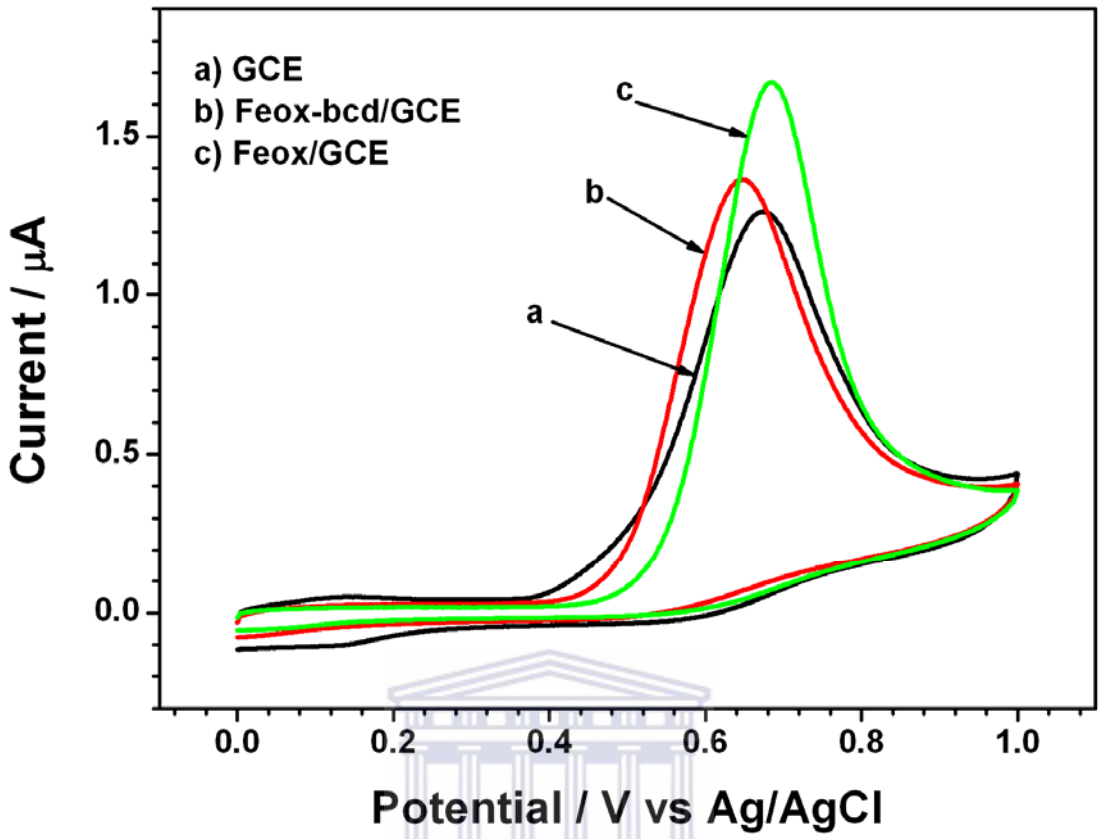

Figure 35: Cyclic voltammograms of TOP (50 x 10^{-6} M) at the bare GCE (curve a), Feox-bcd/GCE (curve b) and Feox (curve c) in aqueous KCl (0.1 M).

The response of the test sensors and control sensor were studied between 0 and 1000 mV where no redox peak occurred for both the modified and unmodified GCE in the blank supporting electrolyte. On addition of TOP to the supporting electrolyte, an irreversible oxidation peak was observed at all sensors (Fig. 35). Compared to the bare GCE (E_{pa} = 674 mV), the TOP oxidation peaks potential at Feox-bcd/GCE is observed at 647 mV and at Feox/GCE observed at 685 mV. Feox-bcd/GCE peak potential shift to less positive value compare to GCE and Feox/GCE. Thus, the iron-oxide material exhibited an electrocatalytic effect. This is actually an advantage gained over the bare GCE for sensing applications. The peak currents for Feox and Feox-bcd modified glassy carbon electrode were well enhanced when compared to the GCE but the highest being once again for the Feox-bcd/GCE. The iron-oxide film without incorporated β-CD showed the highest current-peak height and the

highest peak potential. For the Feox-bcd, the peak potential shifted to a lower value which was smaller by about 38 mV than that for Feox/GCE and by 27 mV from that of the bare GCE. The peak heights were increased significantly by 0.095 µA and 0.398 µA for Feox-bcd and Feox respectively compared to the bare GCE. For the modified electrodes and bare GCE in this work, the oxidation peaks of TOP were observed between 640 - 690 mV (vs Ag/AgCl). Therefore possible causes of the shift of the anodic peak potential to less positive for Feox-bcd/GCE could be the same like explained for BPA in section 5.1.1.

5.2.2 Amperometric TOP sensor

Figures 36 and 37, show cyclic voltammetric and square wave, respectively. Both figures show the responses of Feox-bcd/GCE at different concentrations of TOP in 0.1 M KCl at scan rate of 50 mV/s.

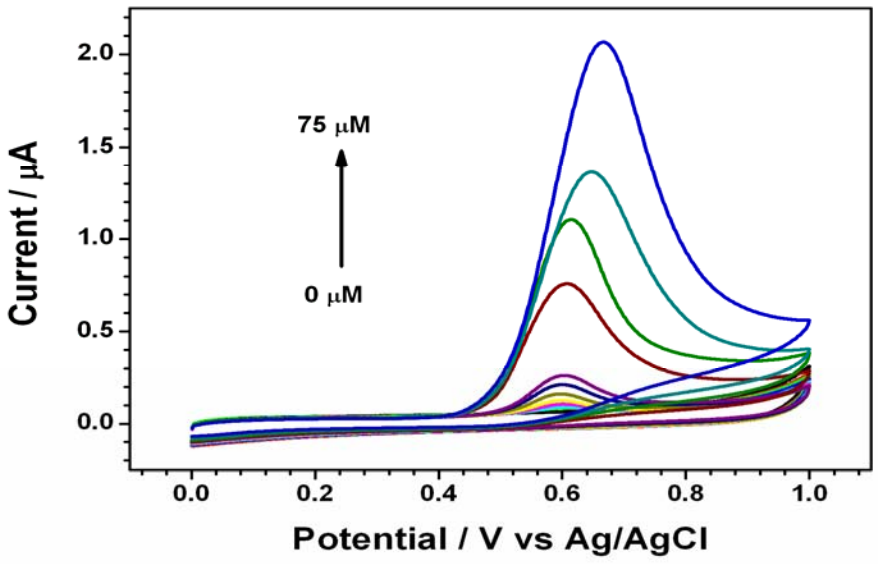

Figure 36: CV response of Feox-bcd/GCE at different concentration of TOP in 0.1 M KCl. Scan rate 50 mV/s

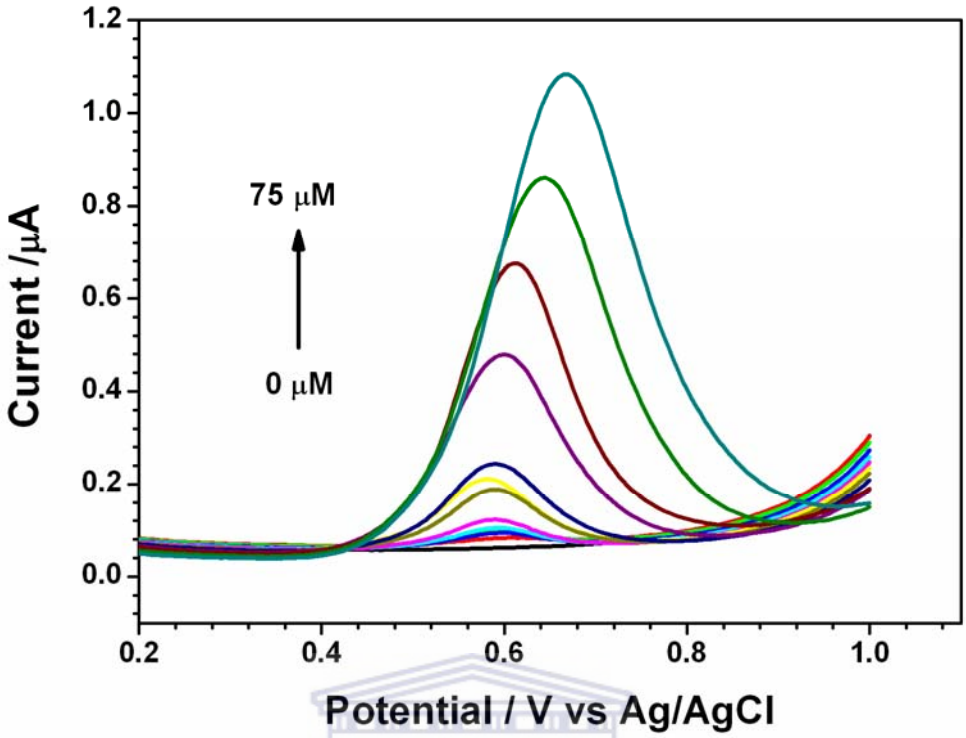

Figure 37: SWV response of Feox-bcd/GCE at different concentration of TOP in 0.1 M KCl. Scan rate 50 mV/s.

In both cases, the peak potentials shifted to more anodic values with increasing concentration. The possible reason may be the adsorption of the TOP on the surface of the film as reported in the literature by Takumi Sannomiya *et al*. [287] by investigating shift of potential with salt concentration on gold nanoparticles modified indium tin oxide (ITO) substrate and Palraj Kalimuthu and S. Abraham John [288] in the determination of folic acid in the presence of interferences using electropolymerized film of 5-amino-2-mercapto-1,3,4-thiadiazole (p-AMT) modified glassy carbon (GC) electrode.

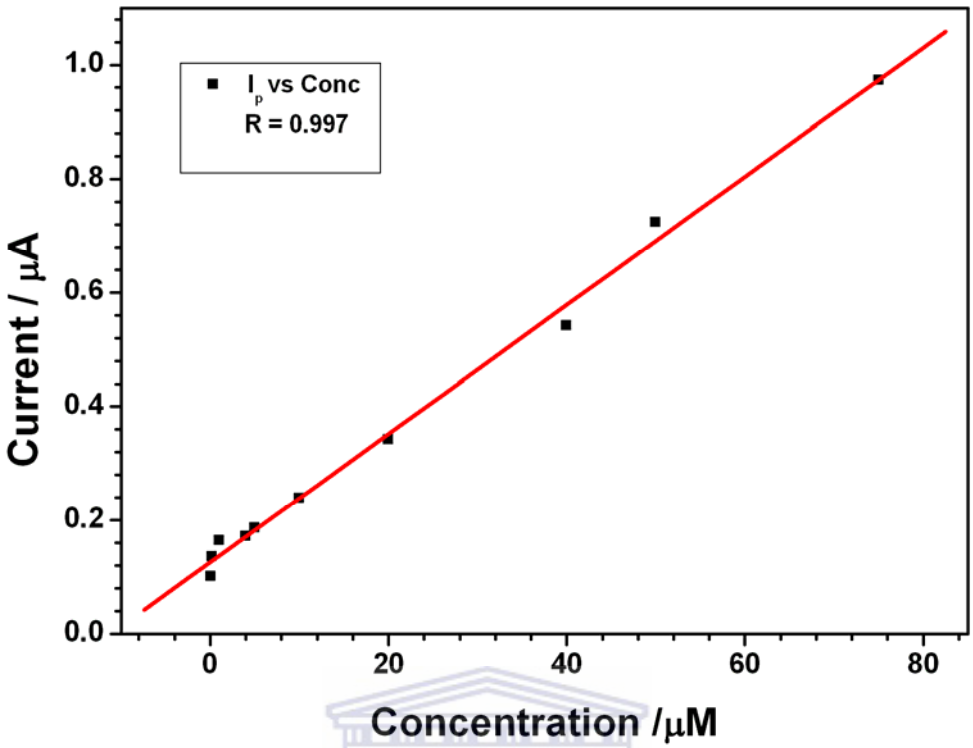

Figure 38: Calibration curve of peak current vs TOP concentration for iron oxide nanoparticle with beta cyclodextrin modified glassy carbon electrode.

As shown in Figure 38, the peak current increased linearly (R = 0.997) with increasing concentration of TOP in the range of 7 x 10^{-7} M to 75 x 10^{-6} M. The corresponding sensitivity and detection limits were 11.31 nA L/mol and 0.249 x 10^{-6} M, respectively and order of magnitude of linearity of 2.00.

5.3 Analysis of stoney ginger beer

A real sample application of the sensor Feox-bcd/GCE was demonstrated using a sample of a commercial soft drink known as STONEY GINGER BEER (SGB). Curve (b) in Figure 39 shows a typical CV recorded for the SGB sample alone (5% v/v) in aqueous KCl (0.1 M). Curve (a) the SGB was recorded in the presence of BPA (6.5 $x10^{-6}$M) after a standard-addition step. The SGB sample exhibited two anodic peaks (I and II) and one cathodic peak (I') at about 360, 600, and 300 mV. On addition of BPA standard, a third anodic peak appeared at +180 mV further from peak II of the SGB sample. Thus, our sensor did not detect any peak at the same position as the peak due to BPA. Furthermore, the level of resolution between these peaks guaranteed that there was no practical interference with BPA determination from the redox active components of this sample. In order to show the utility of the sensor in SGB sample matrix, an artificial real sample was prepared by spiking a standard solution of BPA into a portion of the SGB. The concentration of the spiked BPA (the unknown) was then determined by the standard addition method in a single-blind experiment. Four sensors were prepared simultaneously and their responses (peak heights) to $0.13x10^{-4}$ M BPA were first measured as external reference before recording the CVs of the unknown sample. Adding appropriate volumes of the BPA standard ($0.13x10^{-4}$ M) to four different portions of the contaminated Ginger beer, CVs were recorded for each after taking 500 µL aliquots into separate cells containing 10 mL aq. KCl. The calibration curve (Fig. 40) based on normalized peak heights indicated the BPA in the contaminated Ginger Beer to be between $0.124x10^{-3}$ and $0.136x10^{-3}$ M (130±6 µM). Actually, the BPA concentration added to the Ginger beer was $0.13x10^{-3}$ M.

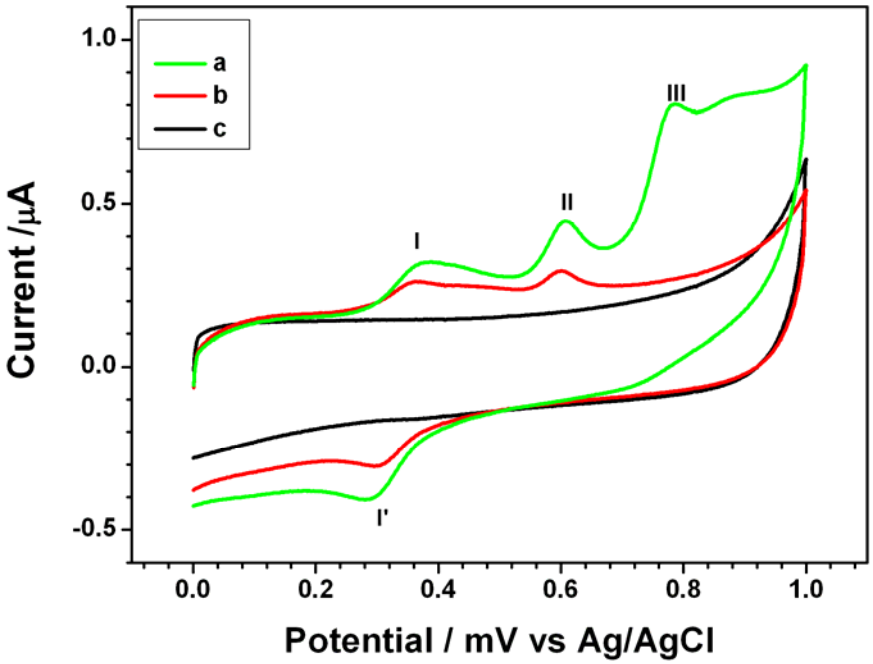

Figure 39: Cyclic voltammograms recorded in aqueous KCl for (a) SGB sample (5% v/v) in the presence of BPA (6.5 μM) and (b) SGB sample only (5% v/v). Curve (c) is the back ground CV for aqueous KCl.

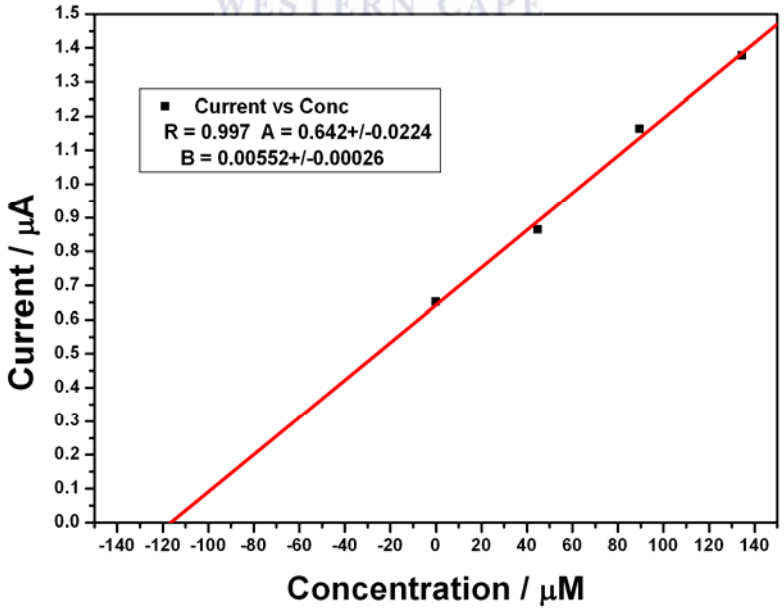

Figure 40: Calibration curve of standard addition run with four different electrodes (Sensors) used to estimate BPA concentration in contaminated ginger beer

CHAPTER 6

CONCLUSION AND RECOMMENDATIONS

6.1 Conclusion

Iron oxide nanoparticles were successfully prepared chemically in the presence and absence of β-cyclodextrin. No difference was found in the structure of nanomaterials synthesized in presence and absence of β-cyclodextrin. The inclusion complex between iron oxide nanoparticles and β-cyclodextrin were confirmed by ATR-FTIR analysis. Sensor measurements of BPA and TOP with the fabricated nanoparticles prepared in presence and absence of β-cyclodextrin modified glassy carbon electrode, in 0.1 M KCl showed that increase in concentration of BPA and TOP led to a proportional increase in catalytic current for both. The enhancement of the electron transfer is greater at the Iron oxide prepare in absence than in presence of β-cyclodextrin for BPA and TOP. The lowest oxidation potential was observed for the iron oxide films without β-cyclodextrin. However, the analytical figures of merit as an amperometric sensor based on cyclic voltammetric peak measurements were the best in the case of the iron oxide product which was synthesized in the presence of β-cyclodextrin. Its two orders of magnitude of linearity, sub-micromolar detection limit, and reproducibility with in experimental error make this sensor potentially exploitable for real sample analysis. The significantly shorter linearity range of the bare GCE indicated that the iron oxide product and its composites with β-cyclodextrin were less prone to passivation by BPA oxidation products. The GCE//Feox-bcd was demonstrated to be useful voltammetric sensor in a selected real sample matrix (Stoney Ginger Beer) with no interference from the

components of the sample. Further studies revealed that the sensors are single shoot for the analysis of phenolic endocrine disruptors.

6.2 Recommendations for future work

Further studies may be considered for the following aspects of the development of an electrochemical sensor for the detection of phenolic endocrine disruptors using iron oxide nanoparticles such as:

- Electrochemical deposition of iron oxide and its optimization.
- Chemical preparation of iron oxide in the presence of functionalized cyclodextrin.
- Chemical preparation of iron oxide in oxygen free environment.
- pH studies and hydrodynamic investigations.
- Selectivities of sensors based on the potential of the BPA and TOP.

REFERENCES

1. Kuch, H.M. and K. Ballschmiter, *Determination of Endocrine-Disrupting Phenolic Compounds and Estrogens in Surface and Drinking Water by HRGC−(NCI)−MS in the Picogram per Liter Range.* Environmental Science and Technology, 2001. **35** (15): p. 3201–3206.
2. NTP, *Draft NTP Brief on Bisphenol A*, in *National Toxicology Program; U.S. Department of Health and Human Services*. 2008.
3. Stuart, J.D., C.P. Capulong, K.D. Launer, and X. Pan, *Analyses of phenolic endocrine disrupting chemicals in marine samples by both gas and liquid chromatography-mass spectrometry.* Journal of Chromatography A, 2005. **1079**(1-2): p. 136-145.
4. Maffini, M.V., B.S. Rubin, C. Sonnenschein, and A.M. Soto, *Endocrine disruptors and reproductive health: The case of bisphenol-A.* Molecular and Cellular Endocrinology, 2006. **254-255**: p. 179-186.
5. Vílchez, J.L., A. Zafra, A. González-Casado, E. Hontoria, and M. del Olmo, *Determination of trace amounts of bisphenol F, bisphenol A and their diglycidyl ethers in wastewater by gas chromatography-mass spectrometry.* Analytica Chimica Acta, 2001. **431**(1): p. 31-40.
6. Rodriguez-Mozaz, S., M.J. López de Alda, and D. Barceló, *Monitoring of estrogens, pesticides and bisphenol A in natural waters and drinking water treatment plants by solid-phase extraction-liquid chromatography-mass spectrometry.* Journal of Chromatography A, 2004. **1045**(1-2): p. 85-92.
7. Ye, X., Z. Kuklenyik, L.L. Needham, and A.M. Calafat, *Automated On-Line Column-Switching HPLC-MS/MS Method with Peak Focusing for the Determination of Nine Environmental Phenols in Urine.* Analytical Chemistry, 2005. **77**(16): p. 5407-5413.

8. Iwuoha, E.I., A.R. Williams-Dottin, L.A. Hall, M. Aoife, G.N. Mathebe, M.R. Smyth, and K. Anthony, *Electrochemistry and application of a novel monosubstituted squarate electron-transfer mediator in a glucose oxidase-doped poly(phenol) sensor.* Pure and Applied Chemistry, 2004. **76**(4): p. 789–799.

9. Jolivet, J.-P., É. Tronc, and C. Chanéac, *Synthesis of iron oxide-based magnetic nanomaterials and composites.* Comptes Rendus Chimie, 2002. **5**(10): p. 659-664.

10. Gupta, A.K. and M. Gupta, *Synthesis and surface engineering of iron oxide nanoparticles for biomedical applications.* Biomaterials, 2005. **26**(18): p. 3995-4021.

11. Jolivet, J.-P., *Metal Oxide Chemistry and Synthesis. From Solution to Solid State*. 2000, Chichester: Wiley.

12. WHO/IPCS. *Global assessment of the state-of-the-science of endocrine disruptors. World Health Organization/International Program on Chemical Safety.* 2002; Available from: www.who.int/pcs/emerg_site/edc/global_edc_ch5. pdf.

13. Kavlock, R.J., G.P. Daston, C. Derosa, P. Fenner-Crisp, L.E. Gray, S. Kaatari, G. Lucier, M. Luster, M. J.Mac, C. Maczka, R. Miller, J. Moore, R. Rolland, G. Scott, D.M. Sheehan, T. Sinks, and H.A. Tilson, *Research Needs for the Risk Assessment of Health and Environmental Effects of Endocrine Disruptors: A Report of the U.S. EPA-Sponsored Workshop.* Environmental Health Perspectives Supplements, 1996. **104**(Supp l4): p. 715-740.

14. Katzenellenbogen, J.A., *The structural pervasiveness of estrogenic activity.* Environmental Health Perspectives, 1995. **103**: p. 99-101.

15. Krishnan, A., P. Stathis, S. Permuth, L. Tokes, and D. Feldman, *Bisphenol-A: an estrogenic substance is released from polycarbonate flasks during autoclaving.* Endocrinology, 1993. **132**(6): p. 2279-2286.

16. Newbold, R., *Cellular and molecular effects of devel opmental exposure to diethylstilbestrol: implications for other environmental estrogens.* Environmental Health Perspectives, 1995. **103**: p. 83-87.

17. Nimrod AC. and B. WH., *Environmental estrogenic effects of alkylphenol ethoxylates.* Critical Reviews in Toxicology, 1996. **26**: p. 335-364.

18. Swart, J.C., *The development and implementation of biomarker assays for estrogenic endocrine disruptors*, in *Medical Biosciences*. 2008, PhD thesis, University of the Western Cape: Cape Town.

19. White, R., S. Jobling, S.A. Hoare, J.P. Sumpter, and M.G. Parker, *Environmentally persistent alkylphenolic compounds are estrogenic.* Endocrinology, 1994. **135**: p. 175-182.

20. Michael, J.K., *Development of polyaniline nanotube electrocatalysts and sensor devices for phenolic-pollutants*, in *chemistry*. 2007, PhD thesis, University of the Western Cape: Cape Town.

21. *WHO/FAO, Bisphenol A (BPA) - Current state of knowledge and future actions by WHO and FAO*. 2009 30 JULY 2010]; Available from: http://www.who.int/foodsafety/publications/fs_management/No_05_Bisphenol_A_Nov09_en.pdf.

22. Allen E. and E. Doisy, *A ovarian hormone: preliminary report on its localization, extraction and partial purification and action in test animals.* Journal of the American Medical Association, 1923. **81**: p. 819.

23. Burlington, H. and V. Lindeman, *Effect of DDT on testes and secondary characters of white leghorn cockerels.* Proceedings of the Society for Experimental Biology and Medicine, 1950. **74**: p. 48-51.

24. Colborn, T., F.S. vomSaal, and A.M. Soto, *Developmental effects of endocrine disrupting chemicals in wildlife and humans.* Environmental Health Perspectives, 1993. **101**: p. 378-384.

25. Rodriquez-Mozaz, S., M.P. Marco, M.J.L.d. Alda, and D. Barceló, *Biosensors for environmental monitoring of endocrine disruptors: a review article.* Analalytical and Bioanalytical Chemistry, 2004. **378**: p. 588-598.

26. *United States Environmental Protection Agency (U.S.E.P.A), Special report on environmental endocrine disruption: an effects assessment and analysis*. 1997, Office of Research and Development: Washington, DC:.

27. Diamanti-Kandarakis, E., J.-P. Bourguignon, L.C. Giudice, R. Hauser, G.S. Prins, A.M. Soto, R.T. Zoeller, and A.C. Gore, *Endocrine-Disrupting Chemicals.* An Endocrine Society Scientific Statement: Endocrine Reviews, 2009. **30**(4): p. 293-342.

28. Giesy, J.P., K. Hilscherova, P.D. Jones, K. Kannan, and M. Machala, *Cell bioassays for detection of aryl hydrocarbon (AhR) and estrogen receptor (ER) mediated activity in environmental samples.* Marine Pollution Bulletin, 2002. **45**(1-12): p. 3-16.

29. Payne, A.H. and B. Dale, *Overview of Steroidogenic Enzymes in the Pathway from Cholesterol to Active Steroid Hormones.* Endocrine Reviews, 2004. **25**: p. 947–970.

30. Encora, *Coastal Portal: Endocrine disrupting compounds*, in *Encora Wiki*, Coastal Wiki.

31. Keith, L., *Environmental endocrine disruptors.* Pure and Applied Chemistry, 1998. **70**: p. 2319-2326.

32. Baker, V., *Session 5: Hot Topics in In Vitro Toxicology. Long-Term Effects, Hormonal Effects, Endocrine disrupters. Endocrine disrupters-testing strategies to assess human hazard.* Toxicology in Vitro, 2001. **15**: p. 413–419.

33. Kuiper, G.G.J.M., J.G. Lemmen, B. Carlsson, J.C. Corton, S.H. Safe, P.T. van der Saag, B. van der Burg, and J.-A. Gustafsson, *Interaction of Estrogenic Chemicals and Phytoestrogens with Estrogen Receptor {beta}.* Endocrinology, 1998. **139**(10): p. 4252-4263.

34. Isselbacher, K.J., A.B. Braunwald, J.D. Wilson, J.B. Martin, A.S. Fauci, and D.L. Kasper, *Harrison's Principles of Internal Medicine*, McGraw-Hill, Editor. 1994: New York.

35. Gaido, K.W., D.P. McDonnell, K.S. Korach, and S.H. Safe, *Estrogenic activity of chemical mixtures: is there synergism? CIIT activities.* Chemical Industry Institute of Toxicology, 1997. **2**: p. 1-7.

36. Villeneuve, D., A.L. Blankenship, and J.P. Giesy, eds. *Interactions between environmental xenobiotics and estrogen receptor-mediated responses. In: Denison, M.S., Helferich, W.G. (Eds.), Toxicant– Receptor Interactions.* 1998, Taylor and Francis: Philadelphia, PA, USA, . 69–99.

37. Stahlschmidt-Allner, P., B. Allner, J. Rombke, and T. Knacker, *Endocrine disrupters in the aquatic environment.* Environmental Science and Pollution Research, 1997. **4**: p. 155–162.

38. Markiewicz, L., J. Garey, H. Adlercreutz, and E. Gurpide, *In vitro bioassays of non-steroidal phytoestrogens.* Steroid Biochemistry and Molecular Biology, 1993. **45**: p. 399–405.

39. Wang, C., T. Makela, T. Hase, H. Adlercreutz, and M.S. Kurzer, *Lignans and flavanoids inhibit aromatase enzyme in human preadipocytes.* Steroid Biochemistry and Molecular Biology, 1994. **50**: p. 205–212.

40. Legler, J., C. Brink, A. Brower, D. Vethaak, P. VanDerSaag, T. Murk, and B. Burg, *Assessment of (anti)estrogenic compounds using a stably transfected luciferase*

reporter gene assay in the human T47-D breast cancer cell line. Organohalogen Compound, 1998. **37**: p. 265–268.

41. Nimrod, A.C. and W.H. Benson, *Xenobiotic interaction with and alteration of channel catfish estrogen receptor.* Toxicology and Applied Pharmacology, 1997. **147**: p. 381–390.

42. Bail, J.C.L., F. Varnat, J.C. Nicolas, and G. Habrioux, *Estrogenic and antiproliferative activities on MCF-7 human breast cancer cells by flavanoids.* Cancer Letters, 1998. **130**: p. 209–216.

43. Safe, S. and K. Gaido, *Phytoestroggounds and anthropogenic estrogenic compounds.* Environmental Toxicology and Chemistry, 1998. **17**: p. 119–126.

44. Celius, T., T.B. Haugen, T. Grotmol, and B.T. Walther, *A sensitive zonagenetic assay for rapid in vitro assessment of estrogenic potency of xenobiotics and mycotoxin.* Environmental Health Perspectives, 1999. **107**: p. 63–68.

45. Sohoni, P. and J.P. Soto, *Several environmental oestrogens are also antiandrogens.* Journal of Endocrinology, 1998. **158**: p. 327–339.

46. Taylor, C.M., B. Blanchard, and D.T. Zava, *Estrogen receptormediated and cytotoxic effects of the antiestrogens tamoxifen and 4-hydroxytamoxifen.* Cancer Research, 1984. **44**: p. 1409–1414.

47. Favoni, R.E. and A. Cupis, *Steroidal and nonsteroidal oestrogen antagonists in breast cancer: basic and clinical appraisal.* Trends in Pharmacological Sciences, 1998. **19**: p. 406–415.

48. Ramkumar, T. and S. Adler, *Differential positive and negative transcriptional regulation by tamoxifen.* journal of Endocrinology, 1995. **136**: p. 536–542.

49. Shelby, M.D., R.R. Newbold, D.B. Tully, K. Chae, and V.L. Davis, *Assessing environmental chemicals for estrogenicity using a combination of in vitro and in vivo assays.* Environmental Health Perspectives, 1996. **104**: p. 1296–1300.

50. Routledge, E.J., J. Parker, J. Odum, J. Ashby, and J.P. Sumpter, *Some alkyl hydroxy benzoate preservatives (parabens) are estrogenic.* Toxicology and Applied Pharmacology, 1998. **153**: p. 12–19.

51. Soto, A.M., C. Sonnenschein, K.L. Chung, M.F. Fernandez, N. Olea, and F.O. Serrano, *The E-SCREEN assay as a tool to identify estrogens: an update on estrogenic environmental pollutants.* Environmental Health Perspectives, 1995. **103**(Suppl. 7): p. 113–122.

52. Sumpter, J.P. and S. Jobling, *Vitellogenesis as a biomarker for estrogenic contamination of the aquatic environment.* Environmental Health Perspectives, 1995. **103**(Suppl. 7): p. 173–178.

53. Kelce, W.R., C.R. Stone, S.C. Laws, L.E. Gray, J.A. Kemppainen, and E.M. Wilson, *Persistent DDT metabolite p,p0-DDE is a potent androgen receptor antagonist.* Nature, 1995. **375**: p. 581–585.

54. Klotz, D.M., B.S. Beckman, S.M. Hill, J.A. Mclachlan, M.R. Walters, and S.F. Arnold, *Identification of environmental chemicals with estrogenic activity using a combination of in vitro assays.* Environmental Health Perspectives, 1996. **104**(10): p. 1084–1089.

55. Soto, A.M., K.L. Chung, and C. Sonnenschein, *The pesticides endosulfan, toxaphene, and dieldrin have estrogenic effects on human estrogen-sensitive cells.* Environmental Health Perspectives, 1994. **102**: p. 380–383.

56. Petit, F., P. Le-Goff, J.P. Cravedi, Y. Valotaire, and F. Pakdel, *Two complementary bioassays for screening the estrogenic potency of xenobiotics: recombinant yeast for*

trout estrogen receptor and trout hepatocyte cultures. Molecular Endocrinology, 1997. **19**: p. 321–335.

57. Asmathbanu, I. and B.B. Kaliwal, *Temporal effect of methyl parathion on ovarian compensatory hypertrophy, follicular dynamics and estrous cycle in hemicastrated albino rats.* Journal of Basic and Clinical Physiology and Pharmacology, 1997. **8**: p. 237–254.

58. Cranmer, J.M., M.F. Cranmer, and P.T. Goad, *Prenatal chlordane exposure: effects on plasma corticosterone concentrations over the lifespan of mice.* Environmental Research, 1984. **35**: p. 204–210.

59. Go, V., J. Garey, M.S. Wolff, and B.G.T. Pogo, *Estrogenic potential of certain pyrethroid compounds in the MCF-7 human breast carcinoma cell line.* Environmental Health Perspectives, 1999. **107**: p. 173–177.

60. Kelce, W.R., E. Monosson, M.P. Gamcsik, S.C. Laws, and L.E. Gray, *Environmental hormone disruptors: evidence that vinclozolin developmental toxicity is mediated by antiandrogenic metabolites.* Toxicology and Applied Pharmacology, 1994. **126**: p. 267–285.

61. Tennant, M.K., D.S. Hill, J.C. Eldridge, L.T. Wetzel, C.B. Breckenridge, and J.T. Stevens, *Possible antiestrogenic properties of chloro-s-triazines in rat uterus.* Toxicology and Environmental Health, 1994. **43**: p. 183–196.

62. Matthiessen, P. and P.E. Gibbs, *Critical appraisal of the evidence for tributyltin-mediated endocrine disruption in mollusks.* Environmental Toxicology and Chemistry 1998. **17**: p. 37–43.

63. Jobling, S., T. Reynolds, R. White, M.G. Parker, and J.P. Sumpter, *A variety of environmental persistant chemicals, including some phtalate plasticizers, are weakly estrogenic.* Environmental Health Perspectives, 1995. **103**: p. 582–587.

64. Servos, M.R., *Review of the aquatic toxicity, estrogenic responses and bioaccumulation of alkylphenols and alkylphenol polyethoxylates.* Water Quality Research Journal of Canada, 1999. **34**: p. 123–177.

65. Beard, A.P., P.M. Bartlewski, and N.C. Rawlings, *Endocrine and reproductive function in ewes exposed to the organochlorine pesticides lindane or pentachlorophenol.* Toxicology and Environmental Health, 1999. **56**: p. 23–46.

66. Safe, S. and V. Krishnan, *Cellular and molecular biology of aryl hydrocarbon (AH) receptor mediated gene expression.* Archives of Toxicology, 1995.(Suppl. 7): p. 99–115.

67. Joyeux, A., P. Balaguer, P. Germain, A.M. Boussioux, M. Pons, and J.C. Nicolas, *Engineered cell lines as a tool for monitoring biological activity of hormone analogs.* Analytical Biochemistry, 1997. **249**: p. 119–130.

68. Matta, M.B., C. Cairncross, and R.M. Kocan, *Possible effects of polychlorinated biphenyls on sex determination in rainbow trout.* Environmental Toxicology and Chemistry, 1998. **17**: p. 26–29.

69. Kramer, V.J., W.G. Helferich, A. Bergman, E. Klasson-Wehler, and J.P. Giesy, *Hydroxylated polychlorinated biphenyl metabolites are anti-estrogenic in a stably transfected human breast adenocarcinoma (MCF7) cell line.* Toxicology and Applied Pharmacology, 1997. **144**: p. 363–376.

70. Chaloupka, K., V. Krishnan, and S. Safe, *Polynuclear aromatic hydrocarbon carcinogens as antiestrogens in MCF-7 human breast cancer cells: role of the Ah receptor.* Carcinogenesis, 1992. **12**: p. 2233–2239.

71. Tran, D.Q., C.F. Ide, J.A. Mclachlan, and S.F. Arnold, *The antiestrogenic activity of selected polynuclear aromatic hydrocarbons in yeast expressing human estrogen*

receptor. Biochemical and Biophysical Research Communications, 1996. **229**: p. 102–108.

72. Clemons, J.H., L.M. Allan, C.H. Marvin, Z. Wu, B.E. McCarry, D.W. Bryant, and T.R. Zacharewski, *Evidence Of estrogen- and TCDD-like activities in crude and fractionated extracts of PM10 air particulate material using in vitro gene expression assay.* Environmental Science and Technology, 1998. **32**: p. 1853–1860.

73. Santodonato, J., *Review of the estrogenic and antiestrogenic activity of polycyclic aromatic hydrocarbons: relationship to carcinogenicity.* Chemosphere, 1997. **34**: p. 835–848.

74. Laskey, J.W. and P.V. Phelps, *Effect of cadmium and other metal cations on in vitro leydig cell testosterone production.* Toxicology and Applied Pharmacology, 1991. **108**: p. 296–306.

75. Ricard, A.C., C. Daniel, P. Anderson, and A. Hontela, *Effects of subchronic exposure to cadmium chloride on endocrine and metabolic functions in rainbow trout Oncorhynchus my kiss.* Archives of Environmental Contamination and Toxicology, 1998. **34**: p. 377–381.

76. Lafuente, A., A. Blanco, N. Marquez, E. Alvarez-Demanuel, and A.I. Esquifino, *Effects of acute and subchronic cadmium administration on pituitary hormone secretion in rat.* Revista Española de Fisiología, 1997. **53**: p. 265–269.

77. Ronis, M.J., J. Gandy, and T. Badger, *Endocrine mechanisms underlying reproductive toxicity in the developing rat chronically exposed to dietary lead.* Toxicology and Environmental Health, 1998. **54**: p. 77–99.

78. Advameg, I. *Endocrine Disruption*. Pollution Issues 2010 [cited 2010 05 May 2010]; Available from: http://www.pollutionissues.com/Ec-Fi/Endocrine-Disruption.html.

79. Carlsen. E., A. Giwercman, N. Keiding, and N.E. Skakkebaek, *Evidence for decreasing quality of semen during last 50 years.* British Medical Journal, 1992. **305**: p. 609-613.

80. Swan, S.H., E.P. Elkin, and L. Fenster, *The question of declining sperm density revisited: an analysis of 101 studies published 1934-1996.* Environmental Health Perspectives, 2000. **Oct; 108**(10): p. 961-966.

81. Europa. *Endocrine disrupters*. 20/02/2007 06 May 2010]; Available from: http://ec.europa.eu/environment/endocrine/definitions/affect_en.htm.

82. McLachlan, J., *Environmental signaling: what embryos and evolution teach us about endocrine disrupting chemicals.* Endocrine Reviews, 2001. **22**: p. 319-341

83. Gore, A. and D. Crews, *Environmental endocrine disruption of brain and behavior.* Hormones, Brain and Behavior, ed. A.A. Pfaff DW, Etgen A, Fahrbach S, Rubin R. 2009, San Diego: Academic Press. 1789–1816.

84. Newbold, R.R., E. Padilla-Banks, and W.N. Jefferson, *Adverse Effects of the Model Environmental Estrogen Diethylstilbestrol Are Transmitted to Subsequent Generations.* Endocrinology, 2006. **147**(6): p. S11–S17.

85. Gail, P.S., W.-Y. Tang, J. Belmonte, and S.-M. Ho, *Developmental exposure to bisphenol A increases prostate cancer susceptibility in adult rats: epigenetic mode of action is implicated.* Cancer Research, 2006. **66**(11): p. 5624-5632.

86. NIEHS. *Endocrine Disruptors*. 2006 June 2006 08 May 2010]; Available from: http://www.niehs.nih.gov/.

87. Newbold, R.R., R.B. Hanson, W.N. Jefferson, B.C. Bullock, J. Haseman, and J.A. McLachlan, *Proliferative lesions and reproductive tract tumors in male descendants of mice exposed developmentally to diethylstilbestrol.* Carcinogenesis, 2000. **Jul;21**(7): p. 1355-1363.

88. Newbold, R.R. and J.G. Liehr, *Induction of Uterine Adenocarcinoma in CD-1 Mice by Catechol Estrogens.* Cancer Research, 2000. **60**: p. 235-237.

89. Fatoki, O.S. and B.O. Opeolu, *Studies on the occurrence and quantification of phenolic endocrine disruptors in water.* Scientific Research and Essay, 2009. **4**(12): p. 1415-1422.

90. Toniolo, R., A. Pizzariello, S. Susmel, N. Dossi, A.P. Doherty, and G. Bontempelli, *An Anionic-Liquid based probe for sequential preconcentration from headspace and direct voltammetric detection of phenols in wastewaters.* Electroanalysis, 2007. **19**(19-20): p. 2141-2148.

91. Barlow, R.J. and J.A.P. Johnson, *Early Life Exposure to Phenols and Breast Cancer Risk in Later Years: fact sheet on phenols*. 2007, University of California, Bay Area Breast Cancer and the Environment Research Center COTC San Francisco.

92. Huang, J., X. wang, Q. Jin, Y. Liu, and Y. Wang, *Removal of phenol from aqueous solution by adsorption onto OTMAC-modified attapulgite.* Journal of Environmental Management, 2007. **84**: p. 229-236.

93. Chaliha, S., K.G. Bhattaryya, and P. Paul, *Catalytic destruction of 4- chlorophenol in water.* Clean, 2008. **36**(5-6): p. 488-497.

94. Gabriel, L.P.F., M. Cyris, W. Giger, and H.E. Kohler, *ipso-substitution: a general biochemical and biodegradation mechanism to cleave alpha-quaternary alkylphenols and bisphenol A.* Chemistry and Biodiversity, 2007. **4**(9): p. 2123-2137.

95. Schmidt-Baumler, K., T. Heberer, and H.J. Stan, *Occurrence and distribution of organic contaminants in the aquatic system in Berlin part II: Substituted phenols in Berlin surface water.* Acta Hydrochimica et Hydrobiologica, 1999. **27**(3): p. 143-149.

96. Jordan, W., H.V. Barneveld, O. Gerlich, and M. Kleine-Boymann, *Phenol*, in *Ullmann's encyclopedia of industrial chemistry*. 1991, Vch Verlagsgesellschaft. p. 299-312.

97. Wallace, J., *Phenol*, in *Kirk-Othmer encyclopedia of chemical technology*. 1996, John Wiley and Sons. p. 592- 602.

98. Scorecard. *The Pollution Information Site, Chemical: Phenol,*. 2005 [cited 2010 13 May]; Available from: http://www.scorecard.org/chemical-profiles/pesticides.tcl?edf_substance_id=108%2d95%2d2.

99. Gupta, Y.K., S. Sharma, I.S. Yadav, and D. Mohan, *Utilization of bagasse fly ash generated in the sugar industry for the removal and recovery of phenol and p-Nitrophenol from wastewater.* Journal of Chemical Technology and Biotechnology, 1998. **71**: p. 180-186.

100. Amiri, F., M.M. Rahman, H. Bornick, and E. Worch, *Sorption behaviour of phenols on natural sandy aquifer material during flow through column experiments: The effect of pH.* Acta Hydrochimica et Hydrobiologica, 2004. **32**(3): p. 214-224.

101. Sulisti, I.A., C. Watson, and E. Senior, *Studies on the co-disposal of o-cresol with municipal refuse.* Journal of Chemical Technology and Biotechnology, 1996. **65**: p. 72-80.

102. Hartung, R., D. Lenoir, B. Henkelmann, S. Schulte-Hostede, and K. Schramm, *Reductive degradation of poly chlorinated phenols by Pd/c formate: An ecoefficient remediation method for aqueous chlorinated phenols.* Clean, 2007. **35**(3): p. 235-238.

103. SHEN, G., G. YU, C. Zhenxiao, and Z. Zulin, *Development of an analytical method to determine phenolic endocrine disrupting chemicals in sewage and sludge by GC/MS.* Chinese Science Bulletin, 2005. **50**(23): p. 2681-2687.

104. Liu, Z.-h., Y. Kanjo, and S. Mizutani, *Removal mechanisms for endocrine disrupting compounds (EDCs) in wastewater treatment -- physical means, biodegradation, and chemical advanced oxidation: A review.* Science of the Total Environment, 2009. **407**(2): p. 731-748.

105. Li, C., X.Z. Li, N. Graham, and N.Y. Gao, *The aqueous degradation of bisphenol A and steroid estrogens by ferrate.* Water Research, 2008. **42**(1-2): p. 109-120.

106. H iroshi, Y., M.L. Howard, S. Yoshihisa, and M. Masatoshi, *Effects of Physical-Chemical Characteristics on the Sorption of Selected Endocrine Disruptors by Dissolved Organic Matter Surrogates.* Environmental Science and Technology, 2003. **37**: p. 2646-2657.

107. Vega, D., L. Agüí, A. González-Cortés, P. Yáñez-Sedeño, and J.M. Pingarrón, *Electrochemical detection of phenolic estrogenic compounds at carbon nanotube-modified electrodes.* Talanta, 2007. **71**(3): p. 1031-1038.

108. Brossa, L., E. Pocurull, F. Borrull, and R.M. Marce, *A Rapid Method for Determining Phenolic Endocrine Disrupters in Water Samples.* Chromatographia, 2002. **56**: p. 573-576.

109. Saad, B., N.H. Haniff, M. Idiris Saleh, N. Hasani Hashim, A. Abu, and N. Ali, *Determination of ortho-phenylphenol, diphenyl and diphenylamine in apples and oranges using HPLC with fluorescence detection.* Food Chemistry, 2004. **84**(2): p. 313-317.

110. Thompson, R., *Determination of phenolic disinfectant agents in commercial formulations by liquid chromatography.* Journal of the Association of Official Analytical Chemists International, 2001. **84**(3): p. 815-822.

111. Fa-Qiong, Z., J. Li, and B.-Z. Zeng, *Coupling of ionic liquid-based headspace single-drop microextraction with GC for sensitive detection of phenols.* Journal of Separation Science, 2008. **31**: p. 3045-3049.

112. Petrovic, M. and D. Barcelo, *Determination of anionic and nonionic surfactants, their degradation products, and endocrine-disrupting compounds in sewage sludge by liquid chromatography/mass spectrometry.* Analytical Chemistry, 2000. **72**(19): p. 4560.

113. Wissiack, R., E. Rosenberg, and M. Grasserbauer, *Comparison of different sorbent materials for on-line solid-phase extraction with liquid chromatography-atmospheric pressure chemical ionization mass spectrometry of phenols.* Journal of Chromatography A, 2000. **896**: p. 159.

114. Takao, Y., H.C. Lee, Y. Ishibashi, S. Kohra, N. Tominaga, and K. Arizono, *Fast screening method for bisphenol A in environmental water and in food by solid-phase microextrac- tion (SPME).* Journal of Health Science, 1999. **45**: p. 39.

115. Mauricio, R., M. Diniz, M. Petrovic, L. Ameral, I. Pers, and F.B.D. Santana, *AA characterization of selected endocrine disruptor compounds in a Portuguese wastewater treatment plant.* Environmental Monitoring and Assessment, 2006. **118**: p. 75-87.

116. Arditsoglou, A. and D. Voutsa, *Determination of phenolic and steroid endocrine disrupting compounds in environmental matrices.* Environmental Science and Pollution Research, 2008. **15**(3): p. 228-236.

117. Bonoli, M., M. Montanucci, T. Gallina Toschi, and G. Lercker, *Fast separation and determination of tyrosol, hydroxytyrosol and other phenolic compounds in extra-virgin olive oil by capillary zone electrophoresis with ultraviolet-diode array detection.* Journal of chromatography A, 2003. **1011**(1-2): p. 163-172.

118. Vaher, M. and M. Koel, *Separation of polyphenolic compounds extracted from plant matrices using capillary electrophoresis.* Journal of chromatography A, 2003. **990**(1-2): p. 225-230.

119. Xiao, J.-p., X.-f. Wang, Q.-x. Zhou, X.-y. Fan, X.-f. Su, H.-h. Bai, and H.-j. Duan, *Rapid determination of phenolic compounds in water samples by alternating-current oscillopolarographic titration.* Journal of Environmental Sciences, 2007. **19**(5): p. 622-627.

120. Zhan, Y.F. and Y.Q. Zhao, *Advances of oscillopolarographic titration.* Journal of Analytical Science, 1999. **15**(4): p. 338–344.

121. Ding, Y., A. Ayon, and C.D. García, *Electrochemical detection of phenolic compounds using cylindrical carbon-ink electrodes and microchip capillary electrophoresis.* Analytica Chimica Acta, 2007. **584**(2): p. 244-251.

122. Campuzano, S., B. Serra, M. Pedrero, F. Villena, and J. Pingarron, *Amperometric flow-injection determination of phenolic compounds at self-assembled monolayer-based tyrosinase biosensors.* Analytica Chimica Acta, 2003. **494**: p. 187-197.

123. Cummings, E.A., S. Linquette-Mailley, P. Mailley, S. Cosnier, B.R. Eggins, and E.T. McAdams, *A comparison of amperometric screen-printed, carbon electrodes and their application to the analysis of phenolic compounds present in beers.* Talanta, 2001. **55**(5): p. 1015-1027.

124. Gaspar, S., K. Habermüller, E. Csöregi, and W. Schuhmann, *Hydrogen peroxide sensitive biosensor based on plant peroxidases entrapped in Os-modified polypyrrole films.* Sensors and Actuators B: Chemical, 2001. **72**(1): p. 63-68.

125. Ngundi, M.M., O.A. Sadik, T. Yamaguchi, and S.-i. Suye, *First comparative reaction mechanisms of [beta]-estradiol and selected environmental hormones in a redox environment.* Electrochemistry Communications, 2003. **5**(1): p. 61-67.

126. Pen˜alver, A., E. Pocurull, F. Borrull, and R.M. Marce, *Method based on solid-phase microextraction–high-performance liquid chromatography with UV and electrochemical detection to determine estrogenic compounds in water samples.* Journal of Chromatography A, 2002. **964**: p. 153–160.

127. Kuramitz, H., M. Matsushita, and S. Tanaka, *Electrochemical removal of bisphenol A based on the anodic polymerization using a column type carbon fiber electrode.* Water Research, 2004. **38**(9): p. 2331-2338.

128. Kuramitz, H., J. Saitoh, T. Hattori, and S. Tanaka, *Electrochemical removal of p-nonylphenol from dilute solutions using a carbon fiber anode.* Water Research, 2002. **36**(13): p. 3323-3329.

129. Huang, W., *Voltammetric Determination of Bisphenol A Using a Carbon Paste Electrode Based on the Enhancement Effect of Cetyltrimethylammonium Bromide (CTAB).* Bulletin of the Korean Chemical Society, 2005. **26**: p. 1560-1564.

130. Wang, F., J. Yang, and K. Wu, *Mesoporous silica-based electrochemical sensor for sensitive determination of environmental hormone bisphenol A.* Analytica Chimica Acta, 2009. **638**(1): p. 23-28.

131. Yin, H., L. Cui, S. Ai, H. Fan, and L. Zhu, *Electrochemical determination of bisphenol A at Mg-Al-CO3 layered double hydroxide modified glassy carbon electrode.* Electrochimica Acta, 2010a. **55**(3): p. 603-610.

132. Yin, H.-s., Y.-l. Zhou, and S.-y. Ai, *Preparation and characteristic of cobalt phthalocyanine modified carbon paste electrode for bisphenol A detection.* Journal of Electroanalytical Chemistry, 2009. **626**(1-2): p. 80-88.

133. Chauke, V., F. Matemadombo, and T. Nyokong, *Remarkable sensitivity for detection of bisphenol A on a gold electrode modified with nickel tetraamino phthalocyanine*

containing Ni-O-Ni bridges. Journal of Hazardous Materials, 2010. **178**(1-3): p. 180-186.

134. Yin, H., Y. Zhou, S. Ai, Q. Chen, X. Zhu, X. Liu, and L. Zhu, *Sensitivity and selectivity determination of BPA in real water samples using PAMAM dendrimer and CoTe quantum dots modified glassy carbon electrode.* Journal of Hazardous Materials, 2010b. **174**(1-3): p. 236-243.

135. Portaccio, M., D. Di Tuoro, F. Arduini, M. Lepore, D.G. Mita, N. Diano, L. Mita, and D. Moscone, *A thionine-modified carbon paste amperometric biosensor for catechol and bisphenol A determination.* Biosensors and Bioelectronics, 2010. **25**(9): p. 2003-2008.

136. Yin, H., Y. Zhou, J. Xu, S. Ai, L. Cui, and L. Zhu, *Amperometric biosensor based on tyrosinase immobilized onto multiwalled carbon nanotubes-cobalt phthalocyanine-silk fibroin film and its application to determine bisphenol A.* Analytica Chimica Acta, 2010c. **659**(1-2): p. 144-150.

137. Hendricks, N.R., T.T. Waryo, O. Arotiba, N. Jahed, P.G.L. Baker, and E.I. Iwuoha, *Microsomal cytochrome P450-3A4 (CYP3A4) nanobiosensor for the determination of 2,4-dichlorophenol--An endocrine disruptor compound.* Electrochimica Acta, 2009. **54**(7): p. 1925-1931.

138. Méndez, M.A., M.F. Suárez, and M.T. Cortés, *Electrochemical impedance spectroscopy of diluted solutions of Bisphenol A.* Journal of Electroanalytical Chemistry, 2006. **590**(2): p. 181-189.

139. Inoue, K., K. Kato, Y. Yoshimura, T. Makino, and H. Nakazawa, *Determination of bisphenol A in human serum by high-performance liquid chromatography with multi-electrode electrochemical detection.* Journal of Chromatography B: Biomedical Sciences and Applications, 2000. **749**(1): p. 17-23.

140. Britt, E.E., *"Bisphenol A under scrutiny". Chemical and Engineering News.* American Chemical Society, 2008. **86**(22): p. 36-39.

141. Saal, F.S.v., B.T. Akingbemi, S.M. Belcher, L.S. Birnbaum, D.A. Crain, M. Eriksen, F. Farabollini, J.r.L.J. Guillette, R. Hauser, J.J.H. HoSM, P.A. Hunt, T. Iguchi, S. Jobling, J. Kanno, R.A. Keri, K.E. Knudsen, H. Laufer, G.A. LeBlanc, M. Marcus, J.A. McLachlan, J.P. Myers, A. Nadal, R.R. Newbold, N. Olea, G.S. Prins, C.A. Richter, B.S. Rubin, C. Sonnenschein, A.M. Soto, C.E. Talsness, J.G. Vandenbergh, L.N. Vandenberg, D.R. Walser-Kuntz, C.S. Watson, W.V. Welshons, Y. Wetherill, and R.T. Zoeller, *Reproductive Toxicology 24(2): 2007.* Reproductive Toxicology, 2007. **24**: p. 131-138.

142. Brotons, J.A., M.F. Olea-Serrano, M. Villalobos, V. Pedraza, and N. Olea, *Xenoestrogens Released from Lacquer Coatings in Food Cans.* Environmental Health Perspectives, 1995. **103**(6): p. 608-612.

143. Calafat, A.M., X. Ye, L.Y. Wong, J.A. Reidy, and L.L. Needham, *Exposure of the U.S. population to bisphenol A and 4-tertiary-octylphenol: 2003–2004.* Environmental Health Perspectives, 2008. **116**: p. 39–44.

144. Lang, I.A., T.S. Galloway, A. Scarlett, W.E. Henley, M. Depledge, R.B. Wallace, and D. Melzer, *Association of Urinary Bisphenol A Concentration With Medical Disorders and Laboratory Abnormalities in Adults.* Journal of the American Medical Association, 2008. **300**(300): p. 1303.

145. Rubin, B. and A. Soto, *Bisphenol A: Perinatal exposure and body weight.* Molecular and Cellular Endocrinology, 2009. **304**(1-2): p. 55–62.

146. Kashiwagi, K., Furuno, Kitamura, Ohta, Sugihara, Utsumi, Hanada, and Taniguchi, *Disruption of Thyroid Hormone Function by Environmental Pollutants.* Journal of Health Science, 2009. **55**: p. 147.

147. Brisken, C., *Endocrine Disruptors and Breast Cancer.* CHIMIA International Journal for Chemistry, 2008. **62**: p. 406–409.

148. Zhu, H., J. Zheng, X. Xiao, S. Zheng, K. Dong, J. Liu, and Y. Wang, *Environmental endocrine disruptors promote invasion and metastasis of SK-N-SH human neuroblastoma cells.* Oncology reports, 2010. **23**(1): p. 129–139.

149. Monje, L., J. Varayoud, M. Muñoz-De-Toro, H. Luque, and G. Ramos, *Neonatal exposure to bisphenol a alters estrogen-dependent mechanisms governing sexual behavior in the adult female rat.* Reproductive toxicology, 2009. **28**(4): p. 435–442.

150. Nagel, S., F. Vom Saal, K. Thayer, M. Dhar, M. Boechler, and W. Welshons, *Relative binding affinity-serum modified access (RBA-SMA) assay predicts the relative in vivo bioactivity of the xenoestrogens bisphenol a and octylphenol.* Environmental Health Perspectives, 1997. **105**(1): p. 70–76.

151. Heemken, O.P., H. Reincke, B. Stachel, and N. Theobald, *The Occurrence of Xenoestrogens in the Elbe River and the North Sea.* Chemosphere, 2001. **45**: p. 245-259.

152. Xie, Z., S. Lakaschus, R. Ebinghaus, A. Caba, and W. Ruck, *Atmospheric concentrations and air–sea exchanges of nonylphenol, tertiary octylphenol and nonylphenol monoethoxylate in the North Sea.* Environmental Pollution, 2006. **142**: p. 170-180.

153. Gunther, K., V. Heinke, B. Thiele, E. Kleist, H. Prast, and T. Raecker, *Endocrine Disrupting Nonylphenols Are Ubiquitous in Food.* Environmental Science and Technology, 2002. **36**: p. 1676-1680.

154. Dodds, E.C. and W. Lawson, *Molecular structure in relation to oestrogenic activity. Compounds without a phenanthrene nucleus.* Proceedings of the Royal Society of London.Series B, 1938. **125**: p. 222-232.

155. Mueller, G.C. and U.-H. Kim, *Displacement of estradiol from estrogen receptors by simple alkyl phenols.* Endocrinology, 1978. **102**: p. 1429-1435.

156. Soto, A.M., H. Justicia, J.W. Wray, and C. Sonnenschein, *p-Nonylphenol, an estrogenic xenobiotic released from 'modified' polystyrene.* Environmental. Health Perspectives, 1991. **92**: p. 167-173.

157. Jobling, S. and J.P. Sumpter, *Detergent components in sewage effluent are weakly estrogenic to fish-An in-vitro study using rainbow-trout (Oncorhynchus mykiss) hepatocytes.* Aquatic Toxicology, 1993. **27**: p. 361-372.

158. Routledge, E.J. and J.P. Sumpter, *Estrogenic activity of surfactants and some of their degradation products assessed using a recombinant yeast screen.* Environmental Toxicology and Chemistry, 1996. **15**: p. 241-248.

159. ENDS, *Industry glimpses new challenges as endocrine science advances.* 1999b, ENDS Report 290. p. 26-30.

160. Ba, J., *Nonaqueous Syntheses of Metal Oxide Nanoparticles and Their Assembly into Mesoporous Materials*, in *chemistry*. 2006, PhD thesis, Max-Planck-Institut für Kolloid- und Grenzflächenforschung: Potsdam. p. 1-134.

161. Livage, J., M. Henry, and C. Sanchez, *Sol-Gel Chemistry of Transition Metal Oxides.* Progress in Solid State Chemistry, 1998. **18**: p. 259-341.

162. Matijevic, E., *Preparation and properties of uniform size colloids.* Chemistry of Materials, 1993 **5**(4): p. 412–426.

163. Tadafumi, A., H. Yukiya, S. Kiwamu, and K. Arai, *Hydrothermal synthesis of metal oxide nanoparticles at supercritical conditions.* Journal of Nanoparticle Research 2001. **3**: p. 227–235.

164. Dawson, W.J., *Hydrothermal Synthesis of Advanced Ceramic Powders.* American Ceramic Society Bulletin, 1988. **67**: p. 1673.

165. Adschiri T., K. Kanazawa., and K. Arai., *Rapid and Continuous Hydrothermal Synthesis of Boehmite Particles in Subcritical and Supercritical Water.* Journal of American Ceramic Society, 1992a. **75**: p. 2615.

166. Hakuta, Y., T. Adschiri, H. Hirakoso, and K. Arai, *Chemical Equilibria and Particle Morphology of Boehmite (AlOOH) in Sub and Supercritical Water.* Fluid Phase Equilibria,1999b. **158–160**: p. 733.

167. Attwood, D., *Microemulsions in Colloidal drug delivery systems*. J. Kreuter ed. 1994, New York: Marcel Dekker.

168. Hoar, T.P. and J.H. Schulman, *Transparent water in oil dispersions: the oleopathic hydromicelle.* Nature, 1943. **152**: p. 102 – 103.

169. zhou, j.x., m.s. zhang, j.m. hong, j.l. fang, and z. yin, *Structural and spectral properties of SnO2 nanocrystal prepared by microemulsion technique.* Applied Physics A, 2005. **81**: p. 177–182.

170. Paul, B.K. and S.P. Moulik, *Uses and applications of microemulsions.* Current Science, 2001. **80**(8): p. 990-1001.

171. José, A.R. and M. Fernández-García, *Synthesis, Properties, and Applications of Oxide Nanomaterials*. 2007, Hoboken, New Jersey: JohnWiley & Sons, Inc.

172. Suslick, K.S., S.-B. Choe, A.A. Cichowlas, and M.W. Grinstaff, *Sonochemical synthesis of amorphous iron.* Nature, 1991. **353**(6343): p. 414-416.

173. Sugimoto, M., *Amorphous characteristics in spinel ferrites containing glassy oxides.* Journal of Magnetism and Magnetic Materials, 1994. **133**(1-3): p. 460-462.

174. Livage, J., *Amorphous Transition Metal Oxides*. Journal de Physique Colloques, 1981. **42**(C4): p. C4-981-C984-992.

175. Perkas, N., Y. Wang, Y. Koltypin, A. Gedanken, and S. Chandrasekaran, *Mesoporous iron-titania catalyst for cyclohexane oxidation.* Chemical Communications, 2001. p. 988-989.

176. Sivarajan, R., K.Y. Prozorov, and R.G. Aharon, *Sonochemical Deposition and Characterization of Nanophasic Amorphous Nickel on Silica Microspheres.* Chemistry of Materials, 1997. **9**(2): p. 546-551.

177. Pol, V.G., R. Reisfeld, and A. Gedanken, *Sonochemical Synthesis and Optical Properties of Europium Oxide Nanolayer Coated on Titania.* Chemistry of Materials, 2002. **14**(9): p. 3920-3924.

178. Chen, J.-F., Y.-H. Wang, F. Guo, X.-M. Wang, and C. Zheng, *Synthesis of Nanoparticles with Novel Technology: High-Gravity Reactive Precipitation.* Industrial and Engineering Chemistry Research, 2000. **39**(4): p. 948-954.

179. Zhang, H. and A.I. Cooper, *Synthesis and applications of emulsion-templated porous materials.* Soft Matter, 2005. **1**(2): p. 107-113.

180. Li, W.-C., A.-H. Lu, C. Weidenthaler, and F. Schüth, *Hard-Templating Pathway To Create Mesoporous Magnesium Oxide.* Chemistry of Materials, 2004. **16**(26): p. 5676-5681.

181. Tian, B., X. Liu, L.A. Solovyov, Z. Liu, H. Yang, Z. Zhang, S. Xie, F. Zhang, B. Tu, C. Yu, O. Terasaki, and D. Zhao, *Facile Synthesis and Characterization of Novel Mesoporous and Mesorelief Oxides with Gyroidal Structures.* Journal of the American Chemical Society, 2003. **126**(3): p. 865-875.

182. Tian, B., X. Liu, H. Yang, S. Xie, C. Yu, B. Tu, and D. Zhao, *General Synthesis of Ordered Crystallized Metal Oxide Nanoarrays Replicated by Microwave-Digested Mesoporous Silica.* Advanced Materials, 2003. **15**(16): p. 1370-1374.

183. Schwickardi, M., T. Johann, W. Schmidt, and F. Schüth, *High-Surface-Area Oxides Obtained by an Activated Carbon Route.* Chemistry of Materials, 2002. **14**(9): p. 3913-3919.

184. Dong, A., N. Ren, Y. Tang, Y. Wang, Y. Zhang, W. Hua, and Z. Gao, *General Synthesis of Mesoporous Spheres of Metal Oxides and Phosphates.* Journal of the American Chemical Society, 2003. **125**(17): p. 4976-4977.

185. Fuertes, A.B., *A general and low-cost synthetic route to high-surface area metal oxides through a silica xerogel template.* Journal of Physics and Chemistry of Solids, 2005. **66**(5): p. 741-747.

186. Chane-Ching, J.Y., F. Cobo, D. Aubert, H.G. Harvey, M. Airiau, and A. Corma, *A General Method for the Synthesis of Nanostructured Large-Surface-Area Materials through the Self-Assembly of Functionalized Nanoparticles.* Chemistry - A European Journal, 2005. **11**(3): p. 979-987.

187. Bard, A.J., G. Inzelt, and F. Scholz, *Electrochemical Dictionary*. 2008, Verlag Berlin Heidelberg, germany: Springer.

188. Waryo, T.T., *Metal Oxide-Modified Carbon Amperometric H2O2-Transducers and Oxidase-Biosensors*, in *chemistry*. 2006, PhD thesis, Karl-Franzens University of Graz: Graz, Austria.

189. Peulon, S., H. Antony, L. Legrand, and A. Chausse, *Thin layers of iron corrosion products electrochemically deposited on inert substrates: synthesis and behaviour.* Electrochimica Acta, 2004. **49**(17-18): p. 2891-2899.

190. Cornell, R.M. and U. Schwertmann, *The Iron Oxides: Structure, Properties, Reactions, Occurrences and Uses*. second ed. 2003, Weinheim, Germany: Wiley-VCH.

191. Teja, A.S. and P.-Y. Koh, *Synthesis, properties, and applications of magnetic iron oxide nanoparticles.* Progress in Crystal Growth and Characterization of Materials, 2009. **55**(1-2): p. 22-45.

192. Klotz, S., G. Steinle-Neumann, T. Strassle, J. Philippe, T. Hansen, and M.J. Wenzel, *Magnetism and the Verwey transition in Fe3O4 under pressure.* Physical Review B, 2008. **77**(1): p. 12411-12414.

193. Laurent, S., D. Forge, M. Port, A. Roch, C. Robic, L.V. Elst, and R.N. Muller, *Magnetic Iron Oxide Nanoparticles: Synthesis, Stabilization, Vectorization, Physicochemical Characterizations, and Biological Applications.* Chemical Reviews, 2008. **108**: p. 2064-2110.

194. Sjogren, C., K. Briley-Saebo, M. Hanson, and C. Johansson, *Magnetic characterization of iron oxides for magnetic resonance imaging.* Magnetic Resonance in Medicine, 1994. **31**(3): p. 268–272.

195. Jolivet, J.-P., C. Chanéac, and E. Tronc, *Iron oxide chemistry. From molecular clusters to extended solid networks.* Chemical Communications, 2004. **5**: p. 481.

196. Augus, I.K. and L.H. John, eds. *Nanocharacterisation*. 2007, The Royal Society of Chemistry: Thomas Graham House, Science Park, Milton Road, Cambridge CB4 0WF, UK.

197. Cherstiouk, O.V., P.A. Simonov, and E.R. Savinova, *Model approach to evaluate particle size effects in electrocatalysis: preparation and properties of Pt nanoparticles supported on GC and HOPG.* Electrochimica Acta, 2003. **48**(25-26): p. 3851-3860.

198. Wafeeq, D., *Consolidated Nanomaterials Synthesized using Nickel micro-wires and Carbon Nanotubes*, in *Chemistry*. 2007, MSc thesis, University of the Western Cape: Cape Town.

199. Yang, L., *Materials Characterization: Introduction to Microscopic and Spectroscopic Methods*. 2008, Singapore: JohnWiley & Sons (Asia) Pte Ltd.

200. Zanello, P., *Inorganic Electrochemistry. Theory, Practice and Application*. 2003, Cambridge CB4 OWF, UK: The Royal Society of Chemistry

201. Ndangili, P.M., *Amperometric Biosensor Systems Prepared on Poly(Anilineferrocenium Hexafluorophosphate) Composites Doped with Poly(Vinyl Sulfonic Acid Sodium Salt)*, in *Chemistry*. 2008, MSc thesis, University of the Western Cape: Cape Town.

202. Joseph, W., *Analytical Electrochemistry*. Second Edition ed. 2000, New York, NY 10158-0012, USA: JohnWiley & Sons, Inc.

.

203. Monk, P.M.S., *Fundamentals of Electroanalytical Chemistry*, ed. C. David J. Ando, Dartford, Kent, UK. 2001, Southern Gate, Chichester, West Sussex PO19 SSQ, England: John Wiley & Sons Ltd.

204. Allen, J.B. and R.F. Larry, *Electrochemical methods : fundamentals and applications*. 2nd ed. ed. 2001, New York, NY 10158-0012, USA: John Wiley & Sons, Inc.

205. David K. Gosser, j., *Cyclic voltammetry:Simulation and Analysis of Reaction Mechanisms* 1993, 220 East 23rd Street New York, NY 10010: VCH Publishers, Inc.

206. Hubert, H. and Girault, *Analytical and Physical Electrochmistry*. First edition ed. 2004, Centre Midi, CH-1015 Lausanne, Switzerland: EPFL Press.

207. Akinyeye, R.O., *Nanostructured Polypyrrole Impedimetric Sensors for Anthropogenic Organic Pollutants*, in *Chemistry*. 2007, PhD thesis, University of the Western Cape: Cape Town.

208. Owino, J.H.O., *Frequency and Voltage-Modulated electrochemical Aflatoxin B1 immunosensor systems prepared on electroactive organic polymer platforms*, in *Chemistry*. 2008, PhD thesis, University of the Western Cape: Cape Town.

209. Macdonald, D.D., *Reflections on the history of electrochemical impedance spectroscopy.* Electrochimica Acta, 2006. **51**(8-9): p. 1376-1388.

210. Macdonald, J.R., J. Schoonman, and A.P. Lehnen, *Applicability and power of complex nonlinear least squares for the analysis of impedance and admittance data.* Journal of Electroanalytical Chemistry, 1982. **131**: p. 77-95.

211. Gamry Instruments. *Basics of Electrochemical Impedance Spectroscopy*. 2007 01 July 2010]; Available from: http://www.gamry.com/App_Notes/EIS_Primer/EIS_Primer_2007.pdf.

212. You, W., H. Xu, J. Zhang, and G. Li, *Electrochemical Sensors for Clinic Analysis.* Sensors, 2008. **8**: p. 2043-2081.

213. Joseph, W., *Electrochemical Sensors for Environmental Monitoring: A Review of Recent Technology*, Office of Research and Development. National Exposure Research Laboratory, U.S. Environmental Protection Agency, Editor.

214. Xiliang, L., A. Morrin, A.J. Killard, and M.R. Smyth, *Application of Nanoparticles in Electrochemical Sensors and Biosensors.* Electroanalysis 2006. **18**(4): p. 319 – 326.

215. Shipway, A.N., M. Lahav, and I. Willner, *Nanostructured Gold Colloid Electrodes.* Advanced Materials, 2000. **12** (13): p. 993 - 998.

216. Shipway, A.N. and I. Willner, *Nanoparticles as structural and functional units in surface-confined architectures.* Chemical Communications, 2001: p. 2035–2045.

217. Crumbliss AL., S. Perine, J. Stonehuerner, K. Tubergen, J. Zhao, R. Henkens, and J. O'Daly, *Colloidal gold as a biocompatible immobilization matrix suitable for the*

fabrication of enzyme electrodes by electrodeposition. Biotechnology and Bioengineering, 1992 **40**(4): p. 483-490.

218. Luo, X.-L., J.-J. Xu, Q. Zhang, G.-J. Yang, and H.-Y. Chen, *Electrochemically deposited chitosan hydrogel for horseradish peroxidase immobilization through gold nanoparticles self-assembly.* Biosensors and Bioelectronics, 2005. **21**(1): p. 190-196.

219. Jianbo, J., B. Wang, A. Wu, G. Cheng, Z. Li, and S. Dong, *A Method to Construct a Third-Generation Horseradish Peroxidase Biosensor: Self-Assembling Gold Nanoparticles to Three-Dimensional Sol-Gel Network.* Analitycal Chemistry, 2002. **74**: p. 2217-2223.

220. Patolsky, F., T. Gabriel, and I. Willner, *Controlled electrocatalysis by microperoxidase-11 and Au-nanoparticle superstructures on conductive supports.* Journal of Electroanalytical Chemistry, 1999. **479**(1): p. 69-73.

221. Liu, Z.-M., H. Wang, Y. Yang, H.-F. Yang, S.-Q. Hu, G.-L. Shen, and R.-Q. Yu, *Amperometric Tyrosinase Biosensor Using Enzyme-Labeled Au Colloids Immobilized on Cystamine/Chitosan Modified Gold Surface.* Analytical Letters, 2004. **37**(6): p. 1079 - 1091.

222. Gu, H.-Y., A.-M. Yu, and H.-Y. Chen, *Direct electron transfer and characterization of hemoglobin immobilized on a Au colloid-cysteamine-modified gold electrode.* Journal of Electroanalytical Chemistry, 2001. **516**(1-2): p. 119-126.

223. He, P. and N. Hu, *Electrocatalytic Properties of Heme Proteins in Layer-by-Layer Films Assembled with SiO_2 Nanoparticles.* Electroanalysis, 2004. **16**(13-14): p. 1122-1131.

224. Pingli, H., N. Hu, and J.F. Rusling, *Driving Forces for Layer-by-Layer Self-Assembly of Films of SiO2 Nanoparticles and Heme Proteins.* Langmuir, 2004. **20**(3): p. 722–729.

225. Zhuo, Y., R. Yuan, Y. Chai, D. Tang, Y. Zhang, N. Wang, X. Li, and Q. Zhu, *A reagentless amperometric immunosensor based on gold nanoparticles/thionine/Nafion-membrane-modified gold electrode for determination of [alpha]-1-fetoprotein.* Electrochemistry Communications, 2005. **7**(4): p. 355-360.

226. Yuan, R., L. Zhang, Q. Li, Y. Chai, and S. Cao, *A label-free amperometric immunosenor based on multi-layer assembly of polymerized o-phenylenediamine and gold nanoparticles for determination of Japanese B encephalitis vaccine.* Analytica Chimica Acta, 2005. **531**(1): p. 1-5.

227. Dianping, T., R. Yuan, Y. Chai, L. Zhang, J. Dai, Y. Liu, and X. Zhong, *Potentiometric Immunosensor Based on Immobilization of Hepatitis B Surface Antibody on Platinum Electrode Modified Silver Colloids and Polyvinyl Butyral as Matrixes.* Electroanalysis, 2005. **17**(2): p. 155-161.

228. Wang, H., J. Li, Y. Ding, C. Lei, G. Shen, and R. Yu, *Novel immunoassay for Toxoplasma gondii-specific immunoglobulin G using a silica nanoparticle-based biomolecular immobilization method.* Analytica Chimica Acta, 2004. **501**(1): p. 37-43.

229. Cai, H., C. Xu, P. He, and Y. Fang, *Colloid Au-enhanced DNA immobilization for the electrochemical detection of sequence-specific DNA.* Journal of Electroanalytical Chemistry, 2001. **510**(1-2): p. 78-85.

230. Zhu, M., M. Liu, G. Shi, F. Xu, X. Ye, J. Chen, L. Jin, and J. Jin, *Novel nitric oxide microsensor and its application to the study of smooth muscle cells.* Analytica Chimica Acta, 2002. **455**(2): p. 199-206.

231. Yu, A., Z. Liang, J. Cho, and F. Caruso, *Nanostructured Electrochemical Sensor Based on Dense Gold Nanoparticle Films.* Nano Letters, 2003. **3**(9): p. 1203-1207.

232. Raj, C.R., T. Okajima, and T. Ohsaka, *Gold nanoparticle arrays for the voltammetric sensing of dopamine.* Journal of Electroanalytical Chemistry, 2003. **543**(2): p. 127-133.

233. You, T., O. Niwa, M. Tomita, and S. Hirono, *Characterization of Platinum Nanoparticle-Embedded Carbon Film Electrode and Its Detection of Hydrogen Peroxide.* Analytical Chemistry, 2003. **75**(9): p. 2080-2085.

234. You, T., O. Niwa, Z. Chen, K. Hayashi, M. Tomita, and S. Hirono, *An Amperometric Detector Formed of Highly Dispersed Ni Nanoparticles Embedded in a Graphite-like Carbon Film Electrode for Sugar Determination.* Analytical Chemistry, 2003. **75**(19): p. 5191-5196.

235. Zen, J.-M., C.-T. Hsu, A.S. Kumar, H.-J. Lyuu, and K.-Y. Lin, *Amino acid analysis using disposable copper nanoparticle plated electrodes.* Analyst, 2 0 0 4. **129**: p. 8 4 1 – 8 4 5.

236. Xu, J.-Z., J.-J. Zhu, H. Wang, and H.-Y. Chen, *Nano-Sized Copper Oxide Modified Carbon Paste Electrodes as an Amperometric Sensor for Amikacin.* Analytical Letters, 2003. **36**(13): p. 2723 - 2733.

237. Fiorito, P.A., V.R. Goncales, E.A. Ponzio, and S.I.C.r.d. Torresi, *Synthesis, characterization and immobilization of Prussian blue nanoparticles. A potential tool for biosensing devices.* Chemical Communications, 2005: p. 366–368.

238. Yi, X., F. Patolsky, E. Katz, J.F. Hainfeld, and I. Willner, *"Plugging into Enzymes": Nanowiring of Redox Enzymes by a Gold Nanoparticle.* Science, 2003. **299**: p. 1877 - 1881.

239. Wang, L. and E. Wang, *Direct electron transfer between cytochrome c and a gold nanoparticles modified electrode.* Electrochemistry Communications, 2004. **6**(1): p. 49-54.

240. Liu, T., J. Zhong, X. Gan, C. Fan, G. Li, and N. Matsuda, *Wiring Electrons of Cytochrome c with Silver Nanoparticles in Layered Films.* ChemPhysChem, 2003. **4**(12): p. 1364-1366.

241. Dongfang, C., P. He, and N. Hu, *Electrochemical biosensors utilising electron transfer in heme proteins immobilised on Fe_3O_4 nanoparticles.* Analyst, 2003. **128**: p. 1268–1274.

242. Lvov, Y., B. Munge, O. Giraldo, I. Ichinose, S.L. Suib, and J.F. Rusling, *Films of Manganese Oxide Nanoparticles with Polycations or Myoglobin from Alternate-Layer Adsorption†.* Langmuir, 2000. **16**(23): p. 8850-8857.

243. Zhang, Y., P. He, and N. Hu, *Horseradish peroxidase immobilized in TiO2 nanoparticle films on pyrolytic graphite electrodes: direct electrochemistry and bioelectrocatalysis.* Electrochimica Acta, 2004. **49**(12): p. 1981-1988.

244. Songqin, L., Z. Dai, H. Chen, and H. Ju, *Immobilization of hemoglobin on zirconium dioxide nanoparticles for preparation of a novel hydrogen peroxide biosensor.* Biosensors and Bioelectronics, 2004. **19**: p. 963–969.

245. Zhou, H., X. Gan, T. Liu, Q. Yang, and G. Li, *Effect of nano cadmium sulfide on the electron transfer reactivity and peroxidase activity of hemoglobin.* Journal of Biochemical and Biophysical Methods, 2005. **64**(1): p. 38-45.

246. Katz, E., I. Willner, and J. Wang, *Electroanalytical and Bioelectroanalytical Systems Based on Metal and Semiconductor Nanoparticles.* Electroanalysis, 2004. **16**(1-2): p. 19-44.

247. Dequaire, M., C. Degrand, and B. Limoges, *An Electrochemical Metalloimmunoassay Based on a Colloidal Gold Label.* Analytical chemistry, 2000. **72**(22): p. 5521-5528.

248. Authier, L., C. Grossiord, P. Brossier, and B. Limoges, *Gold Nanoparticle-Based Quantitative Electrochemical Detection of Amplified Human Cytomegalovirus DNA*

Using Disposable Microband Electrodes. Analytical Chemistry, 2001. **73**(18): p. 4450-4456.

249. Cai, H., Y. Xu, N. Zhu, P. He, and Y. Fang, *An electrochemical DNA hybridization detection assay based on a silver nanoparticle label.* Analyst, 2002. **127**: p. 803 - 808.

250. Cai, H., N. Zhu, Y. Jiang, P. He, and Y. Fang, *Cu@Au alloy nanoparticle as oligonucleotides labels for electrochemical stripping detection of DNA hybridization.* Biosensors and Bioelectronics, 2003. **18**(11): p. 1311-1319.

251. Wang, J., G. Liu, and A. Merkoçi, *Particle-based detection of DNA hybridization using electrochemical stripping measurements of an iron tracer.* Analytica Chimica Acta, 2003. **482**(2): p. 149-155.

252. Merkoçi, A., M. Aldavert, S. Marín, and S. Alegret, *New materials for electrochemical sensing V: Nanoparticles for DNA labeling.* Trac Trends in Analytical Chemistry, 2005. **24**(4): p. 341-349.

253. Wang, J., G. Liu, R. Polsky, and A. Merkoçi, *Electrochemical stripping detection of DNA hybridization based on cadmium sulfide nanoparticle tags.* Electrochemistry Communications, 2002. **4**(9): p. 722-726.

254. Wang, J., G. Liu, and A. Merkoçi, *Electrochemical Coding Technology for Simultaneous Detection of Multiple DNA Targets.* Journal of the American Chemical Society, 2003. **125**(11): p. 3214-3215.

255. Zhu, N., H. Cai, P. He, and Y. Fang, *Tris(2,2'-bipyridyl)cobalt(III)-doped silica nanoparticle DNA probe for the electrochemical detection of DNA hybridization.* Analytica Chimica Acta, 2003. **481**(2): p. 181-189.

256. Luo, X.-L., J.-J. Xu, W. Zhao, and H.-Y. Chen, *A novel glucose ENFET based on the special reactivity of MnO2 nanoparticles.* Biosensors and Bioelectronics, 2004. **19**(10): p. 1295-1300.

257. Jing-Juan Xu, Wei Zhao, X.-L. Luo, and H.-Y. Chen, *A sensitive biosensor for lactate based on layer-by-layer assembling MnO2 nanoparticles and lactate oxidase on ion-sensitive field-effect transistors.* Chemical Communications, 2005: p. 792–794.

258. Luo, X.-L., J.-J. Xu, W. Zhao, and H.-Y. Chen, *Ascorbic acid sensor based on ion-sensitive field-effect transistor modified with MnO2 nanoparticles.* Analytica Chimica Acta, 2004. **512**(1): p. 57-61.

259. Xu, J.-J., X.-L. Luo, Y. Du, and H.-Y. Chen, *Application of MnO2 nanoparticles as an eliminator of ascorbate interference to amperometric glucose biosensors.* Electrochemistry Communications, 2004. **6**(11): p. 1169-1173.

260. Villiers, A., *Sur la fementation de la fècule par l'action du ferment butyrique.* Comptes Rendus de l'Académie des Sciences, 1891. **112**: p. 536.

261. Schardinger, F., *Über Thermophile Bakterien aus verschiedenen Speisen und Milch, sowie über einige Umsetzungsprodukte derselben in kohlenhydrathaltigen Nährlösungen, darunter krystallisierte Polysaccharide (Dextrine) aus Stärke.* Z. Untersuch. Nahr. u. Genussm, 1903. **6**: p. 865–880.

262. Szejtli, J., *Past, present, and future of cyclodextrin research.* Pure and Applied Chemistry, 2004. **76**(10): p. 1825–1845.

263. Loftsson, T. and D. Duchêne, *Cyclodextrins and their pharmaceutical applications.* International Journal of Pharmaceutics, 2007. **329**(1-2): p. 1-11.

264. French, D., *The Schardinger dextrins.* Advances in *Carbohydrate Chemistry*, 1957. **12**: p. 189–260.

265. Horikoshi, K., *Production of Alkaline Enzymes by Alkalophilic Microorganisms, Part I. Alkaline Protease Produced by Bacilius No. 221.* Agricultural Biology and Chemistry, 1971. **35** (9): p. 1407-1414.

266. Horikoshi, K., *Production and industrial applications of b-cyclodextrin.* Process Biochemistry, 1979. **14** (5): p. 26-30.

267. Astakhova, A.V. and N.B. Demina, *Modern Drug Technologies: Synthesis, Characterization, and Use of Inclusion Complexes Between Drugs and Cyclodextrins.* Pharmaceutical Chemistry Journal, 2004. **38** (2): p. 105-108.

268. Kenneth A., C., *The Stability of Cyclodextrin Complexes in Solution.* Chemical Reviews, 1997. **97**: p. 1325-1357.

269. Maestre, I., I. Beà, P. Ivanov, and C. Jaime, *Structural Dynamics of Some Large-Ring Cyclodextrins. A Molecular Dynamics Study: An Analysis of Force Field Performance.* Theoretical Chemistry Accounts, 2007. **117** (1): p. 85-97.

270. Ferancová, A. and J. Labuda, *Cyclodextrins as electrode modifiers.* Fresenius Journal of Analitycal Chemistry, 2001. **370** p. 1-10.

271. Haitao, Y., *UC781: Beta-Cyclodextrin Complexation and Formulation as an Anti-HIV Microbicide*, in *Pharmacy*. 2008, PhD thesis, University of Pittsburgh: Pittsburgh.

272. Shimpi, S., B. Chauhan, and P. Shimpi, *Cyclodextrins: Application in different routes of drug administration.* Acta Pharmaceutica, 2005. **55**: p. 139–156.

273. Numanoğlu, U., T. Şen, N. Tarimci, M. Kartal, O.M.Y. Koo, and H. Önyüksel, *Use of Cyclodextrins as a Cosmetic Delivery System for Fragrance Materials: Linalool and Benzyl Acetate.* Journal of Pharmaceutical Science and Technology, 2007. **8** (4): p. 1-9.

274. Predoi, D., *A Study on iron oxide nanoparticles coated with dextrin obtained by coprecipitation.* Digest Journal of Nanomaterials and Biostructures, 2007. **2**: p. 169-173.

275. Rusling, J.F. and R.J. Forster, *Electrochemical catalysis with redox polymer and polyion-protein films.* Journal of Colloid and Interface Science, 2003. **262**(1): p. 1-15.

276. Keiser, J.T., C.W. Brown, and R.H. Heidersbach, *The Electrochemical Reduction of Rust Films on Weathering Steel Surfaces.* Journal of The Electrochemical Society, 1982. **129**(12): p. 2686-2689.

277. Lin, M. and H. Leu, *A Fe3O4-Based Chemical Sensor for Cathodic Determination of Hydrogen Peroxide.* Electroanalysis, 2005. **17**(22): p. 2068-2073.

278. Waryo, T.T., S. Begic, E.Turkusic, K. Vytras, and K. Kalcher, *Metal Oxide-Based Carbon Amperometric H2O2-Transducers and Oxidase Biosensors*, in *Sensing in Electroanalysis*. 2005, University of Pardubice. p. 145 -191.

279. Henke, C., C. Steinem, A. Janshoff, G. Steffan, H. Luftmann, M. Sieber, and H.-J. Galla, *Self-Assembled Monolayers of Monofunctionalized Cyclodextrins onto Gold: A Mass Spectrometric Characterization and Impedance Analysis of Host−Guest Interaction.* Analytical chemistry, 1996. **68**(18): p. 3158-3165.

280. Finklea, H.O., D.A. Snider, J. Fedyk, E. Sabatani, Y. Gafni, and I. Rubinstein, *Characterization of octadecanethiol-coated gold electrodes as microarray electrodes by cyclic voltammetry and ac impedance spectroscopy.* Langmuir, 1993. **9**(12): p. 3660-3667.

281. Goodhen, P.J., J. humphreys, and R. beanland, *Electron microscopy and analysis* . 2001.

282. Kothiyal, G.P., S.V. Phadnis, V.K. Shrikhande, T. Mirza, M.K. Totlani, and V.C. Sahni, *A study of lead silicate glass degradation behaviour with reference to glasso-metal seal applications.* Anticorrosion Methods and Materials, 2000. **47**(5): p. 280-284.

283. Kandalkar, S.G., J.L. Gunjakar, C.D. Lokhande, and O.-S. Joo, *Synthesis of cobalt oxide interconnected flacks and nano-worms structures using low temperature chemical bath deposition.* Journal of Alloys and Compounds, 2009. **478**(1-2): p. 594-598.

284. McMurry, J., *Organic chemistry fifth edition*. brooks/cole ed. 455-466.

285. Lide, D.R., *Hand book of chemistry and physics*. 86 ed. 2006. 9-87, 89-96.

286. George, W.O. and P.S. Mcintyre , *Infrared Spectroscopy*. 1987: John Wiley and Sons.

287. Sannomiya, T., H. Dermutz, C. Hafner, J. Vörös, and A.B. Dahlin, *Electrochemistry on a Localized Surface Plasmon Resonance Sensor.* Langmuir, 2009. **26**(10): p. 7619-7626.

288. Kalimuthu, P. and S.A. John, *Selective electrochemical sensor for folic acid at physiological pH using ultrathin electropolymerized film of functionalized thiadiazole modified glassy carbon electrode.* Biosensors and Bioelectronics, 2009. **24**(12): p. 3575-3580.

APPENDIX A

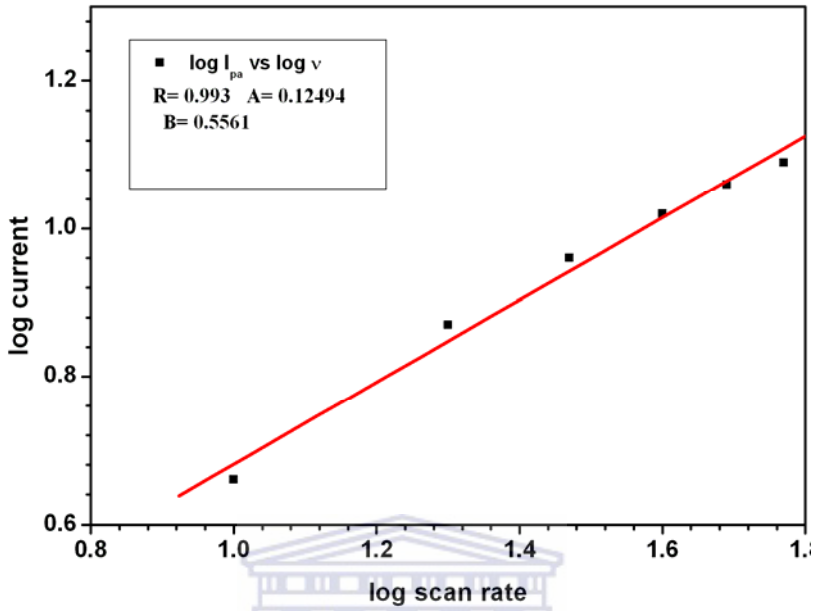

Figure A(i): A plot of log current versus log scan rate for peak a (Ref. Fig. 20)

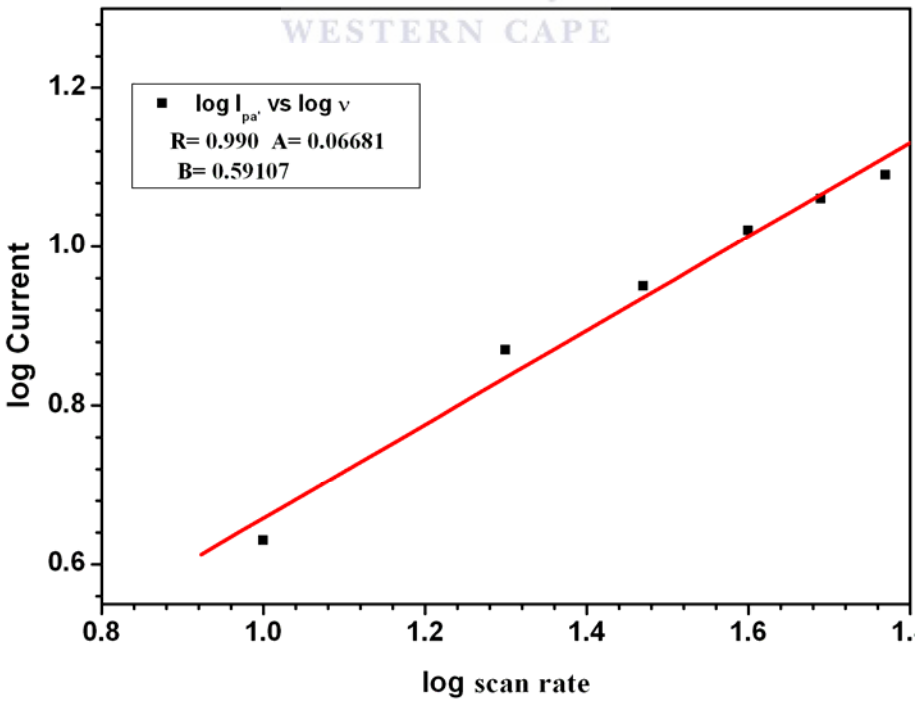

Figure A(ii): A plot of log current versus log scan rate for peak d. (Ref. Fig. 20)

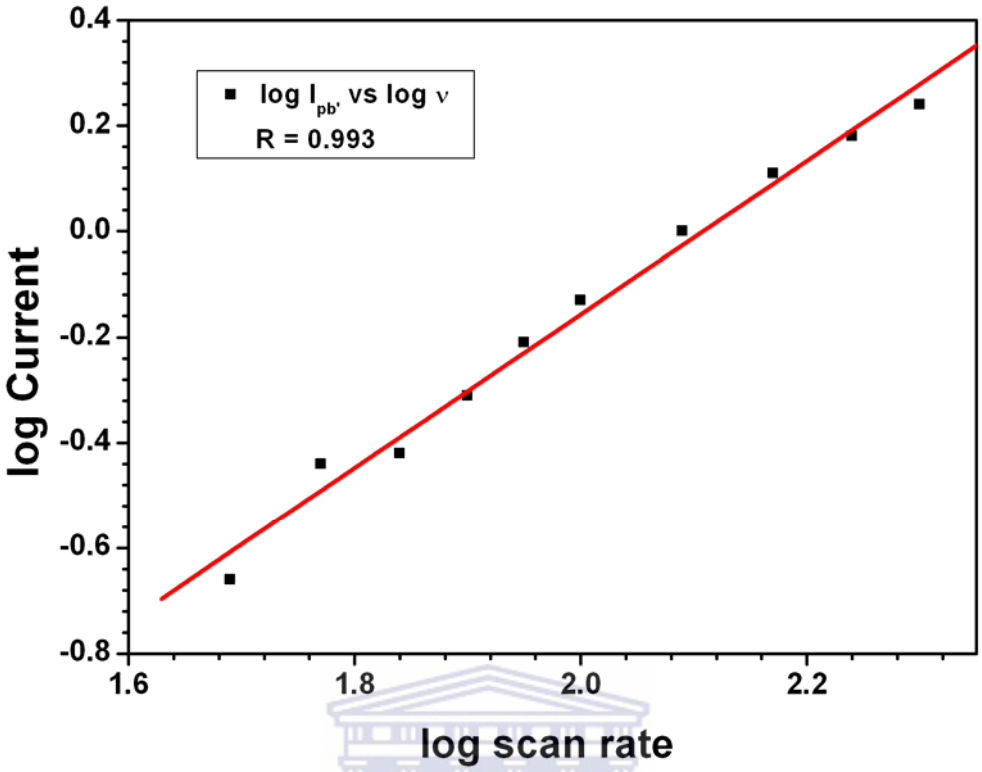

Figure A(iii): A plot of log current versus log scan rate for peak c. (Ref. Fig 20)

APPENDIX B

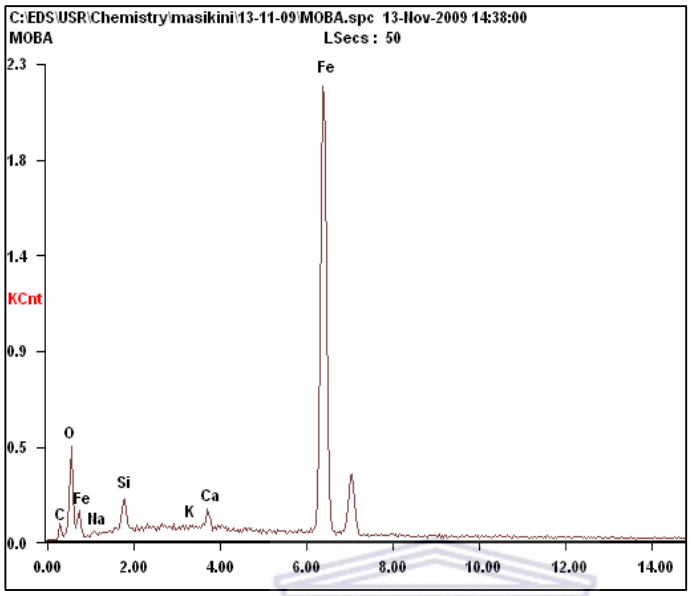

Figure B(i): EDX spectrum for Feox-bcd. (Ref. Fig. 27)

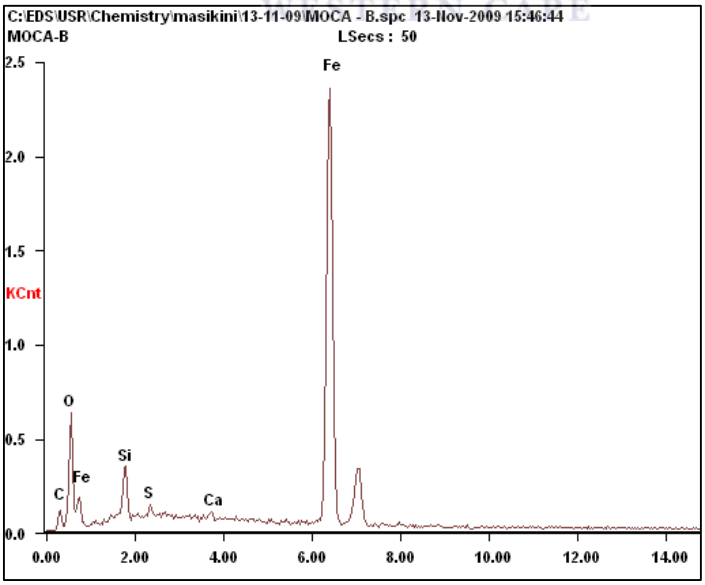

Figure B(ii): EDX spectrum for Feox-cobcd. (Ref. Fig. 27)